Technische Universität München
TUM School of Natural Sciences

TLm

Dynamics of non-classical light generation from semiconductor quantum dots

Lukas Hanschke

Vollständiger Abdruck der von der TUM School of Natural Sciences der Technischen

Universität München zur Erlangung eines

Doktors der Naturwissenschaften (Dr. rer. nat.)

genehmigten Dissertation.

Vorsitz: Prof. Dr. Peter Rabl

Prüfende der Dissertation:

       1.   Prof. Dr. Kai Müller
       2.   Prof. Dr. Stefan Filipp

Die Dissertation wurde am 09.01.2025 bei der Technischen Universität München eingereicht

und durch die TUM School of Natural Sciences am 22.01.2025 angenommen.

Science isn't about why, it's about why not.

- Cave Johnson

Abstract

The advancement of photonic quantum applications is contingent on the availability of pure, bright, and fast single-photon sources. As semiconductor quantum dots nowadays deliver these attributes they represent an auspicious candidate. Despite mastering the high requirements on growth and nanofabrication some properties are inherently limited by the dynamics of the photon generation.

For example the single-photon purity, the property to emit only one photon at a time appears to be inherently perfect when driving a two-level system. The undisturbed system is initially found in its ground state and under absorption of the excitation field lifted to its excited state. From there, spontaneous decay within the excited state lifetime results in the emission of a single photon carrying the transition energy. The cycle restarts then again introducing the temporal separation of subsequently emitted photons. In contrast to a stream of 'clumps' of photons, the emission of single photons is commonly described as antibunched. However, this simple picture breaks down in the presence of a weak excitation field. In this regime, part of the excitation laser is coherently scattered by the two-level system. As a consequence a component of the overall emission features the coherence properties of the laser. This approach suggests the possibility to tailor the emission to gain the narrow linewidth of a laser while maintaining the antibunched emission of a two-level system. However, we find that the origin of photon antibunching lies within the interplay of the coherently scattered component and the emission by spontaneous decay. Furthermore, to retrieve pure single photons from a deterministic source one has to consider the excitation dynamics. The ideal case assumes an instantaneous excitation with subsequent photon emission. This is best reproduced by applying a short laser pulse with a chosen intensity capable to invert the system's population. Typical time scales of this excitation are two orders of magnitude shorter than the decay process and yet allow emission during the presence of the pulse by

the statistical nature of the decay. Considering these decays followed by a second excitation through the remaining pulse sets an upper limit for the resulting photon purity. We even find this re-excitation process being dominant for pulse properties enabling one full rotation of the population. By including an additional excited state via direct excitation of the biexciton adds a second, energetically detuned, decay to the excitation scheme. This cascaded decay strongly reduces the probability of a possible re-excitation process and therefore improves the single-photon purity for each transition by up to two orders of magnitude.

Another key characteristic is the indistinguishability of the emitted photons, crucial for e.g. efficient entanglement swapping for quantum key distribution or error free operation of a photonic quantum computer. Two photons are perfectly indistinguishable when they share the same energy and linewidth, polarization, spatial and temporal mode. While resonant excitation allows near-unity indistinguishable emission, it is strongly degraded in a cascaded decay that creates inseparable photon states. The separability strongly depends on the ratio of the excited state lifetimes and thus, increases by accelerating the first decay. Adding a second laser pulse after initialization of the biexciton state that stimulates the transition to the exciton state artificially breaks the inseparability and restores the indistinguishability of the photons created by the exciton decay while maintaining the excellent single-photon purity provided by the cascaded decay. This excitation scheme also enables spectral separation of the laser and the emitted photons mitigating the inevitable losses from polarization filtering without the need for a asymmetric cavity.

Although our studies were conducted on individual epitaxial quantum dots, our findings are applicable to any quantum two- or few-level system, contributing to the general effort of transitioning quantum systems from the lab to real-world applications.

Zusammenfassung

Der Fortschritt bei photonischen Quantenanwendungen hängt von der Verfügbarkeit reiner, heller und schneller Einzelphotonenquellen ab. Da Halbleiterquantenpunkte heutzutage diese Eigenschaften aufweisen, sind sie ein vielversprechender Kandidat. Trotz der bereits erfüllten hohen Anforderungen an Wachstum und Nanofabrikation sind einige ihrer Eigenschaften durch die Dynamik der Photonenerzeugung von Natur aus begrenzt.

Zum Beispiel scheint die Einzelphotonenreinheit, also die Eigenschaft, jeweils nur ein Photon zu emittieren, beim Anregen eines Zwei-Niveau-Systems von Natur aus perfekt zu sein. Das ungestörte System befindet sich zunächst in seinem Grundzustand und wird durch Absorption des Anregungsfeldes in seinen angeregten Zustand gehoben. Von dort führt ein spontaner Zerfall innerhalb der Lebensdauer des angeregten Zustands zur Emission eines einzelnen Photons, das die Übergangsenergie trägt. Der Zyklus beginnt dann erneut, wodurch die zeitliche Trennung der nacheinander emittierten Photonen sichergestellt wird. Im Gegensatz zu einem Strom aus 'Photonenclustern' wird die Emission einzelner Photonen üblicherweise als 'antibunched' beschrieben. Dieses einfache Bild bricht jedoch in Anwesenheit eines schwachen Anregungsfeldes zusammen. In diesem Regime wird ein Teil des Anregungslasers kohärent vom Zwei-Niveau-System gestreut. Dadurch weist eine Komponente der gesamten Emission die Kohärenzeigenschaften des Lasers auf. Dieser Ansatz deutet darauf hin, dass die Emission so angepasst werden könnte, dass die schmale Linienbreite eines Lasers erhalten bleibt, während die 'antibunched' Emission eines Zwei-Niveau-Systems beibehalten wird. Unsere Ergebnisse zeigen jedoch, dass der Ursprung des Photonen-'antibunching' im Zusammenspiel zwischen der kohärent gestreuten Komponente und der Emission durch spontanen Zerfall liegt.

Darüber hinaus muss man die Anregungsdynamik berücksichtigen, um reine Einzelphotonen aus einer deterministischen Quelle zu gewinnen. Der Idealfall geht

von einer sofortigen Anregung mit anschließender Photonemission aus. Dies wird am besten durch die Anwendung eines kurzen Laserimpulses mit einer geeigneten Intensität erreicht, die in der Lage ist, die Population des Systems vollständig zu invertieren. Typische Zeitskalen dieser Anregung sind zwei Größenordnungen kürzer als der Zerfallsprozess und ermöglichen dennoch aufgrund der statistischen Natur des Zerfalls eine Emission während der Präsenz des Pulses. Wenn man diese Zerfälle betrachtet, gefolgt von einer zweiten Anregung durch den verbleibenden Puls, ergibt sich eine obere Grenze für die resultierende Photonreinheit. Wir stellen sogar fest, dass dieser Wiederanregungsprozess dominant wird, wenn die Pulseeigenschaften eine vollständige Rotation der Population ermöglichen. Die Einbeziehung eines zusätzlichen angeregten Zustands durch direkte Anregung des Biexzitons fügt dem Anregungsschema einen zweiten, energetisch verstimmten Zerfall hinzu. Dieser kaskadierte Zerfall verringert die Wahrscheinlichkeit eines möglichen Wiederanregungsprozesses erheblich und verbessert somit die Einzelphotonenreinheit bei jedem Übergang um bis zu zwei Größenordnungen.

Ein weiteres wichtiges Merkmal ist die Ununterscheidbarkeit der emittierten Photonen, die z. B. für eine effiziente Verschränkungstauschung bei der Quanten-Schlüsselverteilung oder den fehlerfreien Betrieb eines photonischen Quantencomputers entscheidend ist. Zwei Photonen sind perfekt ununterscheidbar, wenn sie dieselbe Energie und Linienbreite, Polarisation sowie räumliche und zeitliche Moden teilen. Während resonante Anregung eine nahezu perfekt ununterscheidbare Emission ermöglicht, wird diese bei einem kaskadierten Zerfall, der untrennbare Photonenzustände erzeugt, stark beeinträchtigt. Die Trennbarkeit hängt maßgeblich vom Verhältnis der Lebensdauern der angeregten Zustände ab und kann durch Beschleunigung des ersten Zerfalls erhöht werden. Durch Hinzufügen eines zweiten Laserpulses nach der Initialisierung des Biexziton-Zustands, der den Übergang zum Exziton-Zustand stimuliert, wird die Untrennbarkeit künstlich aufgehoben und die Ununterscheidbarkeit der durch den Exziton-Zerfall erzeugten Photonen wiederhergestellt, während die hervorragende Einzelphotonenreinheit des kaskadierten Zerfalls erhalten bleibt. Dieses Anregungsschema ermöglicht außerdem eine spektrale Trennung zwischen dem Laser und den emittierten Photonen, wodurch unvermeidliche Verluste durch Polarisationsfilterung reduziert werden, ohne dass ein asymmetrischer Resonator erforderlich ist.

Obwohl unsere Untersuchungen an einzelnen epitaktischen Quantenpunkten durchgeführt wurden, sind unsere Ergebnisse auf jedes Quanten-Zwei- oder -Mehrniveausystem anwendbar und leisten einen Beitrag zu den allgemeinen Bemühungen, Quantensysteme aus dem Labor in reale Anwendungen zu überführen.

Contents

Chapter *1*

Introduction

From the first predictions of the quantum nature of light [Pla01, Ein05] to its experimental proof [Cla74, Kim77a], about seventy years elapsed. In the years that followed, photon entanglement was also demonstrated experimentally [Fre72, Asp81, Asp82] catalyzing a rapidly advancing research field focused on the properties of photon emission. Early experiments relied on sparse beams of atoms, but these were soon succeeded by techniques enabling investigation of single trapped ions and atoms [Neu80, Mig85], as well as the process of parametric down conversion to generate pairs of entangled photons [Ou88, Hor89, Rar90, Kwi95]. These advancements spurred proposals to leverage the quantum properties of light for secure communication [Ben84, Eke91] and realization of quantum computers [Ben80, Kni01, Rau03], bridging the gap between mere academic interest to real world applications.

Quantum key distribution relies on encoding information in a quantum bit, or qubit, in orthogonal bases to generate a secret key that is shared between the communicating parties [Gis02]. Single photons are an ideal platform to realize this concept with the information transferred to its polarization and well conserved due to the weak interaction with the environment [Vaj22]. The encoded information is intrinsically protected by the no-cloning theorem, that states the impossibility to create an identical copy of an unknown quantum state [Par70, Woo82, Die82]. An

eavesdropper needs then to guess the basis of measurement and create a replacement qubit according to the measurement outcome. However, this introduces random qubits in the incorrect basis which the intended receiver detects, leading to the discarding of the transmitted key. To simply approximate packages of single photons it is possible to employ strongly attenuated laser pulses with random phase. Those weak coherent pulses contain statistically less than one photon per pulse in a Poissonian distribution. This introduces a trade-off between transmission rate and security, as stronger pulses are more likely to contain multiple photons, making the transmission vulnerable to a photon number splitting attack [Hut95, Bra00]. By introducing decoy states to more easily detect an eavesdropper, the key transmission rate can be improved, though it remains inferior to that of a pure single-photon source [Hwa03, Lo05].

For quantum computers, the focus is on discovering and implementing algorithms capable of solving computational tasks that are beyond the reach of classical computers. One prominent example is Shor's algorithm that retrieves the prime factors of an integer [Sho94]. However, the potential lies in the efficient simulation of quantum systems, which could, for example, aid in discovering room-temperature superconducting materials or advancing drug discovery. Additionally, other complex systems, such as financial risk management, traffic optimization and cargo distribution, could also see significant improvements. Building such a quantum computer requires scalable qubits and high-fidelity controlled gate operations. While a full scale quantum computer is still elusive, many prototypes with few qubits were already realized using superconducting qubits [Bar14, Kan17, Aru19], trapped atoms [Jak05, Blo12, Par22] or ions [Ben08, Gae16, Pog21], gate-defined quantum dots (QD) [Yan20, Hen21, Mą22, Zwe22] or photons [Zho20, Mad22, Mar24]. On a photonic quantum computer the different gate operations between the qubits can be realized with variable phase shifter and beam splitter which can be directly implemented on chip. However, a reliable and efficient single-photon source is essential to provide the qubits. Furthermore, the photons must be indistinguishable to ensure fault-free operation, that requires even multiple identical sources to scale the number of usable qubits without multiplexing.

Motivated by those powerful applications a variety of quantum emitters were discovered, such as single dye molecules bound in organic crystals [Bas92], defect centers in diamond [Kur00, Bro00, Wan06, Neu11, Iwa15, Iwa17], silicon carbide [Cas14,

Loh16], silicon [Lee23] and boron nitride [Tra16] or functionalized carbon nanotubes [Ma15], broadening the range of systems to study and harness single-photon emission.

And with the advances in material growth by molecular beam epitaxy (MBE) formation of nanometer sized islands of InAs grown on top of GaAs was achieved [Gol85, Leo93]. Those structures, coined as QDs, provide a confinement potential for charge carriers resulting in a quantized energy level structure due to their small size. Following this property they are also referred to as artificial atoms and provide another platform to emit single photons undergoing a spontaneous decay from an excited state [Mic00a, San01]. Coherent and deterministic control of the excited state [Sti01, Kam01, Hto02, Zre02] and the high quality of the emitted photons being indistinguishable [San02b] proofed that QDs are a promising source for potential applications. However, the semiconductor matrix embedding the QDs introduces some drawbacks, like an unstable electrical environment. Random charging of the QD and spectral wandering lead to blinking of the emission [Ngu12, Dav14b] as well inhomogeneous linewidth broadening [Kuh13b]. In addition, undirected emission and the high reflective index of the surrounding bulk material causing total internal reflection strongly reduces the collection efficiency of the created photons. While the semiconductor host of the QDs is the source of those detriments, it also offers opportunities to overcome them. Incorporating doped layers above and below the QDs during epitaxial growth forms a diode structure that stabilizes the electrical environment and enables precise tuning of the ground charge state [War00, Kuh15]. Furthermore, mirror structures can be directly implemented during the growth and combined with advanced nanofabrication techniques allow forming efficient cavities to funnel the emission towards a collecting lens or fiber. [Gé98]. With all this methods at hand and improving excitation techniques [Kuh13a], the field underwent a rapid development bearing bright single-photon sources with high indistinguishability [Din16b, Som16], unrivaled single-photon purity [Sch18a] and polarization entangled photon pairs with near-unity concurrence [Hub18]. Moreover, by employing an open cavity to efficiently collect and separate the emission of a single QD from the excitation laser an overall system efficiency exceeding 70% was demonstrated [Tom21, Din23]. Even fundamental studies of the quantum nature of light, often first investigated in intrinsically pure systems like single atoms, became possible showing the squeezing of light

with single photons [Sch15]. To further push this system towards applications in communication, significant efforts were made to tune the emission wavelength to the telecom O- and C-band [Miy05, All05, War05, Sem08], enabling low-loss quantum key distribution through optical fibers [Int09, Tak10, Tak15].

Despite three decades of extensive research and impressive progress on this quantum system, several fundamental questions remain unresolved, which we address within this thesis. We start in Chapter 2 by introducing the growth of epitaxial QDs and their resulting discrete energy level structures. Additionally, it discusses the integration of diode structures during the growth process, which is completed through the nanofabrication of metal contacts, enabling charge control to select the either negatively charged trion transition for investigations of a true two-level system or the exciton-biexciton complex to expand the system to a quantum three- or four-level system. Building on the foundation of the studied quantum system, Chapter 3 covers its interaction with a resonant light field, leading to the observation of Rabi oscillations. The experimental setup to achieve this is described, along with the methods used to analyze the purity and indistinguishability of the resulting emission. Besides the aforementioned coherent population dynamics introduced by resonant excitation, Chapter 4 focuses on the impact on the level structure. The bare energy level structure of a QD is modified by the interacting light field, forming a new set of dressed states that give rise to the Mollow triplet. Perfect agreement with the fundamental theory, which models the QD as a pure two-level system, validates the quality of our samples and techniques. Chapter 5 addresses the underlying origin of photon antibunching of resonance fluorescence (RF) in the weak driving regime. There, a portion of the incoming light field is coherently scattered by the two-level system contributing a component to the overall emission which inherits the coherence properties of the laser [Ste15, Mey07]. Early studies suggested that in this excitation regime the emission can be tailored to combine the narrow linewidth of a laser with the antibunched emission of a two-level system [Ngu11, Mat12]. On the other hand, we find that the origin of photon antibunching lies within the interplay of the coherently scattered component and the emission by spontaneous decay [Han20, Phi20]. This, at first, renders the idea of using weak excitation to obtain a single-photon source with sub-natural linewidth unusable but delivers the comprehension to maintain the crucial balance of the coherent and incoherent component under narrow spectral

filtering by admixing an external coherent field [LC18]. In addition, a detailed study of the pulsed excitation and decay dynamics reveal potential re-excitation processes that inherently limit the single-photon purity [Fis18a], and opens up methods to either enhance dominant two-photon emission [Fis17] or further suppress these processes [Han18]. The second key focus of this thesis, the indistinguishability of the generated photons, is further examined in Chapter 6. The decay dynamics play a crucial role, potentially imposing a fundamental limit on the achievable indistinguishability of photons emitted in a cascade. By artificial tuning of the decay rates, we study this impact and can mitigate it to overcome this limitation. Finally we summarize the major results in Chapter 7 and conclude with remarks on the significance of our findings and their potential contribution to the collective endeavor toward quantum applications.

Chapter 2

Semiconductor QDs: Growth and Properties

Contents

2.1 QDs Growth

Solid state nanostructures composed of semiconductors with different bandgaps can create a confinement potential for charge carriers. If the size of such a structure is in the range of the carrier de Broglie wavelength, the energy states become quantized [Bim99]. Thus, confinement in all three dimensions can be utilized to realize a simple and easily accessible quantum two-level system [War98, Haw99, Fin01b]. In this thesis we performed experiments on two different kinds of QDs. InGaAs QDs

grown by the Stranski-Krastanow mode embedded in GaAs [Sta04] and GaAs QDs formed by localized droplet etch in an AlGaAs matrix [DS21].

2.1.1 Stranski Krastanov - InGaAs QDs

To grow the desired nanostructures with high quality we use MBE which allows deposition of materials with precise control of the growth rate and composition. As a first step 300 nm of GaAs is deposited on a commercially available GaAs wafer to heal out crystal defects caused by wafer cutting. Next, nominally 3 - 7 monolayers of $In_{0.4}Ga_{0.6}As$ are grown as depicted in Figure 2.1a. Despite the up to 7% larger lattice constant of InGaAs compared to GaAs it first forms a highly strained two-dimensional layer [Gol85, Moi94] (Figure 2.1b). After reaching a critical thickness the strain is released by formation of lens shaped islands, as shown in Figure 2.1c, with a diameter of around 20 nm and height of 5 nm [Fry00a, Fry00b, Kre05a]. Leaving only a thin InGaAs layer, the so called wetting layer, since the surface free energy of InGaAs is smaller than that of GaAs [Poh08]. Due to the passive nature of the formation of the QDs, they are often referred to as self-assembled. In a final step the QDs are capped by GaAs, illustrated in Figure 2.1 d), to passivate surface states and to provide full three dimensional confinement.
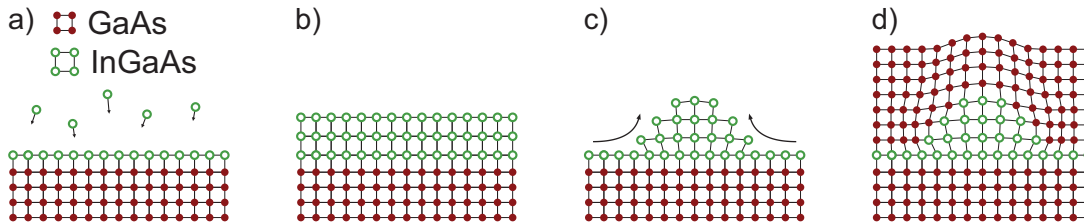
Figure 2.1 | Stranski-Krastanov growth of InGaAs QDs a, Deposition of InGaAs on the GaAs subtrate. **b**, Despite the smaller lattice constant of GaAs compared to InGaAs the grown layer continue with the same crystal structure. **c**, The strain inside the few monolayers thick InGaAs becomes strong enough to energetically favor the formation of small islands. **d**, The QD layer is capped with GaAs.

The formation and density of those QDs is extremely sensitive on the amount of deposited InGaAs. The geometry of the MBE system and the material effusion cells combined with stopped rotation of the substrate result in a position dependent

deposition rate. This gradient in layer thickness translates in a QD density gradient across the wafer. To identify the region with suitable dot density $< 1\,\mu m^{-2}$, we perform a macro photoluminescence (PL) scan over the whole wafer under above band excitation at $10\,K$, as presented in Fig. 2.2a. Here, the integrated intensity of the QD ensemble is shown with a bright signal in the bottom left and no QD PL in the top right region. The example spectrum in the high density region shows bright ensemble emission centered at $905\,nm$ (Fig. 2.2c red) that shifts to longer wavelength with reduced density (blue) and finally only features emission from the wetting layer (green). All spectra exhibit emission at $815\,nm$ from exciton recombination in the GaAs matrix. The ideal region is found between the blue and green marked positions and is verified by a high resolution widefield PL image, shown in Fig. 2.2b, where a single QD creates a bright spot.
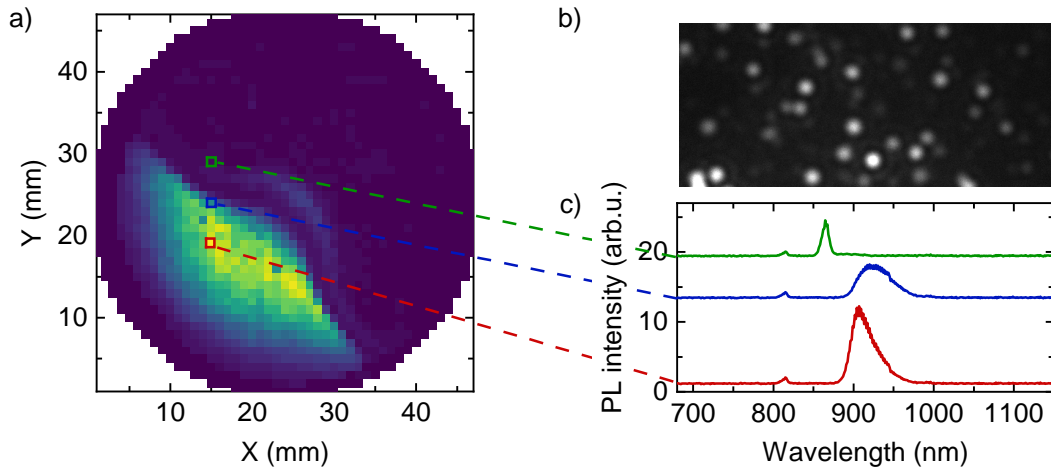
Figure 2.2 | Macro PL of QDs grown by Stransky-Krastanov method. a, Spatially resolved integrated intensity of QD PL of a gradient-grown wafer acquired at $T = 10\,K$. **b**, High resolution image of QD emission under wetting layer excitation. **c**, Emission spectra along the gradient of the grown wafer. The red and blue spectra show dominant QD ensemble emission, while the green spectrum exhibits mainly emission from the wetting layer. The signal of free exciton recombination in GaAs at $\sim 815\,nm$ is visible at each position.

2.1.2 Aluminum Droplet Etch - GaAs QDs

Another approach to create QDs is the localized droplet etching method. After the growth of a GaAs buffer layer on a GaAs wafer a $200\,nm$ thick AlGaAs layer
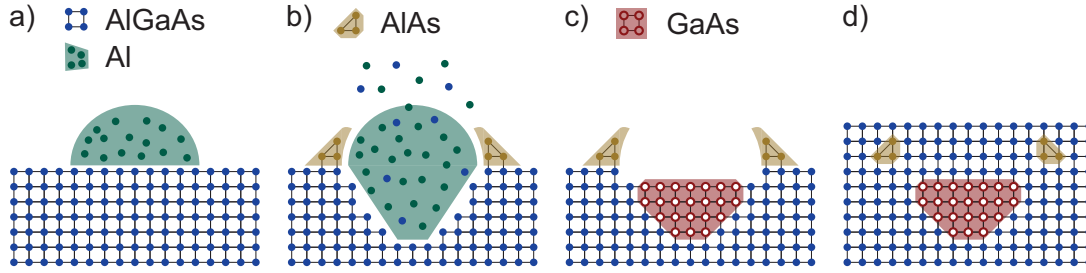
Figure 2.3 | Localized droplet etching method for GaAs QD growth a, Formation of Al droplets on AlGaAs subtrate with the Volmer Weber growth mode **b,** During annealing As diffuses into the droplet leading to a liquefaction of the substrate while AlAs crystallizes at the edges. The remaining droplet is desorbed leaving a nanohole in the substrate **c,** The holes are filled with GaAs **d,** As a final step, the QDs are overgrown by AlGaAs

is deposited. Changing the environment to a low arsenic pressure in the growth chamber while maintaining the Al flux leads to formation of Al droplets on the sample surface [Son12], as presented in Fig. 2.3a. Increasing the temperature of the substrate allows the As atoms from the substrate to diffuse into the Al droplet resulting in liquefaction of the remaining material. Thus, a hole of the size of the droplet is etched into the sample. The dissolved As crystallizes at the edges of the droplet forming an optically inactive AlAs lobe around the hole, as illustrated in Fig. 2.3b [Wan07, Hey09a, Hey11]. Simultaneously the droplet is being desorbed into the chamber, leaving an empty hole [Hey09a]. In the next step, shown in Fig. 2.3c, 2 nm GaAs is deposited followed by an annealing step facilitating the diffusion of the material into the etched holes. The QD growth is finalized by embedding the GaAs dots fully in AlGaAs , depicted in Fig. 2.3d [Hey09b, Huo13].

2.2 Energy Levels and Spin Configurations

Both growth methods result in nanometer sized islands of a direct semiconductor encapsulated in a material with larger band gap. The band gap of GaAs at $4.2\,\mathrm{K}$ of $E_{g,GaAs} = 1.52\,\mathrm{eV}$ ensures charge carrier confinement in InGaAs with a nominal In content of 40% and band gap of $E_{g,InGaAs} = 0.96\,\mathrm{eV}$ [Pau91]. On the other hand, $\mathrm{Al_{0.4}Ga_{0.6}As}$ with a band gap of $E_{g,AlGaAs} = 2.04\,\mathrm{eV}$ [Asp76, Sax80] provides a
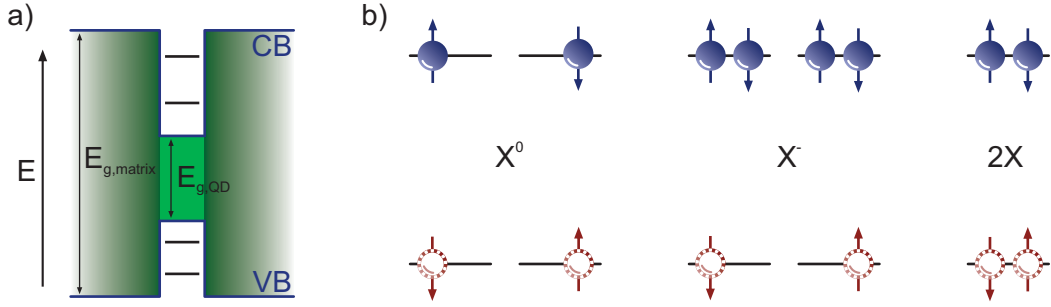
Figure 2.4 | Bandstructure and excited states of a QD a, Simplified bandstructure of a small bandgab semiconductor embedded in a matrix of a semiconductor with larger bandgab. The resulting energy structure ot the formed quantum well is discrete. **b**, Spin configurations of the neutral, negatively charged and bi-exciton.

suitable matrix for GaAs QDs. The creation of such a three-dimensional confinement potential, as schematically depicted in Fig. 2.4a, finally results in the formation of discretized energy states [Bim99]. Due to the significantly smaller size of the QD along the growth direction, only the lowest energy conduction level and the highest energy valence level are relevant, whereas in the lateral direction, multiple sub-bands with quantized energy levels, which are labeled s, p, d, . . . -shell in analogy to atomic levels [Haw99, War98, Haw03], are present. The confined electrons maintain a s-type wavefunction and, thus, the total angular momentum is only given by the electron spin with two possible values $m_{s,z}^{e} = \pm 1/2$ for the spin pointing up or down. On the other hand, the hole wavefunction can be predominantly considered p-type, carrying an additional orbital angular momentum of $l^{h} = 1$ [Dya08]. It follows that the total projection of the angular orbital momentum allows four values $m_{j,z}^{h} = \pm 1/2, \pm 3/2$. While those states are degenerate in a bulk semiconductor, the different confinement energies lift the degeneracy of the so called heavy and light holes by a few tens of meV. Since we focus our investigations to the QD ground states we can omit the light hole states from our considerations [Bra59, Ehr60]. This leaves the four possible spin configurations $S_z = m_{s,z}^{e} + m_{s,z}^{hh} = \{-2, -1, 1, 2\}$ for an exciton in the s-shell. Given the angular momentum carried by a single photon, that does not posses an additional orbital angular momentum, light can only couple efficiently to $S_z = \pm 1$ states [Urb13]. The two possible spin configurations of the electron (blue) and the hole (red) forming a neutral exciton are depicted in Fig. 2.4b [Fin01b]. In

the ideal case those two states are energetically degenerate. However, a deviation from the radial symmetry of the QD results in the electron-hole exchange interaction forming new eigenstates by superposition of the initial states $|\uparrow\Downarrow\rangle$, $|\downarrow\Uparrow\rangle$. Those states are separated by the fine structure splitting δ_{FSS}. Adding an additional charge carrier cancels either the electron or hole spin and therefore neglects the exchange interaction, with the two charged states being again energetically degenerate in the absence of an external magnetic field [Bay02b]. This is achieved by deterministically charging the QD with e.g. an electron. The ground state is then negatively charged and the trion X^- the excited state. The possible spin configurations are depicted in the second panel of Fig. 2.4b. Finally, as shown in the last panel of Fig. 2.4b, the fully occupied s-shells allow only one spin configuration according to the Pauli principle. The energy level of this so called biexciton $2X$ deviates from twice the exciton energy, due to Coulomb interaction, by the biexciton binding energy E_b [Bru94].

Including higher excited states or a strong chirp in the laser pulse combined with a magnetic field allows also the generation of the 'dark' exciton with $S_z = \pm2$ [Haw99], which through its long lifetime can be used to generate a cluster state of entangled photons or serve as a shelving state for the generation of time-bin entangled photon pairs [Poe10, Sch16, Kap24].

2.3 Diode Structure and Distributed Bragg Reflector

The epitaxial growth of our samples offers the possibility to incorporate additional functional layers. Embedding the QDs in two conducting layers forms a diode that creates a constant electric field in the reverse biased region [War00, Fry00a, Fin01a]. This is realized by adding silicon as dopant in GaAs creating an n-contact separated by a thin tunnel barrier of intrinsic GaAs below the QD layer, as depicted in Fig. 2.5a. Following the growth process we define contact pads on the surface by optical lithography and e-beam evaporation of Ni, Ge and Au, marked in red in Fig. 2.5b. After the lift-off process the sample is annealed for $90\,\mathrm{s}$ at $420\,^\circ\mathrm{C}$ to form a Ge-Au eutectic stabilized by Ni which diffuses into the sample establishing an ohmic contact with the n-doped layer [Rob75]. In another lithography step a $4.5\,\mathrm{nm}$ thin titanium layer is deposited which creates a semi-transparent Schottky contact on the sample surface (grey and gold area) preserving optical access from the top. As

last step gold windows (golden area) with $20\,\mu m$ wide cutouts are deposited onto the titanium layer as orientation markers and to facilitate wire bonding.

The final structure creates a build-in electric field that bends the valence and conduction band as schematically depicted in Fig. 2.5c. By applying an external voltage this bending and therefore the charge carrier tunnel dynamics can be tuned.
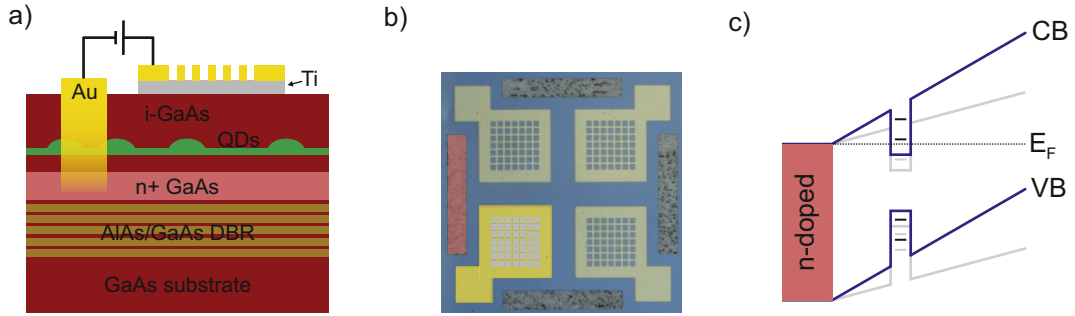
Figure 2.5 | n-i-Schottky diode structure a, Schematic QD sample structure featuring a n-doped GaAs contact below the QD layer and a Ti/Au contact on the surface. **b**, Microscope image of the fabricated contact pads. The colored regions correspond to the layers in a). **c**, Band diagram of the diode structure. Applying an external voltage lowers the bands. This allows deterministic tunnel charging of the QD from the n-doped region.

A similar diode structure is realized by replacing the Schottky contact with a p-doped layer. This requires etching of mesa structures to avoid a short circuit between the doped layers. The schematic layer structure is presented in Fig. 2.6a and a microscope image showing the etched mesas (purple) and the contact pads (yellow) in Fig. 2.6b. Additionally, the top contact is replaced by a sequence of Pd/Zn/Pd/Au to achieve a good ohmic contact with the p-doped GaAs [Bru90]. One advantage of this design is the lower absorption of the doped top layer and the possibility to combine the diode structure with a nanofabricated cavity. An example of a fully fabricated sample piece is shown in the photograph in Fig. 2.6c. Prior to wire bonding the sample is glued onto a ceramic chip carrier that allows connection to a voltage source.

Both kind of diode structures exhibit a wide reverse bias voltage range with remaining leakage current below the resolution limit $(30\,pA)$ of our source meter, as can be seen in Fig. 2.7a. In this voltage range a constant electric field between the two contact layers is created, thus, providing a stable electrical environment
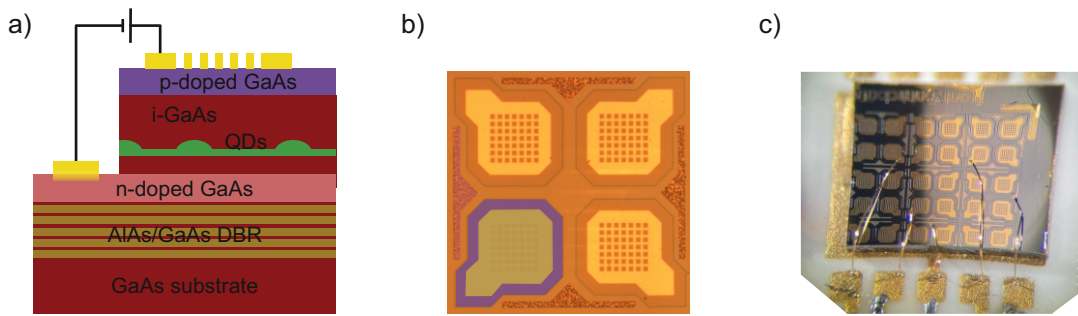
Figure 2.6 | n-i-p diode structure a, Schematic QD sample structure with etched mesas to access the doped layers. **b**, Microscope image of the etched mesas and deposited contacts. **c**, Fully fabricated, cleaved and wire bonded sample piece on a ceramic chip carrier.

quenching charge noise experienced by the QDs [Kuh13b, Kuh15]. The impact on the emission of the QD is studied by voltage dependent PL measurements under wetting layer excitation. A typical result of such a measurement is presented in Fig. 2.7b.
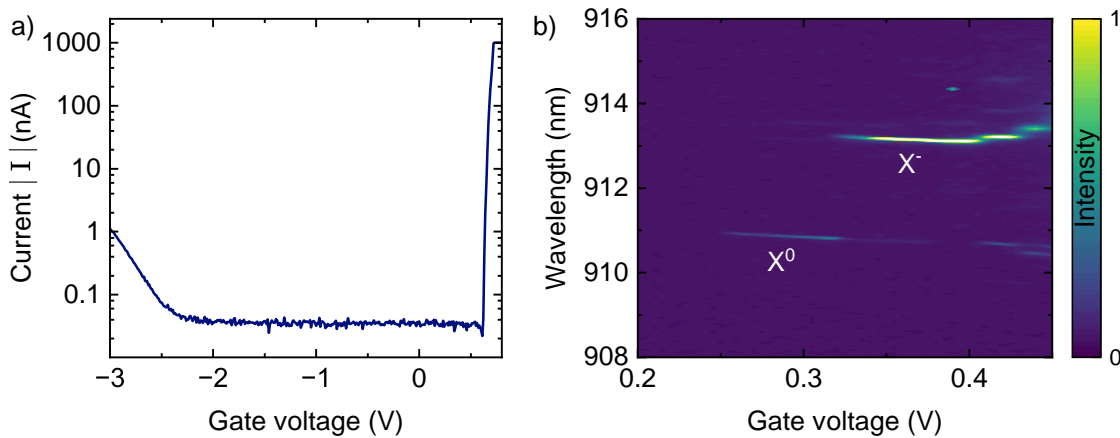
Figure 2.7 | Diode structure tuning a, Typical diode characteristic of a n-i-Schottky sample. The absolut current falls in the reverse biased region $-2.4\,\text{V}$ to $0.7\,\text{V}$ below the resolution limit of the source meter. **b**, The voltage dependent PL measurement reveals distinct charging plateaus.

Over a large range within the reverse bias region ($V < 0.25\,\text{V}$) the charge carrier tunnel rate to the contact layers exceeds the recombination rate resulting in a photo current and quenching of PL [Fry00b]. Increasing the applied voltage shifts the

rate ratio towards radiative recombination resulting in the observation of emission of the neutral exciton X^0, here at $\lambda_{X^0} = 910.87\,\text{nm}$. Further increasing the bias voltage $(V > 0.32\,\text{V})$ shifts the electron s-shell below the Fermi level leading to electron tunneling from the back contact to the QD [War00]. This quenches the emission from the neutral exciton and gives rise to PL from the negatively charged trion X^-, here at $\lambda_{X^-} = 913.15\,\text{nm}$. At $V = 0.40\,\text{V}$ another electron is able to tunnel to the QD shifting the emission to the double charged exciton X^{2-}. This sequential charging eventually continues until tunneling from the QD to the front contact takes over, allowing a constant current of charge carriers and consequently vanishing radiative recombination. In addition, within a charge plateau the transition energy is shifted by the quantum confined Stark effect (QCSE) through control of the electric field by the applied voltage [Fry00a, Fin01a]. For the presented data set the neutral exciton can be tuned over a range of $\Delta_{X^0} = 172\,\mu\text{eV}$ corresponding to a tuning rate of $2.867\,\frac{\text{meV}}{\text{V}}$ while the negative trion shows a similar behaviour with $\Delta_{X^-} = 157\,\mu\text{eV}$ and tuning rate $2.096\,\frac{\text{meV}}{\text{V}}$. This tuning ability provides a huge advantage for applications which require two or more quantum emitter to operate at the exact same wavelength [Zha22]. Moreover, it facilitates bringing the transition energy in resonance with an excitation laser or cavity.

Besides the incorporated diode structure we include a distributed Bragg reflector into the sample design. Placed below the QD layer, this dielectric mirror prevents loss of emission intensity to the bottom of the sample. The high reflectivity of such a mirror is achieved by constructive interference of the partial reflections on a superlattice of two materials with a high and low refractive index [Tan95, Ali04]. This condition is matched when the individual layers thickness fulfills:

$$d = \frac{\lambda}{4n} \tag{2.1}$$

Here λ is the design wavelength and n the refractive index. The epitaxial growth requires materials with matching lattice constants to avoid stress and crystal defects. Suitable materials are GaAs and AlAs, which also exhibit a sufficiently high contrast of refractive indices with $n_{GaAs} = 3.50$ and $n_{AlAs} = 2.92$ at $T = 10\,\text{K}$. We include 17 alternating pairs of GaAs and AlAs to achieve a high reflectivity $> 90\%$ over a $> 100\,\text{nm}$ wide stop band. Fig. 2.8a shows the measured reflectivity normalized to a

reference gold mirror with the stop band centered at 937 nm. Due to the nonuniform deposition rate during growth, the center wavelength of the stopband exhibits a radial gradient over the whole wafer. We characterize this by measuring a spatial map of the reflectivity. The result of such a map with the determined center wavelength ranging from 940 nm in the center of the waver to 880 nm at the edge is presented in Fig. 2.8b. Together with the macro PL shown in Fig. 2.2a, this data allows us to select the piece of the wafer with the desired dot density and matching DBR. In addition, the DBR forms a weak planar cavity with the sample surface, further increasing the extraction efficiency of emitted photons. An additional DBR with lower reflectivity can be used as the top mirror of such a weak cavity to further improve its performance.
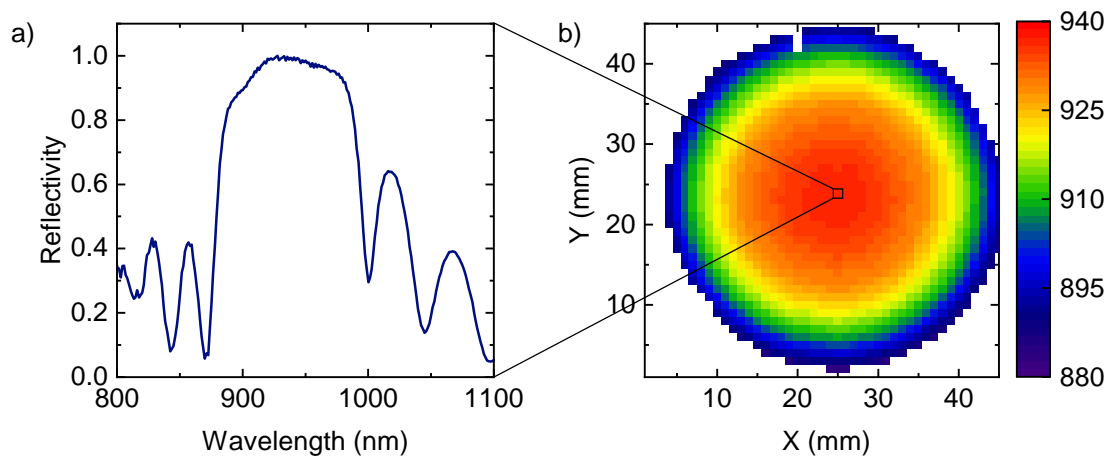
Figure 2.8 | Incorporated distributed Bragg reflector a, Reflectivity as a function of wavelength. The stop band is centered at 937 nm at $T = 10$ K. **b**, The spatial map of the DBR center wavelength of a full wafeß ws a radial dependency with increasing wavelength towards the center.

Chapter *3*

Quantum Optics Concepts Realized with QDs

Contents

3.1 Rabi Oscillations in QDs

In this chapter we provide a brief introduction of the interaction of QDs with resonant laser fields. Since the different charge configurations are discrete in energy and well separated we can reduce our considerations to a quantum mechanical two-level system, shown in Fig. 3.1a, with the ground state given e.g. by an empty QD

$$|g\rangle = \begin{pmatrix} 0 \\ 1 \end{pmatrix} \tag{3.1}$$

and the excited state represented by the neutral exciton.

$$|e\rangle = \begin{pmatrix} 1 \\ 0 \end{pmatrix} \tag{3.2}$$

The energy separation is given by $\hbar\omega_0$ and the ground state is chosen to be at zero energy. The atomic free-evolution Hamiltonian is then given by [Scu97]:

$$H_0 = \hbar\omega_0 |e\rangle\langle e| \tag{3.3}$$

The interacting laser is assumed as a classical monochromatic light field [Mol69,
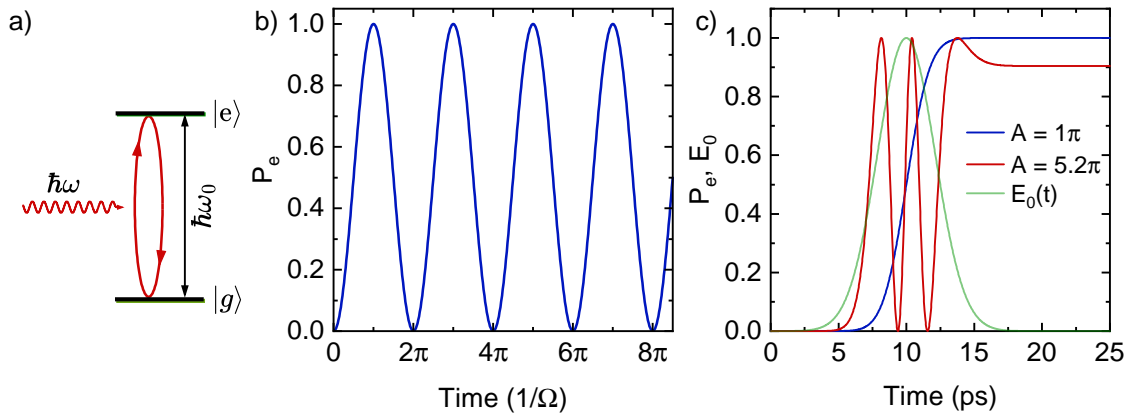
Figure 3.1 | Rabi oscillations a, Two-level system with ground state $|g\rangle$ and excited state $|e\rangle$ separated by $\hbar\omega_0$ interacting with a light field of energy $\hbar\omega$. **b**, Under resonant excitation the excited state population undergoes oscillations with period $T = 2\pi/\Omega$. **c**, Gaussian pulsed excitation (green) makes the Rabi frequency $\Omega(t)$ time dependent. A pulse with area π (blue) inverts the system's population. Exemplary pulse area of 5.2π (red) demonstates the speed up and slow down of the oscillation as the light pulse interacts with the system finally leaving it at $P_e \approx 0.9$.

Scu97, All75]. Since the wavelength is much larger than the QD, we can apply the dipole approximation and neglect the spatial dependence of the electric field [CT98].

$$\mathbf{E}(t) = \hat{\varepsilon}E_0 cos(\omega t) = \hat{\varepsilon}\frac{E_0}{2}(e^{-i\omega t} + e^{i\omega t}) \tag{3.4}$$

Here, ω is the angular frequency of the field and $\hat{\varepsilon}$ is the unit polarization vector. The Hamiltonian for the dipole interaction of electric field and the two-level system

can then be written [CT98, Mey07]:

$$H_{int} = -\mathbf{d} \cdot \mathbf{E} \tag{3.5}$$

With **d** denoting the dipole moment operator that is given by [Fox06]:

$$\mathbf{d} = \hat{r}d \cdot (|e\rangle \langle g| + |g\rangle \langle e|) \tag{3.6}$$

where d represents the dipole matrix element and $\hat{r}$ is a unit vector that defines the dipole's orientation. Considering only a linearly polarized light field aligned with the dipole in x-direction d_x allows us to rewrite the interaction Hamiltonian:

$$H_{int} = -d_x \frac{E_0}{2} \cdot (e^{-i\omega t} + e^{i\omega t})(|e\rangle \langle g| + |g\rangle \langle e|) \tag{3.7}$$

$$= -\frac{\hbar\Omega}{2} \cdot (e^{-i\omega t} + e^{i\omega t})(|e\rangle \langle g| + |g\rangle \langle e|) \tag{3.8}$$

where we have defined the Rabi frequency as [Scu97, Fox06]:

$$\Omega = \frac{d_x \cdot E_0}{\hbar} \tag{3.9}$$

The full system Hamiltonian is then the combination of the free-evolution and interaction Hamiltonian:

$$H = H_0 + H_{int} = \begin{pmatrix} \hbar\omega_0 & -\frac{\hbar\Omega}{2} \cdot (e^{-i\omega t} + e^{i\omega t}) \\ -\frac{\hbar\Omega}{2} \cdot (e^{-i\omega t} + e^{i\omega t}) & 0 \end{pmatrix} \tag{3.10}$$

To investigate now the temporal dependence of the system's states we define its wavefunction:

$$|\psi\rangle = c_g(t) |g\rangle + c_e(t) |e\rangle \tag{3.11}$$

and using the Schrödinger equation $i\hbar\partial_t |\psi\rangle = H |\psi\rangle$ with the Hamiltonian 3.10 gives us a set of coupled differential equations [Gri19]:

$$i\hbar\partial_t c_g = -\frac{\hbar\Omega}{2}(e^{-i\omega t} + e^{i\omega t})c_e \tag{3.12}$$

$$i\hbar\partial_t c_e = \hbar\omega_0 c_e - \frac{\hbar\Omega}{2}(e^{-i\omega t} + e^{i\omega t})c_g \tag{3.13}$$

This pair of coupled equations contains terms oscillating at optical frequencies. Considering only a resonant light field, these precessions become phase-locked and should vanish in the appropriate coordinate system. We therefore perform a transformation of the excited state probability into the rotating frame of the laser field with frequency ω to eliminate the rapid oscillations [Ste15].

$$\tilde{c}_e := c_e e^{i\omega t} \tag{3.14}$$

By expressing the equations of motions in terms of $\tilde{c}_e$, we obtain:

$$i\hbar\partial_t c_g = -\frac{\hbar\Omega}{2}(1 + e^{-2i\omega t})\tilde{c}_e \tag{3.15}$$

$$i\hbar\partial_t c_e = \hbar\Delta\tilde{c}_e - \frac{\hbar\Omega}{2}(e^{2i\omega t} + 1)\tilde{c}_g \tag{3.16}$$

Where $\Delta = \omega_0 - \omega$ is the detuning between the laser and the transition. In addition, for small detunings it follows that $|\Delta| \ll \omega + \omega_0$ which allows us to apply the rotating wave approximation which omits rotating terms at optical frequencies by replacing them with their zero average value and focuses on slow dynamics [All75, Ste15]. As this removes all of the explicit time dependence the remaining evolution of the system is solely given by the varying amplitude $\tilde{c}_e$.

$$\partial_t c_g = -i\frac{\Omega}{2}\tilde{c}_e \tag{3.17}$$

$$\partial_t \tilde{c}_e = i\Delta\tilde{c}_e - i\frac{\Omega}{2}c_g \tag{3.18}$$

Interestingly $|e\rangle$ remains an eigenstate of H_0, with eigenvalue $\hbar\omega_0 - \hbar\omega = -\hbar\Delta$. This means the transformation to the rotating frame effectively lowers the energy of the excited state by $\hbar\omega$ [Ste15].

To finally decouple equations (3.17) and (3.18) we differentiate and substitute them in the initial equations and obtain:

$$\partial_t^2 c_g = -\left(\frac{\Omega}{2}\right)^2 c_g \tag{3.19}$$

$$\partial_t^2 \tilde{c}_e = -\left(\frac{\Omega}{2}\right)^2 \tilde{c}_e \tag{3.20}$$

These equations represent the equation of motion of an undamped harmonic oscillator. For simplicity we will here only consider the case for exact resonant driving of the two-level system ($\Delta = 0$) and assume the system to be initially in the ground state. The solution is then given by:

$$c_g(t) = cos\left(\frac{\Omega t}{2}\right) \tag{3.21}$$

$$\tilde{c}_e(t) = -sin\left(\frac{\Omega t}{2}\right) \tag{3.22}$$

And we can find the probability of the system to be in a certain state:

$$P_g(t) = |c_g(t)|^2 = cos^2\left(\frac{\Omega t}{2}\right) \tag{3.23}$$

$$P_e(t) = |\tilde{c}_e(t)|^2 = sin^2\left(\frac{\Omega t}{2}\right) \tag{3.24}$$

Thus, the population of the system exhibits Rabi oscillations between the ground and excited state with angular frequency Ω, and therefore a period of $T = {2\pi}/{\Omega}$, when driven by a continuous and resonant laser field as depicted in Fig. 3.1b. In the experiments we typically work with pulsed excitation which introduces a time dependence to the electric field amplitude $E_0(t)$ and therefore a varying Rabi frequency $\Omega(t)$. Considering first a rectangular pulse, we can easily see that the system performs a half rotation for a pulse duration of $T/2$. Such a pulse is called π-pulse and interchanges the population of the ground and excited state. If the system is initially in the ground state it will be fully driven to the excited state. This consideration persists also for a time dependent field amplitude given that the integrated pulse area equals π [Gib73, Rod87].

$$A = \int dt \Omega(t) = \pi \tag{3.25}$$

This example is presented in Fig. 3.1c (blue) for a Gaussian pulse shape (green). For the case of $A = 5.2\pi$ (red) the oscillation becomes faster with increasing electric field and decelerates at the falling edge of the pulse. After a little more than two and half rotations the final excited state population reaches $P_e \approx 0.9$.

3.2 Resonance Fluorescence

For the investigation of single QDs and their optical response under resonant excitation we employ a confocal micro-PL setup with cross-polarized suppression of the back reflected laser beam [Kuh13a]. In addition, the QD sample needs to be held at cryogenic temperatures to freeze out phonons [Bay02a]. This is realized with a dip stick setup combined with an optical head.

The dip stick consists of a removable steel tube which can be sealed to a top plate with a cryo window for optical access. The whole microscope assembly is held by a construction of four steel rods fastened to the top end and reaches all the way down. At the bottom is a stack of three cryogenic temperature compatible nano positioners onto on which the sample is fixed. This enables precise three dimensional movement with respect to a fixed lens to navigate on the sample and adjust the focus of the incident laser beam. To reduce the thermal contact of this assembly to the environment the sealed stick is evacuated and filled with a small amount of helium gas. This ensures that the sample has proper thermal contact to the liquid helium bath in which the stick is immersed while the heat transfer from the top part is minimized. Moreover, this prevents the formation of ice from air and water on the sample and other components.

Since the setup is bound to a helium dewar the optical components need to be attached directly to it. They are organized in four different functional layers as sketched in Fig. 3.2. In the excitation layer the laser is outcoupled from a polarization maintaining fiber with an adjustable collimator. The beam alignment is done with an independent pair of mirrors. A linear polarizer mounted in a precision rotation stage enables control of the polarization of the laser and suppresses elliptical components. The beam is then reflected by a polarizing beam splitter towards the steering unit at the bottom of the optical head. Before entering the stick assembly and being focused on the sample it passes through a λ-quarter plate to correct for any elliptical component that was introduced. The back reflected laser and the QD signal are then separated by the polarizing beam splitter and an additional polarizer in the detection plane increases the rejection of remaining laser light [Kuh13a]. The QD emission is coupled into a fiber and can be guided to various setups to investigate its properties. For a proper cross-polarized suppression it is important to be able to adjust the polarization optics with < 5 mdeg accuracy. The polarization is required to be
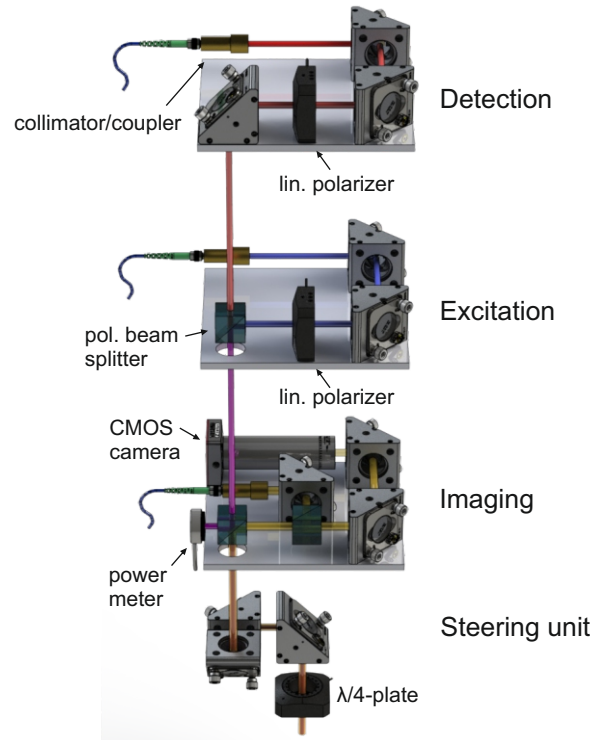
Figure 3.2 | Optical head assembly for RF The cross-polarization components, consisting of a linear polarizer in the excitation and detection layer each, the polarizing beam splitter and the $\lambda/4$-plate, in combination with spatial filtering through coupling into a single mode fiber, allow efficient rejection of the excitation laser in the detection path. The imaging plane hosts a fiber coupled LED and a CMOS camera for a Köhler illumination of the sample allowing navigation and alignment.

aligned along the s- or p-plane of each mirror to avoid the introduction of elliptical polarized components. As a consequence the steering unit is overdefined with a third mirror to bring the beam to the center of the optical head. Also a mismatch to a possible birefrigend axis of the sample needs to be avoided. However, the part of the strongly focused laser backreflected from the sample gains a component with orthogonal polarization due to internal reflection. The spatial mode of this component has a clover leaf pattern with a pronounced intensity minimum in the center and can be therefore separated by spatial filtering [Nov01]. Coupling the beam into a single mode fiber as a spatial filter is already sufficient to achieve suppression of the laser by seven orders of magnitude. This fact emphasizes the importance of proper mechanical stability of the whole assembly and the reduction of vibrations.

Finally the imaging plane integrates a fiber coupled LED for uniform illumination of the sample and a monochromatic CMOS camera to capture the sample image. This allows precise navigation and alignment of the sample in the field of view.

3.3 Pulse Shaping Techniques

Efficient pulsed excitation of a QD is usually done by few picosecond long laser pulses. One reason is that the intensity for a given pulse area scales inversely with the duration. Consequently, the required intensity for a π-pulse is lower for a longer pulse, making it easier to sufficiently suppress it in a resonant experiment. In addition, longer pulses are less affected by the dispersion experienced in fibers and acquire less chirp that can affect the excitation dynamics. On the other hand, the pulse has to be much shorter than the excited state lifetime. The impact of the pulse duration on the emission purity will be discussed in detail in Chapter 5.2 and 5.4. Such pulses are realized with a passively mode locked Ti:Sa laser emitting 150 fs long pulses, a confocal beam expander to increase the beam diameter and a $4f$ pulse shaper line [Wei88, Wei95, Wei00, Mon10]. The $4f$ line consists of an optical grating that disperses the pulse, a lens at a distance f, which also corresponds to its focal length, that focuses the single spectral components in the back focal plane or Fourier plane, an identical lens in confocal configuration to collimate the components again and another grating combining all the spectral components in a single beam. The name "$4f$" refers to the spacing of all the components. Such a setup has no dispersion and the outgoing laser pulse is identical to the initial one. However, modulation of the intensity or phase in the Fourier plane enables also modulation in the temporal domain of the pulse. In the simplest case a spectral cut-out from the fs-pulse is performed. A Gaussian intensity profile results then in a Gaussian temporal shape as the conversion is given by Fourier transformation. In our setup, as illustrated in Fig. 3.3, the Gaussian shape is approximated by an adjustable slit of rectangular shape smoothed by a Gaussian beam profile. Using a blazed diffraction grating with 1800 grooves per mm, a plano-convex lens with $f = 300\,\mathrm{mm}$ and an incoming beam diameter of $w_{dia} \cong 5\,\mathrm{mm}$ we achieve a spectral resolution of $\delta\lambda = 0.08\,\mathrm{nm}$. This translates to a maximum of $\tau \cong 15\,\mathrm{ps}$ long pulses for a center wavelength $\lambda = 915\,\mathrm{nm}$.

Furthermore the $4f$ geometry is folded by inserting a mirror in the Fourier plane,
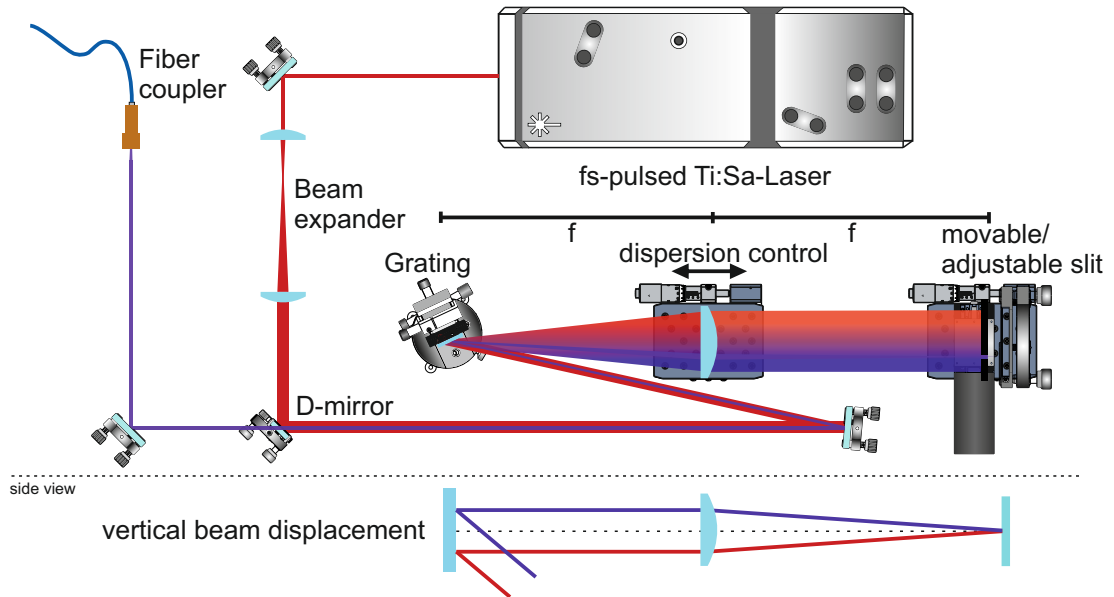
Figure 3.3 | Picosecond pulse shaper setup The initially fs-long pulse is shaped in a folded $4f$ line consisting of a grating, a lens in distance of its focal length and a folding mirror in the back focal plane. A slit close to the Fourier plane cuts out a variable spectral window of the dispersed pulse altering it also in the temporal domain. Increasing the spatial beam profile with the confocal beam expander increases the spectral resolution. The side view demonstrates how a vertical offset from the optical axis introduces a displacement between the incoming and outgoing beam.

making the setup more compact and easier to align. To separate the incoming beam from the shaped pulse without intensity loss, the beam enters the pulse shaper offset to the optical axis of the lens. The lens and the folding mirror introduce a vertical displacement in the beam path as shown in the lower part of Fig. 3.3, allowing separation of the two path by a D-shaped mirror.

3.4 Time-Resolved and Correlated Photons

In chapter 3.1 we described the interaction of a two-level system with a resonant laser field but omitted the interaction of the transition dipole with the vacuum electromagnetic field. This introduces emission of a single photon by spontaneous transition from the excited to the ground state. The excited state lifetime can be investigated by combining the aforementioned methods. A resonant laser field,

realized with a short laser π-pulse, drives the quantum system's population to the excited state while the subsequent emission is measured with a time resolving detector. Correlating the detector clicks with a trigger signal from the pulsed laser produces a temporal histogram of the decay, as presented in Fig. 3.4a. The onset and exponential decay is here broadened by the timing jitter of the detector (≈ 350 ps) which is taken into account for the analysis by the convolution with a Gaussian curve (red). We obtain an excited state lifetime of $\tau = 502$ ps which represents a typical value for Stransky-Krastanov mode grown InAs QDs [Pai00, Lan04, Dal08, Urb13]. The
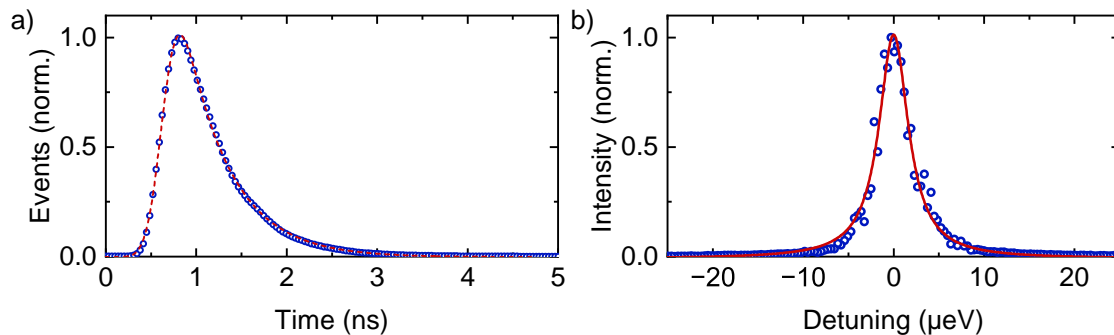
Figure 3.4 | Spontaneous emission a, Time-resolved fluorescence from an excited two-level system shows an exponential decay (blue). The theoretical fit (red), consists of a monoexponential decay convolved with a Gaussian curve to account for the detector's timing resolution. It closely matches the measured data and yields an excited state lifetime of $\tau = 502$ ps. **b**, Emission intensity as a function of the laser detuning reveals a Lorentzian line shape with $\delta\omega_{FWHM} = 3.97$ µeV.

limited lifetime of the excited state causes a broadening of its energy spectrum, in accordance with the uncertainty principle [Lan04, Mey07]. To probe the linewidth we scan a narrow continuous wave laser across the transition and monitor the emission intensity. The result is presented in Fig. 3.4b and exhibits a Lorentzian shape, characteristic of exponential decay, with $\delta\omega_{FWHM} = 3.97$ µeV. Here, inhomogeneous broadening from spin and charge noise increases the linewidth to nearly three times the expected Fourier limit [Kuh13b].

Since a two level system emits only a single photon through the spontaneous decay of its excited state it must be re-excited before it can emit another photon. This enables conversion of pulses with Poissonian photon statistics interacting with the two level system to a stream of single photons. This emission property can be investigated using an Hanbury Brown and Twiss (HBT) setup [Bro56], as illustrated

in Fig. 3.5. The beam is divided by a 50:50 beam splitter and directed to single-photon detectors. A time tagger records the detection times from both detectors, enabling the extraction of the temporal correlation between the signals. This data is
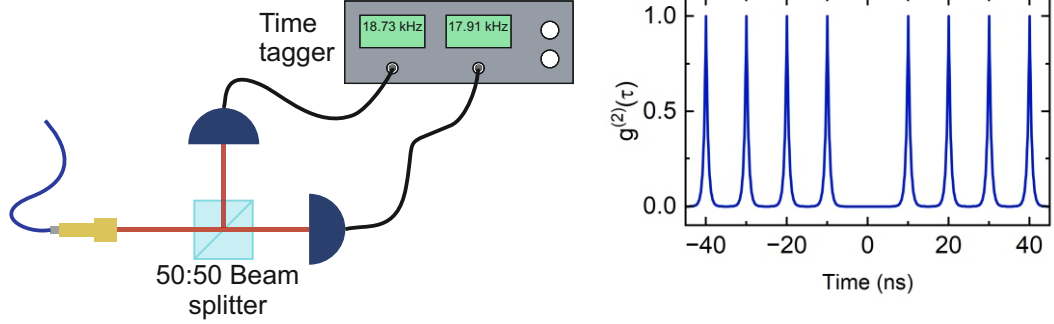
Figure 3.5 | Hanbury Brown and Twiss setup The intensity autocorrelation of a photon stream is measured using an HBT setup, which generates a temporal correlation from the outputs of a 50:50 beam splitter. For an ideal deterministic single-photon source, both detectors cannot register a photon simultaneously, resulting in the absence of a peak in the correlation histogram.

then used to calculate the second-order correlation function. Which in the classical picture is given by [Fox06]:

$$g^{(2)}(\tau) = \frac{\langle I(t)I(t+\tau)\rangle}{\langle I(t)\rangle\langle I(t+\tau)\rangle} \tag{3.26}$$

Here, $I(t)$ denotes the intensity of the light beam at time t. It can be shown that any classical light field fulfills

$$g^{(2)}(0) \geq 1 \tag{3.27}$$

To account for a stream of photons we need to substitute the intensity with the number of photons $n_i(t)$ impinging on detector i at time t.

$$g^{(2)}(\tau) = \frac{\langle n_1(t)n_2(t+\tau)\rangle}{\langle n_1(t)\rangle\langle n_2(t+\tau)\rangle} \tag{3.28}$$

The $g^{(2)}(\tau)$ function can now be understood as the probability to detect a photon at time t at detector 1 while getting a click from detector 2 at time $t + \tau$. In the case of a pulsed driven single-photon source with repetition rate $1/\tau_{rep}$ each photon has a 50% chance to be detected at either of the outputs. So when a photon generates a

click at detector 1 at time t the next photon might get detected at output 2 adding an event at time τ_{rep} to the correlation histogram. On the other hand, a single photon can only be detected at one of the beam splitter outputs which prevents simultaneous detection events and consequently [Kim76, Kim77b]:

$$g^{(2)}(0) = 0 \qquad (3.29)$$

This violates clearly the classical relation (3.27) and is a proof of the quantum nature of light. In addition, the photons in the stream are well separated in time and are often referred to as "antibunched". In contrast, the photons in a beam of coherent light, like emitted by a laser, are randomly distributed and therefore the probability to find a correlation event for time τ is equal for all times, giving $g^{(2)}(0) = 1$. For a source that emits bunched photons the chance for both detectors to click at the same time or shortly one after another is increased compared to longer time scales leading to $g^{(2)}(0) > 1$. It follows that the observable value $g^{(2)}(0)$ provides insight into the temporal order of photons in a stream. Furthermore it can be shown for a Fock state $|n\rangle$ with the photon number $n \geq 1$ that [Wal08, Grü19]:

$$g^{(2)}(0) = 1 - \frac{1}{n} \qquad (3.30)$$

Therefore, $g^{(2)}(0) \geq 0.5$ for a Fock state with $n \geq 2$. On the other hand, this implies that a single-photon component is present for $g^{(2)}(0) < 0.5$. In conclusion, measuring the second order correlation function can confirm the single-photon nature of a source and provide additional insights into the single-photon purity.

We continue to examine the indistinguishability of the emitted photons with a Hong-Ou-Mandel (HOM) type experiment [Hon87, Fea89]. Therefore, two subsequently generated photons from a single QD are interfered at a $50:50$ beam splitter. Denoting the two beam splitter input ports a and b and the output ports c and d simplifies description of the beam splitter interaction by photon-creation operators $\hat{x}^{\dagger}$. The outcome for a single photon entering the beam splitter at port a is then given by:

$$|1\rangle_a \overset{beamsplitter}{\longrightarrow} \frac{1}{2}\left(\hat{c}^{\dagger} + i\hat{d}^{\dagger}\right)|0\rangle_c|0\rangle_d = \frac{1}{\sqrt{2}}\left(|1\rangle_c|0\rangle_d + i|0\rangle_c|1\rangle_d\right) \qquad (3.31)$$

The complex phase of i is gained upon reflection while the photon in the case of

transmission is not affected. The result is determined by the photon having a 50% chance of being detected at each output. Adding a second photon impinging the beam splitter on input port b extends the description to:

$$
\begin{aligned}
|1\rangle_a |1\rangle_b &\stackrel{beamsplitter}{\longrightarrow} \frac{1}{2} \left(\hat{c}^\dagger + i\hat{d}^\dagger \right) \left(i\hat{c}^\dagger + \hat{d}^\dagger \right) |0\rangle_c |0\rangle_d \\
&= \frac{1}{2} \left(i\hat{c}^{\dagger 2} + \hat{c}^\dagger \hat{d}^\dagger - \hat{d}^\dagger \hat{c}^\dagger + i\hat{d}^{\dagger 2} \right) |0\rangle_c |0\rangle_d
\end{aligned}
\tag{3.32}
$$

If the two photons entering the beam splitter are indistinguishable the two creation operators commute $[\hat{c}^\dagger, \hat{d}^\dagger] = 0$. Taking this into account reduces the outcome to:

$$
= \frac{1}{\sqrt{2}} \left(i |2\rangle_c |0\rangle_d + |0\rangle_c |2\rangle_d \right)
\tag{3.33}
$$

This means that two indistinguishable photons have to exit the beam splitter at the same port together [San02b]. Therefore, measuring the intensity correlation function of the two outputs results in that case in an absence of coincidences at zero time delay. To realize this two-photon interference in the experiment the QD transition of interest is subsequently excited twice with a π-pulse and a fixed time delay. This transforms the two pulses into two single photons with the given delay τ which are guided to an unbalanced Mach-Zehnder interferometer, as depicted in Fig. 3.6. Such
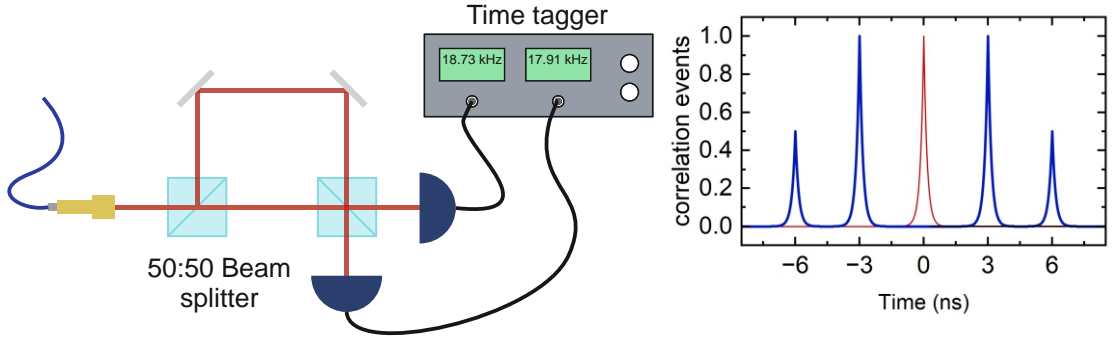
Figure 3.6 | Hong-ou-Mandel interference The unbalanced Mach Zehnder interferometer allows HOM interference between two sequentially generated photons by splitting the incoming beam and introducing a time delay τ between the two path, allowing them to interfere at the second beam splitter. Indistinguishable photons exit the beam splitter together, surpressing correlation events at zero time delay.

a setup consists of a $50:50$ beam splitter where the photons enter in one port and

the two outputs are connected to the second $50:50$ splitter. The two paths between the beam splitters have an optical length difference corresponding to the time delay of the generated photon pair. Monitoring the exit ports with single-photon detectors connected to a time tagging device allows the generation of a correlation histogram and therefore the analysis of coincidences of the two outputs for zero time delay.

With the photon pair impinging on the first beam splitter there are in principle three different scenarios which path they can take. If the first photon is traveling through the delayed arm of the interferometer while the later one takes the shorter path the distance between the two is doubled and an coincident event at 2τ is registered. Interchanging the two detectors adds a minus sign to the determined correlation time. Another possibility is that both photons follow the same path and therefore maintain the initial delay of τ. Since this can happen in either of the arms it results in peaks at $\pm\tau$ in the correlation histogram with twice the area compared to the one at $\pm2\tau$. And finally the first photon can be delayed in the longer path while the later one travels through the short arm allowing them to enter the second beam splitter at the same time. This enables interference of the two with a vanishing probability to register a coincidence event at zero time delay for indistinguishable photons [San02b]. On the other hand, two distinguishable photons have the ability to produce a click at both detectors at the same time. As a consequence this results in a correlation peak with the same area as the adjacent peaks considering that the two detectors are interchangeable. We define the HOM visibility as follows:

$$\mathrm{V_{HOM}} = 1 - \frac{2A_3}{A_2 + A_4} \tag{3.34}$$

Given a high purity of the source and splitting ratios close to 50% makes this value a direct measure of the indistinguishability of the interfered photons.

Chapter *4*

Two-Level System under Strong Continuous and Coherent Driving

Contents

4.1 The Mollow Triplet

In section 3.1 we examined the interaction between a quantum two level system and a resonant laser field to determine the evolution of the state populations, which result in Rabi oscillation. This finally provides a method to coherently invert the population of the system using a short pulse. Building on this framework, we now introduce the dressed state picture, from which the emergence of the so called Mollow triplet in RF can be understood [Mol69].

We start by recalling the equations of motion in the rotating frame (3.17) and

(3.18) and rewrite them in the matrix form [Ste15]:

$$\partial_t \begin{bmatrix} \tilde{c}_e \\ c_g \end{bmatrix} = -i \begin{bmatrix} -\Delta & \Omega/2 \\ \Omega/2 & 0 \end{bmatrix} \begin{bmatrix} \tilde{c}_e \\ c_g \end{bmatrix} \tag{4.1}$$

Following the Schrödinger equation we can extract the rotating frame Hamiltonian as

$$\tilde{H} = (\tilde{H}_0 + \tilde{H}_{int}) = \hbar \begin{bmatrix} -\Delta & \Omega/2 \\ \Omega/2 & 0 \end{bmatrix} \tag{4.2}$$

With the Hamiltonian at hand we find the new eigenstates based on the bare states of the system.

$$|\alpha\rangle = sin\theta \, |g\rangle + cos\theta \, |e\rangle \tag{4.3}$$

$$|\beta\rangle = cos\theta \, |g\rangle - sin\theta \, |e\rangle \tag{4.4}$$

With the so called Stückelberg angle θ defined by

$$tan2\theta = -\frac{\Omega}{\Delta} \quad \left(0 \leq \theta < \frac{\pi}{2}\right) \tag{4.5}$$

And finally the eigenenergy of the dressed states can be calculated.

$$E_{\alpha,\beta} = -\frac{\hbar\Delta}{2} \pm \frac{\hbar\tilde{\Omega}}{2} \tag{4.6}$$

Where we have introduced the generalized Rabi frequency $\tilde{\Omega} = \sqrt{\Omega^2 + \Delta^2}$. It becomes evident that the newly formed dressed states are split by $\hbar\tilde{\Omega}$.

However, to describe the Mollow triplet in the dressed state picture, a fully quantum mechanical treatment of the two level system interacting with the light field is required. We can qualitatively extend the semi-classical dressed state model by introducing the quantized field with n photons [Ste15]. This results in a ladder of replicated bare states in the rotating frame, with energy separation of $\hbar\omega$, corresponding to the number of field quanta. One set of degenerate states consists of the uncoupled two level system in the ground state $|g\rangle$ with n photons in the field mode, and the bare excited state $|e\rangle$ with the reduced photon number $n-1$, as shown on the left side of Fig. 4.1a. The degeneracy of those states becomes clear since the energy difference

of the bare system in the ground state and in the excited state corresponds to the energy of a single photon for a resonant field. Adding or subtracting a photon from the system moves it one step up or down the ladder, respectively. Including the interaction of the two level system and the light field, splits each set of degenerate states by $\hbar\tilde{\Omega}$ under the formation of the dressed states α and β, in analogy to the semi-classical treatment. Emission from theses dressed states reduces the photon number by 1, allowing four possible transitions between two sets, as illustrated on the right side of Fig. 4.1a. The two decays shown with purple arrows result in emission with the original resonance energy $\hbar\omega$, while the red and blue arrows represent shifted transitions by $-\hbar\tilde{\Omega}$ and $+\hbar\tilde{\Omega}$, respectively. For exact resonant excitation, the new eigenstates are an equal superposition of the bare ground and excited state, leading to an equal probability for each transition [Rud98, Gus18].
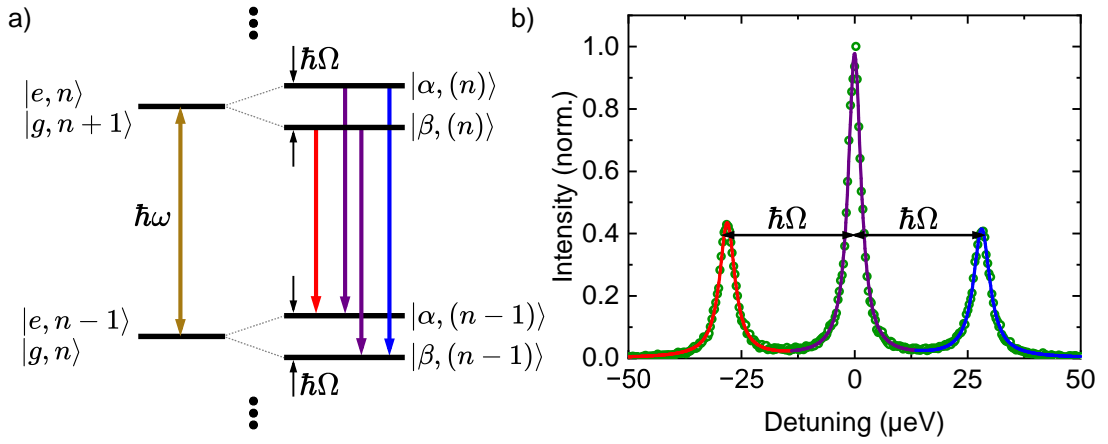
Figure 4.1 | Mollow triplet a, Combined energy level scheme of the bare two-level system $|g\rangle$, $|e\rangle$ and the field mode with n photons. Considering the coupling between laser and QD forms the dressed states $|\alpha\rangle$ and $|\beta\rangle$ split by the Rabi energy $\hbar\Omega$ **b**, RF of the negative trion transition under strong continuous driving exhibits the Mollow triplet as a result of the formation of dressed states.

We confirm this deduction experimentally by driving the negative trion transition with a resonant continuous wave laser and analyze the emission with a high resolution (300 MHz) scanning Fabry-Perot cavity. The obtained spectrum is shown in Fig. 4.1b by green points and consists of three in energy equally spaced Lorentzian peaks (solid line) [Ulh13]. The center peak is found at exactly the laser energy with twice the integrated intensity compared to each side peak. The energy shift of the side

peaks is then given by the Rabi energy $\hbar\Omega = 28.1\,\mu\text{eV}$. The cumulative fit is colored corresponding to the transitions in Fig. 4.1a.

We finally introduce the main features of the fully quantum mechanical model for completeness [Str71, CT77, CT98]. Here, the quantum system is placed in a lossless cavity with volume V and coupled to a single mode of the light field with average photon number $\langle n \rangle$ [CT98]. In analogy to the semi-classical picture the light field is described as a harmonic oscillator, however with the Hamiltonian [Scu97]:

$$H_L = \hbar\omega \left(a^\dagger a + \frac{1}{2} \right) \tag{4.7}$$

Where a is the annihilation operator and $a^\dagger$ the creation operator, removing or adding a photon to the field, respectively. While the two level system is still described by the Hamiltonian H_0 given in equation (3.3) we need to include the interaction to complete the picture. The quantized interaction Hamiltonian considering the rotating wave approximation can be found to be [Mey07]:

$$H_{q,int} = \hbar g(\sigma a^\dagger + \sigma^\dagger a) \tag{4.8}$$

Here g denotes the cavity QED coupling constant [Ste15]

$$g = d_x \sqrt{\frac{\omega}{2\epsilon_0 \hbar V}} \tag{4.9}$$

with the vacuum permittivity ϵ_0, while σ and $\sigma^\dagger$ represent the lowering and raising operator of two level system, respectively. The interaction can be understood such that either a photon is removed from the field mode exciting the system or the two-level system is lowered to the ground state returning a photon to the cavity. Since we focus on the interaction with a strong laser field we can apply the assumption that $\langle n \rangle$ and V tend to infinity while maintaining their ratio. In addition, this ratio is proportional to the amplitude of the electric field of the laser [Gri19].

$$E_0 = 2\sqrt{\frac{\hbar\omega\langle n \rangle}{2\epsilon_0 V}} \tag{4.10}$$

And draws a connection to the coupling constant g,

$$\frac{d_x \cdot E_0}{\hbar} = \Omega = 2g \langle n \rangle \tag{4.11}$$

which is also referred to as the one-photon Rabi energy. With this at hand, we can write the full Hamiltonian:

$$H_{quantum} = \hbar\omega \, |e\rangle \, \langle e| + \hbar g(\sigma a^\dagger + \sigma^\dagger a) + \hbar\omega \left(a^\dagger a + \frac{1}{2} \right) \tag{4.12}$$

And find the dressed states for exact resonant excitation.

$$|\alpha, (n)\rangle = \frac{1}{\sqrt{2}}(|g,n+1\rangle + |e,n\rangle) \tag{4.13}$$

$$|\beta, (n)\rangle = \frac{1}{\sqrt{2}}(|g,n+1\rangle - |e,n\rangle) \tag{4.14}$$

with the eigenenergies

$$E_{\alpha/\beta,n} = \hbar\omega \left(n + \frac{1}{2} \right) \pm \hbar g\sqrt{n+1} \tag{4.15}$$

Recalling the valid assumption that $n \gg 1$ for an intense laser field ensures equal splitting of adjacent pairs of dressed states equal, thus justifying the level scheme introduced in Fig. 4.1a [Scu97, CT98].

4.2 Power and Detuning Dependence

Next we perform a measurement series of high-resolution spectra while increasing the excitation laser power. The transition of the bare system is carefully tuned into resonance with the laser by first adjusting the laser wavelength precisely to the measured emission wavelength and finally fine tuning the transition via the QCSE. The resonance is determined by finding the maximum emission intensity while tuning the transition energy. To obtain an accurate result, the laser is attenuated far below the saturation regime. With the laser and transition in perfect resonance, the laser power is then increased in quadratic steps from 1 nW to 2.21 µW. We are also interested in the properties of the center peak, which overlaps with a weak but significant residual laser signal. This residual signal arises from imperfect suppression

by the RF setup. To address this, we acquire a second spectrum for each power step with the QD tuned far off resonance using the QCSE. Those spectra, obtained under otherwise exactly identical conditions, contain only the unsurpressed laser component. We then subtracted them from each resonant spectrum to isolate the desired signal. For the lowest driving power applied, the spectrum exhibits only a single peak, as can be seen as yellow line in Fig. 4.2a. At already $P_{exc} = 9\,\text{nW}$ we observe shoulders emerging from the single line which further split off with increasing driving strength and are well separated for $P_{exc} = 49\,\text{nW}$. Further increasing the laser power increases the Rabi energy and therefore the separation of the triplet. The spectra are offset in vertical direction for better visual presentation. Fitting
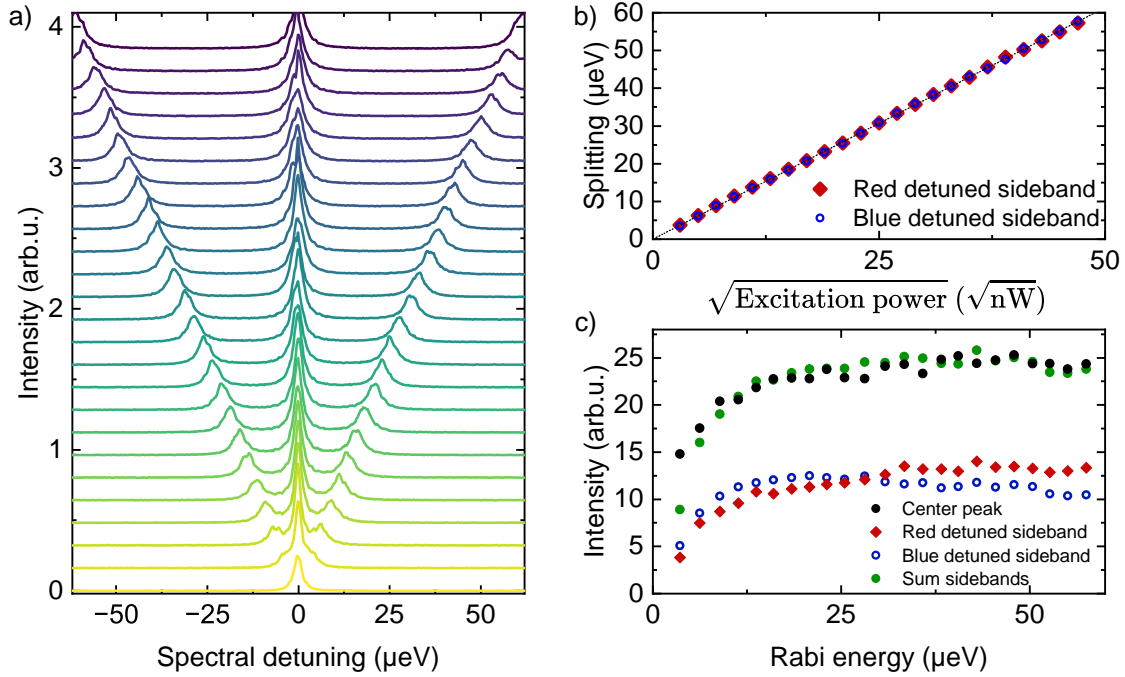
Figure 4.2 | Power dependent Mollow triplet a, High resolution spectra of the resonantly driven negative trion transition for increasing laser power from $1\,\text{nW}$ to $2.21\,\mu\text{W}$ in quadratic increasing steps. As the laser power increases, the Mollow triplet evolves from a single emission line to a maximally measurable splitting of $60\,\mu\text{eV}$. **b**, The extracted energy splitting of Mollow sidebands exhibits a symmetric and linear increase as a function of the square root of the excitation power. **c**, The integrated intensity of the three emission peaks saturates quickly for a Rabi energy of $\sim 12\,\mu\text{eV}$, while the sidebands maintain approximately half of the intensity compared to the center transition. This becomes even clearer when comparing the sum of the side peaks (green) with the center peak (black).

each spectrum with three Lorentzian curves enables a more precise quantitative analysis. The extracted center energy of each peak provides the splitting between the side peaks and the center peak, which is plotted in dependence of the square root of the excitation power in Fig. 4.2b. Both side peaks are perfectly symmetrically shifted with a linear dependence as the driving increases. The linear fit (dashed line) shows excellent agreement for all data points and tends to zero for vanishing laser power. As given by equation (4.6) and (4.15) the splitting of the sidebands corresponds to the Rabi energy $\hbar\Omega$ which is direct proportional to the electric field E_0 and therefore as well to the square root of the laser power $\sqrt{P_{exc}}$. The integrated intensity, shown in Fig. 4.2c, first increases for all emission lines until they saturate at a Rabi energy of $\sim 12\,\mathrm{\mu eV}$. The side peaks exhibit a similar spectral weight and about half of the center transition, as expected from the introduced picture with for equally probable transitions where two coincide in energy and contribute to the center peak. Comparing the sum of the side peaks $I_{red} + I_{blue}$ (green) with the integrated intensity of the center peak I_{center} (black) confirms the doubled transition probability for the center emission.

$$\frac{I_{center}}{I_{red} + I_{blue}} = 0.987 \pm 0.032 \tag{4.16}$$

The small deviations from perfectly balanced transitions can originate from energy drifts of the laser or the two-level system over time or a detuning introduced by heating through the laser itself. Thus, we continue with the investigation of the impact of detuning on the RF in the strong driving regime. For this measurement the laser power is kept constant to a Rabi energy of $\hbar\Omega = 21\,\mathrm{\mu eV}$ while the laser energy is varied corresponding to a detuning to the bare transition from $-42\,\mathrm{\mu eV}$ to $45\,\mathrm{\mu eV}$. The resulting spectra centered at the laser energy are shown in Fig. 4.3a as a color plot. Detuning the laser results in a symmetrically increasing splitting of the Mollow triplet. The center of the side peaks are marked by red and blue points. Recalling the eigenenergies of the dressed states from equation (4.6) shows that the splitting follows the effective Rabi energy $\tilde{\Omega} = \sqrt{\Omega^2 + \Delta^2}$ (solid lines) in excellent agreement with our measurements. Moreover, the center transition is offset by $\hbar\Delta$ fixing the resulting Mollow triplet to the laser energy instead on the uncoupled QD transition. Regarding the emission intensity, we observe a symmetry breakdown in the Mollow triplet where the red shifted side band weakens significantly to the point where it
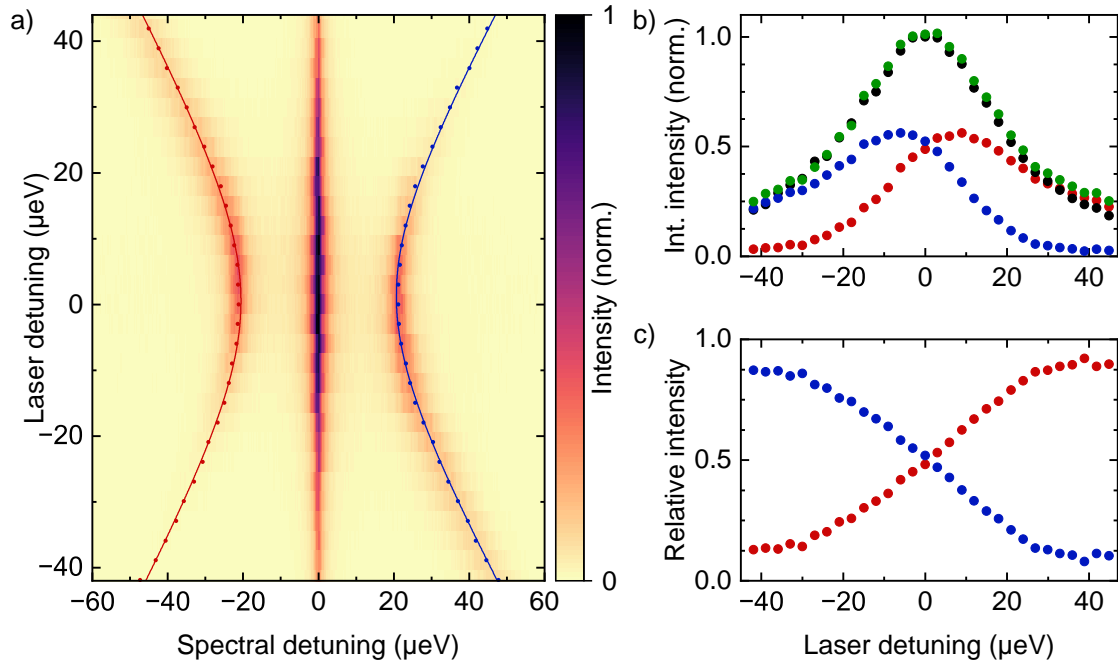
Figure 4.3 | Detuning dependent Mollow triplet a, Emission spectra of a detuning series. Each spectrum is centered on the corresponding laser energy. With increasing detuning the effective Rabi energy and therefore the side band splitting increases. The fitted side band energies (points) follow the effective Rabi energy $\hbar\tilde{\Omega}$ (solid lines) **b**, The integrated intensity of each transition decreases as the laser is detuned. The center peak (black) exhibits a symmetric behaviour while the red shifted side band (red) nearly vanishes for negative detunings and vice versa for the blue shifted side peak (blue). The equal balance of the sum of the sidebands (green) and the center peak remains constant. **c**, Relative intensity of the side peaks switches from blue to red as the laser is tuned towards positive detuning.

nearly vanishes as the laser is negatively detuned $\Delta < 0$. An identical behaviour is observed for the blue detuned side peak for positive detuning. The integrated intensity of all peaks, presented in Fig. 4.3b, provides a quantitative basis to examine the dependence on detuned excitation in detail. For the resonant case the system behaves exactly as described before, with balanced side peaks and combined spectral weight (green) equal to the center transition (black). Increasing the laser energy reduces the emission of the center and blue peak, while the red shifted emission first remains unaffected before it also loses intensity as the laser is further detuned. The situation is inverted for the red and blue side band as the laser is tuned to lower

energy, while the main transition exhibits a symmetric behaviour. Interestingly, the equilibrium of the sum of the side bands and the center peak perpetuates for all detunings.

The impact of detuning on the emission spectrum originates from the admixture of the dressed states and their transition rates. In the resonant case the formed dressed states are composed in equal parts of the ground and excited state of the bare system. This results in equal population of the dressed states as well as identical transition probabilities. Detuning the laser, e.g. to lower energy $\Delta < 0$, transforms $|\alpha\rangle$ to have a larger contribution of the excited state $|e\rangle$, while $|\beta\rangle$ gains contribution of the ground state. Due to the detuned light field the population of the excited state is reduced and consequently the population of the state $|\alpha\rangle$ as well. On the other hand, the increased excited state character increases the transition probability. Considering that the observed emission intensity is proportional to the product of the population and the transition rate, the asymmetry introduced by the detuned field is effectively compensated [Ulh12, Gus18]. This holds only true in the absence of pure dephasing, which destroys the coherence of the driving between the states of the two-level system and induces non-radiative transitions within rungs of the dressed states ladder [Ulh13, Gus18]. For our example of negative detuning $\Delta < 0$ the population of α increases, disturbing the balance of the side bands in favour for a stronger emission of the blue shifted line. For positive detunings the situation is inverse, so that transitions from the $|\beta\rangle$ state gain intensity. Since the center transition of the Mollow triplet arises from the two decay paths $|\alpha\rangle \rightarrow |\alpha\rangle$ and $|\beta\rangle \rightarrow |\beta\rangle$, any population asymmetry is canceled out. Directly comparing the relative intensities of the side bands $I_{red/blue}/(I_{red} + I_{blue})$, shown in Fig. 4.3c, illustrates the shift of spectral weight induced by the detuned light field in perfect agreement with our model.

Chapter 5

Generation of Single-Photon and Multi-Photon States from Single QDs

Contents

The results of this chapter are published in [Han20, Fis18a, Fis17, Han18]. The theoretical model and calculations for section 5.1 were provided by Juan Camilo López Carreño, Eduardo Zubizarreta Casalengua, Elena del Valle and Fabrice P. Laussy. The numerical simulations for section 5.2, 5.3 and 5.4 were performed with the Quantum Optics Toolbox in Python (QuTiP) [Joh13] by Kevin A. Fischer, who also provided the theoretical model together with contributions from Daniil Lukin, Shuo Sun and Rahul Trivedi.

5.1 Antibunching in Resonance Fluorescence

Already in one of the earliest experiments demonstrating the quantum nature of light RF was employed [Kim77a]. And it remains often the excitation method of choice to realize efficient single-photon sources [Som16, Din16a, Sni18, Upp20]. In particular, it offers the advantage for semiconductor QDs to directly excite the desired state rather than generating charge carriers in higher excited states or in the surrounding region which get trapped in the quantum well before they recombine under emission of a single photon [Mic00b]. The unstable electrical environment caused by this quasi or off-resonant excitation, among other factors, is a drawback that results in spectral wandering of the photon emission [Che16]. However, with the improvements of optical elements that permit efficient polarization filtering, RF has become possible with QDs facilitating fundamental studies of the properties of the emitted photons [Kuh13a]. A typical emission spectrum of a single QD under resonant continuous excitation of the trion transition is shown in Fig. 5.1a with just one distinct line being observable. On closer examination using a logarithmic scale, two Lorentzian components of the QD emission become evident. (Fig. 5.1b) [Kon12]. The blue fit exhibits a linewidth of (28 ± 6) MHz and is predominantly limited by the resolution of the scanning Fabry-Perot interferometer. This distinct characteristic results from the laser being coherently scattered by the two-level system [Hei54]. It thus inherits the laser's narrow sub-natural linewidth and coherence [Ngu11, Mat12, Mat13]. On the other hand, the green curve represents the incoherently scattered component. This emission occurs when a QD absorbs laser light, creating an exciton, which subsequently recombines and emits a single photon. Thus, the linewidth is limited by the lifetime of the trapped charge carriers. From the presented data we extract a FWHM of (890 ± 60) MHz. The proportion of the two components strongly depends on the driving strength of the applied laser field. It can be deduced that the annihilation operator of the two-level system σ can be expressed as the sum of the coherent term $\langle\sigma\rangle$ and the quantum, or incoherent, term $\varsigma \equiv \sigma - \langle\sigma\rangle$.

$$\sigma = \langle\sigma\rangle + \varsigma \tag{5.1}$$

Here ς represents an operator. This allows the calculation of the respective intensities of the components as a function of the driving Ω and emission rate γ_σ

and are found to be [Mey07]:

$$|\langle\sigma\rangle|^2 = \frac{4\gamma_\sigma^2\Omega^2}{(\gamma_\sigma^2 + 8\Omega^2)^2} \quad \text{and} \quad \langle\varsigma^\dagger\varsigma\rangle = \frac{32\Omega^4}{(\gamma_\sigma^2 + 8\Omega^2)^2} \tag{5.2}$$

The calculated components as a function of the driving strength are presented in Fig. 5.1c. The blue line represents the coherent component while the green line depicts the incoherent part. For weak driving, Rayleigh scattering of the incident laser light prevails while it is negligible in the strong driving regime where the incoherent emission dominates. The dashed line indicates the driving used in the experiment and was extracted from the ratios of the two components by the Lorentzian fit. From both components one can calculate the total emission intensity by:

$$n_\sigma \equiv \langle\sigma^\dagger\sigma\rangle \tag{5.3}$$

which gives us

$$n_\sigma = |\langle\sigma\rangle|^2 + \langle\varsigma^\dagger\varsigma\rangle + 2\text{Re}(\langle\sigma\rangle^*\langle\varsigma\rangle) \tag{5.4}$$

indicating interference between the two fields with the last term. However, this is not the case since $\langle\varsigma\rangle = 0$ by definition as ς has no mean field.
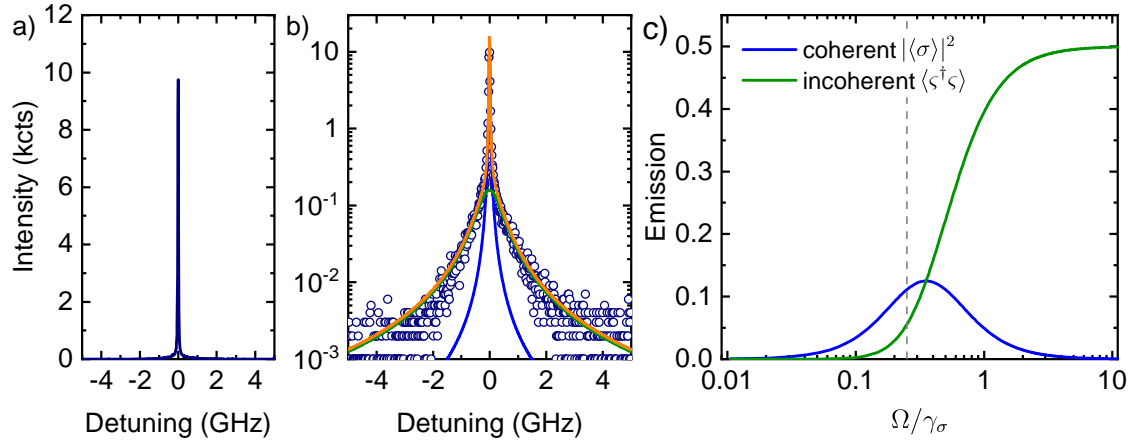
Figure 5.1 | RF of a two-level system a, Emission spectrum of the trion decay of a continuous weakly excited QD. **b**, High-resolution spectrum of the RF. The cumulative Lorentz fit reveals the coherently and incoherently scattered components. **c**, Calculated contribution of the incoherent and coherent scattering to the total emission.

On the contrary, for higher-order photon correlations the coherent component,

which inherits the laser photon statistics, and the incoherent emission feature interferences. To quantify this interference at the two-photon level we introduce the coefficients $\mathcal{I}_k$ to calculate the degree of second-order coherence $g^{(2)}(0)$ [Man82, Car85, Vog91].

$$g^{(2)}(0) = 1 + \mathcal{I}_0 + \mathcal{I}_1 + \mathcal{I}_2 \tag{5.5}$$

where:

$$\mathcal{I}_0 = \frac{\langle \varsigma^{\dagger 2} \varsigma^2 \rangle - \langle \varsigma^\dagger \varsigma \rangle^2}{\langle \sigma^\dagger \sigma \rangle^2}, \tag{5.6a}$$

$$\mathcal{I}_1 = 4 \frac{\Re[\langle \sigma \rangle^* \langle \varsigma^\dagger \varsigma^2 \rangle]}{\langle \sigma^\dagger \sigma \rangle^2}, \tag{5.6b}$$

$$\mathcal{I}_2 = \frac{\langle :X_{\varsigma,\phi}^2: \rangle - \langle X_{\varsigma,\phi} \rangle^2}{\langle \sigma^\dagger \sigma \rangle^2}, \tag{5.6c}$$

with $X_{\varsigma,\phi} \equiv (e^{i\phi}\varsigma^\dagger + e^{-i\phi}\varsigma)/2$ being the ς-field quadrature and the phase locked to $\phi = \pi/2$ in RF. Here, $\mathcal{I}_0$ characterizes the sub-Poissonian character of the quantum fluctuations for values < 0 or the super-Poissonian behavior for positive values. $\mathcal{I}_1$ describes its so called anomalous moments [Man82, Vog91] and $\mathcal{I}_2$ describes its squeezing when negative [Wal81, Lou84]. The contributions of these coefficients to anti-bunching as a function of the drive in relation to the decay rate are presented in Fig. 5.2a. The anti-bunching is maintained over the whole depicted range where $\mathcal{I}_0$ exhibits a transition from 1 to -1, by $\mathcal{I}_2$ holding the balance by transitioning from -2 in the Rayleigh regime to 0 for strong driving. It follows that in the strong driving regime, where the emission is completely dominated by the quantum fluctuation ($\sigma \approx \varsigma$) and the system is found in a statistical mixture of the ground and excited state $\rho = \frac{1}{2}(|0\rangle \langle 0| + |1\rangle \langle 1|)$, anti-bunching results only from the character of a sub-Poissonian emitter with $\mathcal{I}_0 = -1$ reaching its minimum. On the other hand, in the Rayleigh regime the quantum fluctuations are squeezed ($\mathcal{I}_2 = -2$) and interfere with the coherent component $\langle \sigma \rangle$. Surprisingly, the incoherent component exhibits super-Poissonian statistics but by interfering with the coherence of the mean field this leads to anti-bunching of the overall emission [ZC20]. This contribution is given by $\mathcal{I}_2$ in the weakly driven case while in the intermediate drive regime, where the

quantum state obtains a skewed squeezing, the anomalous correlation term $\mathcal{I}_1$ takes over.

Considering that the interplay of the coherent and incoherent component is crucial to achieve anti-bunching in the two-level system emission for weak driving disproves the claim of emission of single photons with simultaneous sub-natural linewidth [Höf97, Ngu11, Mat12]. Consequently, any spectrally sharp absorption or detection process disregards the super-Poissonian quantum fluctuations and therefore destroys the balance of the two-photon interference terms leading to a loss of anti-bunching.

For a weak driving strength the theory allows to determine the interference coefficients as a function of the filtering Γ [Zub20]:

$$\mathcal{I}_0 = \frac{\Gamma^2}{(\Gamma + \gamma_\sigma)^2} \qquad \mathcal{I}_1 = 0 \qquad \mathcal{I}_2 = -\frac{2\Gamma}{\Gamma + \gamma_\sigma} \tag{5.7}$$

This simplifies the degree of second-order coherence to:

$$g^{(2)}(0) = \left(\frac{\gamma_\sigma}{\Gamma + \gamma_\sigma} \right)^2 \tag{5.8}$$

It can be seen, that the process of filtering has a stronger impact on the statistics of ς rather than on the squeezing of its quadratures.

To experimentally investigate this we drive the trion transition of a single QD resonantly with a weak continuous wave laser and measure the second-order correlation function of the emitted photons. In addition, the emission is spectrally filtered prior to the HBT-setup to artificially disturb the ratio of the coherent and incoherent components. For experimental feasibility the driving strength was chosen to be in the intermediate regime. The obtained auto-correlation functions are presented in Fig. 5.2b and offset in vertical direction by values of one for clarity. Using a broad filter, compared to the linewidth of the incoherent emission, with $\Gamma = (19.0 \pm 0.5)\,\text{GHz}$ does not affect the composition of the quantum light and thus clean anti-bunching with $g^{(2)}(0) = 0.022 \pm 0.011$ is observed (red circles). Decreasing the filter width leaves the coherent component unaffected but reduces the intensity of the photons emitted by spontaneous decay. The unbalanced two-photon interference results then in an increased degree of second-order coherence and ultimately a Poissonian distribution of the remaining quantum light (purple circles).

Using an exact theory of time- and frequency-resolved photon correlations provides a

Parameter	γ_σ	Ω	Γ_1	Γ_2	Γ_3	Γ_4	Γ_5
Fitting (MHz)	900	225	11403	1324	709	535	28
Data (MHz)	890	198	19000	1550	780	390	28
(Error)	(60)	(7)	(500)	(320)	(160)	(80)	(6)

Table 5.1 | Summary of the parameters used to measure and theoretically reproduce the second-order coherence function of the filtered emission.

quantitative approach to validate the experimental results [Del12]. Excellent agreement is achieved (Fig. 5.2b solid lines) by a global fitting routine with the filter width Γ and driving strength Ω as free parameters and a fixed decay rate $\gamma_\sigma = 900\,\mathrm{MHz}$ of the two-level system. All parameters used in the experiment and extracted from the theory are listed in table 5.1.

As given by Eqn. (5.8) we can study the two-photon coincidence correlation function in dependence of the filter width as shown in Fig. 5.2c as a dashed red line. Since the experiment was conducted in the intermediate driving regime $\mathcal{I}_1$ becomes non negligible. Taking this into account gives us for the normalized zero-delay coincidences:

$$
g^{(2)}(\tau = 0) = \frac{\left(48\Gamma^2\Omega^4 F_{21} + 4\Gamma\Omega^2 F_{31}\left(17\Gamma^3 + 29\Gamma^2\gamma_\sigma + 18\Gamma\gamma_\sigma^2 + 4\gamma_\sigma^3\right) + F_{11}F_{21}^2 F_{31}^2 F_{12}F_{32}\right)}{F_{21}F_{31}\left(F_{11}F_{21} + 4\Omega^2\right)\left(F_{31}F_{32} + 8\Omega^2\right)\left(F_{12}F_{11}^2 + 4\Gamma\Omega^2\right)^2} \cdot
$$
$$
\cdot F_{11}\left(\gamma_\sigma^2 + 4\Omega^2\right)\left(F_{11}F_{12} + 8\Omega^2\right)
$$

$$(5.9)$$

Where $F_{kl} \equiv k\Gamma + l\gamma_\sigma$. This analytical expression is plotted for the parameters used in the experiment in Fig. 5.2c as a solid blue line and yields perfect quantitative agreement with the experimentally determined $g^{(2)}(0)$-values (blue circles).

In conclusion, the experimental demonstration of the loss of antibunching of the filtered RF in the Rayleigh regime confirms the theoretical description of its origin as the interference of coherently and incoherently scattered light. This contradicts the idea of exploiting the coherent scattering as a source of sub-natural linewidth single photons. However, based on this insight the restoration of antibunching in the presence of spectral filtering can be achieved by introducing an external coherent field. Such a homodyne setup would reduce the excess of coherently scattered light and balances out the two components again [LC18].

Considering that applications based on single photons usually require those photons
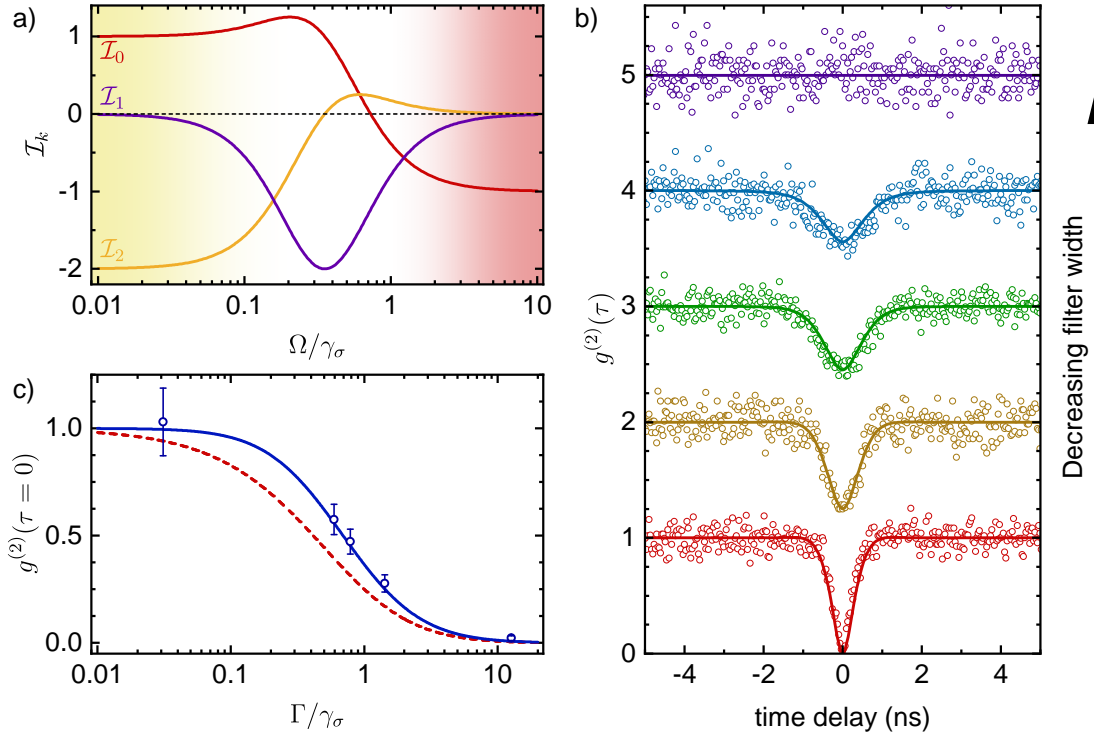
Figure 5.2 | Impact of spectral filtering on RF a, Two-photon interference terms of the emission as a function of the driving strength **b**, Second-order correlation functions of the RF in the weak driving regime for decreasing spectral filter width **c**, Second-order coherence of the RF in the Rayleigh regime in dependence of the filter width. Narrow filtering leads to loss of antibunching.

to be deterministically generated favors pulsed excitation in the strong driving regime. In this case the coherent component becomes negligible and the antibunching originates purely from the sub-Poissonian character of the incoherent emission. In the following section we investigate the intrinsic limitation of single-photon purity under pulsed resonant excitation of a quantum two-level system.

5.2 The Area Theorem and its Breakdown

The simple quantum two-level system is the perfect candidate to realize a deterministic single-photon source. Once prepared in the excited state it decays under emission of a single photon back to the ground state. An additional excitation is intrinsically impossible which inhibits multi-photon events leading to a pure single-photon source.

However, when realizing this in the laboratory the photon purity is usually found to deviate from the idealistic picture. Common reasons are for example back scattered excitation laser, broad background emission or emission from energetically close transitions which mixes with the stream of the desired single photons [Fox24]. In recent years experimental methods significantly improved, but a perfectly pure single-photon source is still elusive. In addition, a second emission event occurring shortly after the first photon was emitted triggered by a single excitation cycle affects the purity of the source as it is defined by the number of emitted photons per excitation [Fis18a].

An efficient way to excite a two-level system is to apply a resonant short laser pulse on the ground to excited state transition $|0\rangle \rightarrow |1\rangle$. The pulse can be characterized by its pulse area [Sti01, Fox06, Fis18a]:

$$A(t) = \int_0^t dt' \frac{\mu \cdot E(t')}{\hbar} \tag{5.10}$$

where μ is the system's dipole moment and $E(t')$ is the envelope of the electric field. The pulse coherently drives the population between the two states, the so called Rabi oscillations. Assuming the system initially in the ground state gives us the state after the pulse interaction as:

$$|\psi_f(A)\rangle = \sqrt{1 - P_e(A(t))} \, |0\rangle + e^{-i\phi} \sqrt{P_e(A(t))} \, |e\rangle \tag{5.11}$$

where ϕ is a phase given by the electric field and $P_e(A(t))$ describes the probability to find the system in the excited state. This probability is found to be sinusoidal with the interacted pulse area:

$$P_e(A(t)) = \sin^2\left(A(t)/2\right) \tag{5.12}$$

Therefore a pulse with area $A = \pi$ is capable to invert the population of the system while interaction with a pulse area $A = 2\pi$ leads to a full rotation, so the system is finally found again in its initial state. Description of the systems final excited state population as a function of the interacted pulse area of a resonant laser pulse is known as the area theorem [All75, Rod87].

However the system is also interacting with the outside world allowing spontaneous decay. Such a decay interrupts the sinusoidal behavior of the driven two-level

system and instantaneously resets its population to the ground state [Lew86, Dad16, Fis17]. To take this into account the system's state evolution can be expressed by the stochastic Schrödinger equation which describes the Rabi oscillations and the spontaneous emission [Car93]. Such a quantum trajectory is shown in Fig. 5.3a for two exemplary trajectories of π-pulse excitation. The blue curve shows the ideal case where the system is found with unity probability in the excited state after full absorption of the laser pulse. In the other case (green line) a spontaneous decay happens after interaction with half the laser pulse under emission of a single photon, resetting the system to the ground state and restarting the Rabi oscillation. Following such a trajectory can result in the emission of a second photon after the system-pulse interaction. To ascertain the emitted photon number probabilities of such a two-level system interacting with a laser pulse with given duration we calculate multiple random trajectories. On the other hand, the trajectory formalism also allows finding direct analytical expression of the probability densities [Fis18a]. The probability for a single-photon emission after interaction with a pulse with area of π is then given by:

$$P_1(A = \pi) \approx e^{-\gamma T/2} \left(1 + \frac{3\gamma T}{8}\right) \tag{5.13}$$

with T describing the pulse duration and γ being the decay rate of the excited state. While the probability for two-photon emission events reads:

$$P_2(A = \pi) \approx e^{-\gamma T/2} \left(\frac{\gamma T}{8} + (\gamma T)^2 \left(\frac{3}{4\pi^2} - \frac{5}{64}\right)\right) \tag{5.14}$$

The calculated one- and two-photon emission probabilities as a function of the pulse duration are presented in Fig. 5.3b. Increasing the pulse duration increases the probability for an emission event during the presence of the laser pulse and therefore leads to a more likely two-photon emission. For short pulses, compared to the excited state lifetime, the probability to emit a single photon is near unity while the two-photon events gain importance as the pulse becomes longer. Importantly, the simplified analytical model (solid lines) agrees well with the numerical exact simulations (dashed lines) for pulses up to the duration of the lifetime of the excited state.

The calculated photon number probabilities allow us to determine the degree
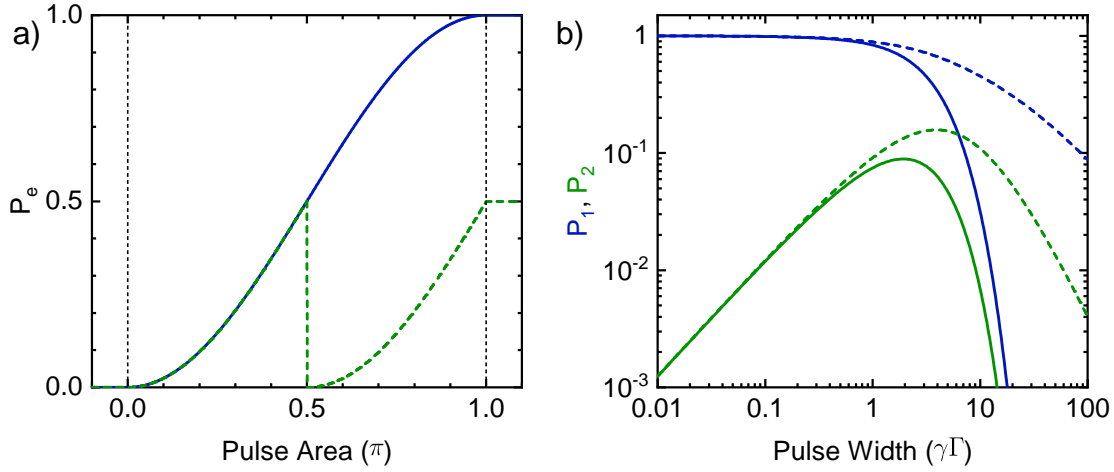
Figure 5.3 | Re-excitation dynamics of a two-level system during resonant π-pulse excitation a, Two possible quantum trajectories of the system with no spontaneous emission during the pulse-system interaction (blue line) and emission after absorption of half the excitation pulse (green dashed). **b**, Probability of one photon P_1 (blue) and two photon emission P_2 (green). The solid lines are calculated with the simplified analytical model, dashed lines represent numerical exact simulations.

of second-order coherence of the emitted photons which is also experimentally accessible [Fis16].

$$g^{(2)}[0] = \frac{\sum_k k(k-1)P_k}{(E[n])^2} \tag{5.15}$$

with

$$E[n] = \sum_k kP_k \tag{5.16}$$

which denotes the expected photon number. For the excitation of the system with a short laser pulse where the analytical model is applicable the ratio of events with three or more photons is negligible small which reduces Eqn. (5.15) to:

$$g^{(2)}[0] \approx \frac{2P_2}{(P_1 + 2P_2)^2} \tag{5.17}$$

This approximated calculated degree of second-order coherence is shown in Fig. 5.4a in red. The exact numerically simulated curve is shown in blue indicating strong antibunching for short pulses and approaching Poissonian statistics for very long

ones. The analytical model allows accurate predictions up to a pulse length of the order of excited state lifetime $\gamma T \approx 1$.

To experimentally access the degree of second order coherence of the photons emitted from a two-level system, the negative trion of a single QD is resonantly excited and the emission is analyzed with an HBT Setup, as introduced in section 3.4. The result is presented in Fig. 5.4b and exhibits qualitative agreement with the theoretical curve. The offset of the experimental data with respect to the simulated curve can be attributed to the temporal pulse shape. While in the experiment a Gaussian-like pulse is used the calculations were performed for simplicity with a temporal rectangular pulse. In addition, for very short pulses the cross-polarized suppression of the excitation laser in the detection path is imperfect since shorter pulses require a higher intensity to reach an area of π.
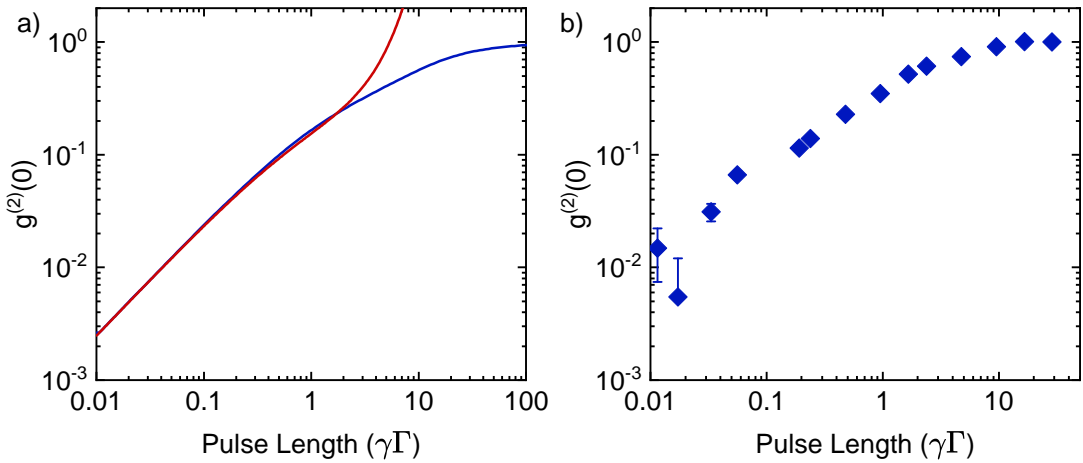
Figure 5.4 | Degree of second-order coherence of the photon emission of a two-level system under resonant π-pulse excitation a, Theoretical calculation of the $g^2(0)$ value as a function of the applied pulse duration. The analytical model (red line) is in good agreement with the numerical calculation (blue line) for short pulses. **b**, Experimental data measured on the negative trion transition of a single QD.

In summary, we have introduced the area theorem which describes the final excited state population purely as a function of the pulse area. This translates ideally to the probability of the system to emit a single photon. However, spontaneous decay during the pulse interaction interrupts and resets the Rabi oscillation inducing the possibility of a second photon emission. Taking this process into account allowed the

study of single-photon purity as a function of the excitation pulse duration, where shorter pulses are beneficial to achieve high purity. In the following section we extend this analysis to the dependence of the pulse area.

5.3 Signatures of Two-Photon Pulses

The ideal quantum two-level system follows Rabi oscillations under a resonant and coherent drive. As described in sections 3.1 and 5.2 above this can be realized for example with a short laser pulse where the probability to find the system in the excited state P_e can be calculated as a function of the pulse area. This is shown in Fig. 5.5a as a green dashed line. The system follows a sinusoidal behavior where it can be found in the excited state for odd π-pulse areas and is again driven down to its ground state for even π pulse areas [Sti01, Zre02, Ram10a]. If spontaneous emission and re-excitation events during the pulse-system interaction are considered the probability to find the system in the excited state P_e does not describe the system very well any more since the dynamics are not captured. Therefore, the expected number of photons emitted by the system during and after the pulse interaction is a better description and is shown in Fig. 5.5a in blue. The pulse duration for the simulations was chosen to be $\tau_{FWHM} = \tau_e/10$ for the remainder of this section. The expected photon number follows mainly the same oscillation. However, a small deviation can already be seen for a pulse area of 1π with a mean photon number exceeding one while the difference is largest for even π pulse areas. We observe a similar behavior in the experiment when we drive the negative trion transition resonant with an $80\,\mathrm{ps}$ ($\sim 0.13\tau_e$) long pulse and measure the emitted photon intensity (Fig. 5.5b). To reproduce the experimental data with the quantum simulations (solid line) excitation induced dephasing and a chirped laser pulse have to be considered [Ram10a, Deb12, Kuh15].

While the previous section 5.2 covered the impact of re-excitation events in dependence of the pulse duration for a π-pulse excitation we use now the quantum trajectory approach and assisting experiments to further investigate the consequence of excitation with a finite pulse duration for different pulse areas.

We start the discussion with the case of a π-pulse excitation where a typical quantum trajectory is shown in Fig. 5.6a as green line. The pulse is capable to
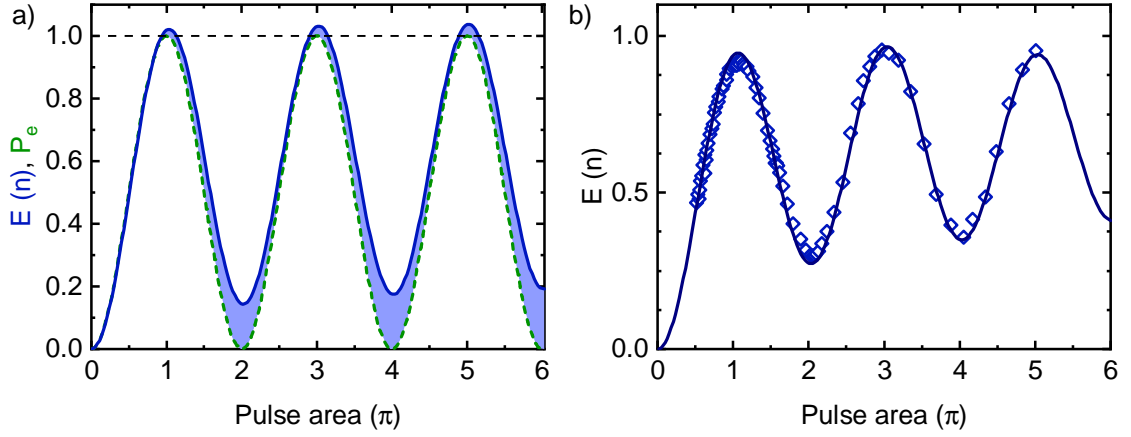
Figure 5.5 | Rabi rotation under consideration of re-excitation a, Simulated probability to find a two-level system in the excited state after pulsed and resonant excitation as a function of the pulse area (green dashed line). The expected photon number (solid blue line) deviates from the ideal Rabi oscillation. **b**, Measured Rabi rotation exhibits considerable emission for even pulse areas.

drive the system fully to the excited state where it remains for a certain time, given by the lifetime of the excited state, until it spontaneously decays under the emission of a single photon. The lifetime can be extracted from the temporal evolution of the probability to find the system in the excited state which follows a clean monoexponential decay (blue line). Considering a finite temporal width of the laser pulse (grey dashed line) leads to a smeared out onset of the excitation compared to a theoretically ideal instantaneous preparation. Using the statistical nature of the computed quantum trajectories allows to determine the photon number distribution [Joh13], shown as an inset, which exhibits mainly single-photon events ($P_1 = 97.9\%$). This confirms the usefulness of a quantum two-level system driven by a resonant short pulse as a deterministic single-photon source. However, a small fraction of the events result in the emission of two photons ($P_2 = 2.1\%$) while higher photon number emissions are negligible. This can be indirectly accessed in the experiment by measuring the second-order correlation function of the QD emission under π-pulse excitation and the resulting correlation histogram is shown in Fig. 5.6b. For an ideal single-photon source there are no correlation events for zero time delay. However, the measurement produces a small peak indicating two- or multi-photon emission events. The $g^{(2)}(0) = 0.096 \pm 0.009$ still proofs dominant single-photon

emission in agreement with the simulations.
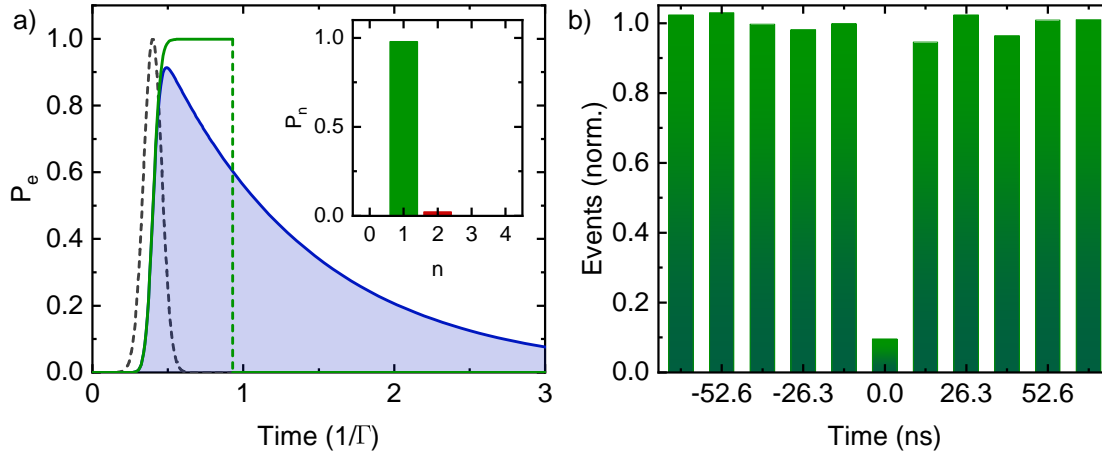
Figure 5.6 | Resonant π-pulse excitation of a two-level system a, Simulated temporal evolution of the probability to find the system in the excited state (solid blue line). An exemplary quantum trajectory is shown in green while the dashed part depicts the collapse of the system to the ground state under emission of a single photon. The excitation pulse is indicated by the black dashed line. Inset: Photon number probabilities indicating near-unity single-photon emission. **b,** Measured auto-correlation histogram showing clear anti-bunching, a proof of predominant single-photon emission.

For 2π-pulse excitation the two-level system is expected to be finally found again in its initial state after the pulse interaction. But after absorption of half the laser pulse the system has a near unity probability to be found in its excited state. In that period of time there is a significant chance for a spontaneous decay. Such an event resets the system to the ground state and restarts the Rabi oscillation with the remaining pulse area. An exemplary quantum trajectory is depicted in Fig. 5.7a in red for the case of an emission event exactly when the excited state probability reaches one. This means that a pulse area of 1π is still available to drive the population to the excited state leading to a second photon emission at a later time. Simulation of the temporal evolution of the excited state probability therefore yields a sharp peak centered at the excitation pulse with a weak tail for longer times. Further insight is given by the calculated photon number distribution, presented in the inset, where in most cases there is no photon emission at all ($P_0 = 92\%$). But surprisingly for the case of any photon emission the two-photon emission dominates over single-photon events while three or more photons per excitation pulse have a negligible portion. We

experimentally verify this finding by exciting the QD on resonance with a 2π-pulse and recording the correlation of the output of an HBT-Setup. In the case for a sparse two-photon source this produces a peak at zero time delay of the normalized correlation histogram which exceeds one indicating the bunching of the arriving photons as it is presented in Fig. 5.7b. It is important to note, that the center peak in a high resolution correlation histogram still features a dip at exactly zero time delay since in the case of a two-photon bundle emission the first emission conditions the subsequent emission of the second photon with a delay governed by the lifetime of the excited state [Mn14]. However, using the laser pulse as the on-demand trigger for photon emission requires taking into account all resulting emission events.
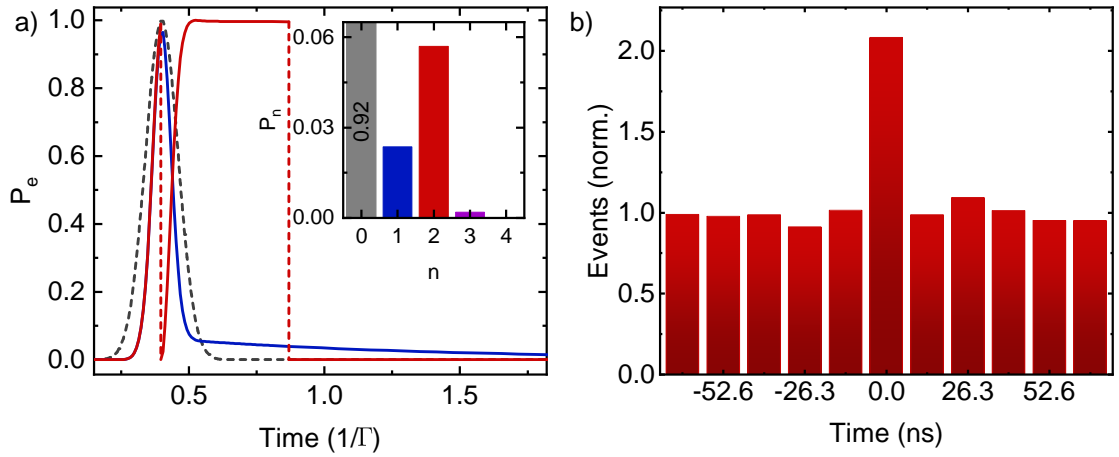
Figure 5.7 | Resonant 2π-pulse excitation of a two-level system a, Simulated temporal evolution of the probability to find the system in the excited state (solid blue line). After interaction with half the laser pulse the system is found with near-unity probability in the excited which increases the chances for a photon emission. The remaining pulse is able to drive the system again to the excited state resulting in a second photon emission (solid red line). Inset: Photon count distribution shows dominating two photon emission for all emission events. **b**, Strong bunching of the center peak in the auto-correlation measurement of the emitted photons indicates dominating two-photon emission.

While in the case of resonant excitation with a pulse area of π the two-level system predominantly emits a single photon, a 2π-pulse can unexpectedly initiate the emission of a two-photon bundle. To gain further insight when the two-photon emission surpasses the single-photon events we simulate the photon count distribution in dependence of the applied pulse area. The result is presented in Fig. 5.8a where

we find that the single-photon probability P_1 (solid green line) follows the Rabi oscillations with its maxima at even π-pulse areas. In contrast, the probability to emit two photons per excitation pulse P_2 (solid red line) oscillates out of phase while three-photon processes stay negligible for all pulse areas (purple line). The picture becomes even clearer by renormalizing the photon count distribution by neglecting the vacuum component which gives us the photon number purities π_n depicted as dashed lines [Mn14]. Here the alternating behavior between single- and two-photon emission with increasing pulse area becomes evident. The photon count distribution gives also access to the degree of second-order coherence of the QD emission which we can verify experimentally. Keeping the pulse duration constant but increasing the intensity of the applied resonant laser pulse reproduces then the scenario investigated theoretically before. We analyze the QD emission with an HBT-setup and extract the corresponding $g^{(2)}(0)$-value as shown in Fig. 5.8b. The autocorrelation measurement reveals $g^{(2)}(0)$-values smaller than 0.5 and therefore mainly single-photon emission for pulse areas up to 1.5π but super-Poissonian statistics for pulse areas around 2π and 4π indicating the bunched nature of the emission as two-photon bundles. Notably, the two-level system also acts as a good single-photon source for a pulse area of 3π. In addition, the degree of second-order coherence already increases with the pulse area for very low excitation power with the consequence that a single-photon source with higher purity might be realized at the cost of excitation efficiency.
The theoretical calculation of $g^{(2)}(0)$ factors in the extracted dephasing rate and laser pulse chirp from the measured and fitted Rabi oscillation shown before (Fig. 5.5b). In addition, using the experimentally determined pulse duration and excited state lifetime of the QD leaves no free parameter to match the experimental results (solid line in Fig. 5.8b). The excellent agreement between experiment and theory further proves the validity of our model.

As indicated by the presented exemplary quantum trajectory of the two-level system under resonant excitation with a 2π-pulse, the two photons are not emitted at the same time but consecutively. The first photon is created during the presence of the laser pulse while the second one is emitted at a later random time within the lifetime of the excited state. While the temporal detector resolution inhibits experimental insight into this dynamics we can use our theoretical model to study the time resolved photon emission in detail. Therefore we investigate the time resolved
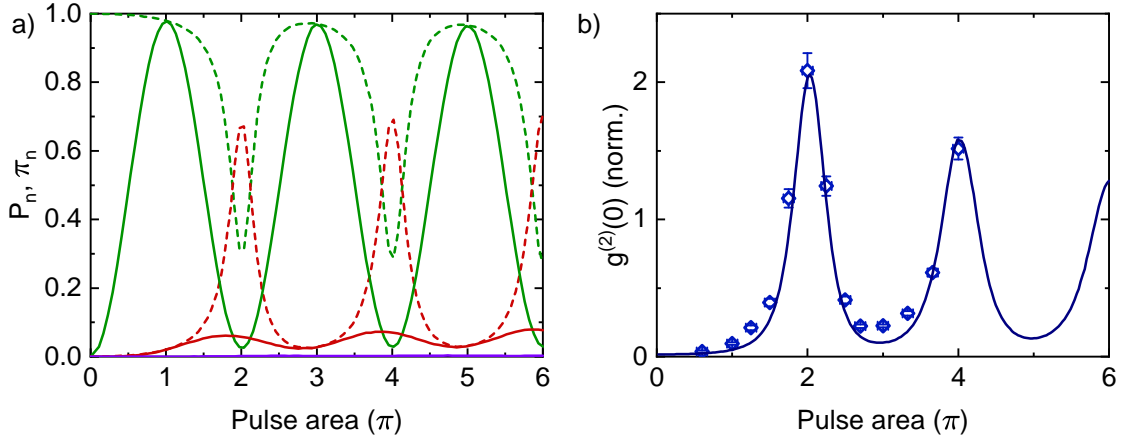
Figure 5.8 | Photon count distribution of a resonantly driven two-level system a, Calculated probability to emit one (green solid line), two (red solid line) or three photons (purple) as function of the area of the applied pulse. The single-photon emission probability retraces the Rabi oscillations of the system while the two-photon emission occurrence oscillates out of phase. Omitting the probability that the pulse interaction leads to no photon emission gives the photon number purities for one photon π_1 (green dashed line) and two-photons π_2 (red dashed line) **b**, Measured (diamonds) and simulated (solid line) degree of second order coherence in dependence of the pulse area.

probability mass function for photodetection given by [Lou00]:

$$P_1 = \int_{\mathbb{R}} \mathrm{d}t_1 p_1(t_1) \quad \text{and} \quad P_2 = \iint_{\mathbb{R}^2} \mathrm{d}t_1 \mathrm{d}t_2 p_2(t_1, \tau) \tag{5.18}$$

Here $p_1(t_1)$ describes the case for only a single-photon emission at time t_1 while $p_2(t_1, \tau)$ represents the probability density for an initial first emission event at time t_1 with a subsequent second radiative decay happening at time $t_1 + \tau$. The probability mass functions are presented in Fig. 5.9 for a pulse area of 2π a), 4π b) and 6π c) with the excitation pulse centered around $t_1 = 0.15$. For an easier accessibility $p_2(t_1, \tau)$ can be integrated along τ and t_1 to separately study each photon emission. The resulting $p_2(t_1)$ then gives insight into the probability distribution when the first photon is emitted given that a second emission is happening at a later time. For a 2π pulse we obtain a single peak with its maximum nearly reaching unity after interaction with half of the laser pulse. This trace can be directly compared to $p_1(t_1)$ which exhibits a dip at the pulse center. Thus, if a photon is emitted during that time window it is likely that a second photon emission will follow at a later

time. The probability density for the second photon $p_2(\tau)$ resembles the temporal evolution of a simply excited two-level system. The probability density is rising during interaction with the pulse followed by an exponential decay. Analysis of the behavior under excitation with a pulse with area of 4π reveals a second peak in the probability density $p_2(t_1)$. The first photon has a high probability to be emitted after interaction with π of the pulse leaving an area of 3π for further excitation. This gives rise to two probable scenarios for the second photon to be emitted: The system is driven again to the excited state with an additional pulse area of π and emits a photon with then an area of 2π left capable of performing a full Rabi rotation. Or on the other hand the system interacts with the full 3π before the second photon is emitted after the interaction during the lifetime of the excited state. The additional Rabi oscillation is also clearly visible in $p_2(\tau)$. If the first photon emission happened after absorption of 3π the second one is very likely to take place after the interaction with the residual π, copying the evolution under 2π-pulse excitation. However, three or multi-photon processes remain unlikely since after the first emission event the pulse is always converted to an odd π-area pulse which predominantly produces single-photon events. For a pulse area of 6π an additional Rabi rotation is possible, adding a further copy of the 2π-pulse scenario to the probability density functions.

Until now the discussion was limited to relatively short pulses ($\tau_{FWHM} = \tau_e/10$) resulting in strong photon bunching for even π-pulse areas where three or higher photon number events play a negligible role but their impact increases for longer pulses. Therefore we investigate the degree of second-order coherence for excitation with pulses of different durations but with fixed pulse area of 2π (Fig. 5.10). For an ideal two-level system (dashed line) we obtain strong bunching for very short pulses. There, the highest ratio of two- to one-photon processes combined with an overall low probability to emit any photon, roughly given by τ_{FWHM}/τ_e, leads to high $g^{(2)}(0)$-values. Longer pulse durations facilitate spontaneous decays during the pulse interaction so multi-photon events gain significance resulting in the pulse wise photon statistics approaching a Poissonian distribution. Introducing excitation induced dephasing disturbs the coherent drive and hence, the Rabi oscillations which reduces the probability of re-excitation during the pulse interaction and therefore also the degree of second-order coherence (short dashed curve). Since the dephasing scales with the intensity of the laser pulse its impact is stronger for short pulses
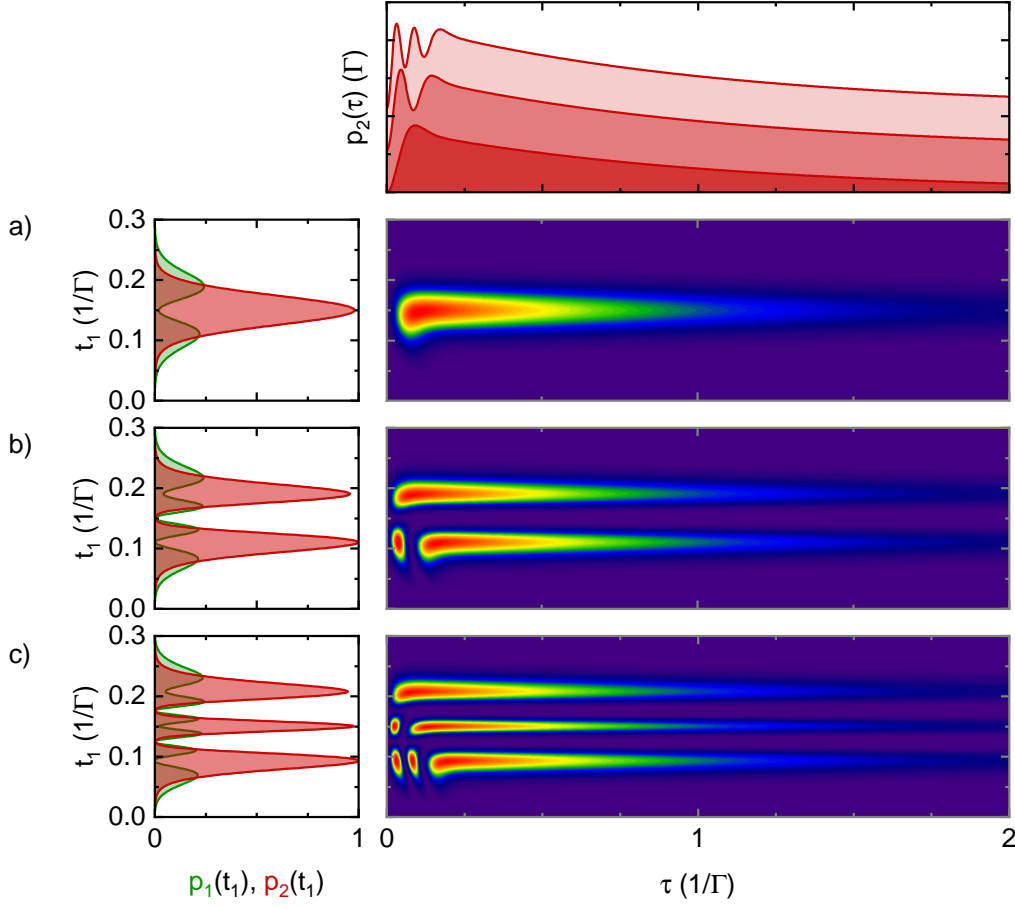
Figure 5.9 | Simulated time-resolved probability densities for the emission of one or two photons from an ideal two-level system under resonant a) 2π b) 4π and c) 6π pulse area excitation

until the system is solely incoherently driven and thus resulting in anti-bunched single-photon emission. The $g^{(2)}(0)$-value is further reduced when laser pulse chirp is taken into account (solid line) which also prevents clean Rabi oscillations due to the ability to adiabatically drive the QD to the excited state. Including those effects in the simulation allows good agreement with the experimental data (diamonds) with the exception of the shortest measured pulse where a stronger chirp needs to be assumed (dotted line).

Finally we explore the emission spectrum of such a two-photon bundle. Given the short temporal window during the laser pulse interaction for the first emission suggests an alternated linewidth due to the time-frequency uncertainty. Therefore we
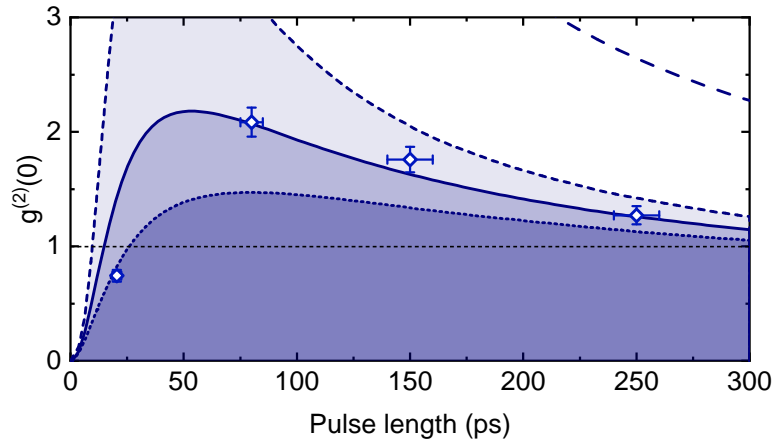
Figure 5.10 | Degree of second order coherence of the emission of a two-level system resonantly driven by a 2π-pulse in dependence of the pulse duration. Including dephasing strongly reduces $g^{(2)}(0)$ (short dashed line) in comparison to an ideal two-level system (dashed line). Taking a slightly chirped laser pulse into account, matching the experimental conditions (diamonds), further reduces the degree of second order coherence (solid and dotted line).

simulated the emission for a 2π-pulse excitation which is presented in Fig. 5.11a and exhibits a broader spectrum of order $1/\tau_{FWHM}$ compared to the natural linewidth of the two-level system (dashed line) caused by the first emitted photon of the bundle. Additionally, the emission spectrum inherits an intensity oscillation similar to an emerging dynamical Mollow triplet for 4π- and 6π-excitation due to undergoing Rabi oscillations during the pulse interaction. High-resolution spectroscopy of the QD emission allows experimental insight and is presented in Fig. 5.11a for π-pulse excitation. A Gaussian fit reproduces the measured data very well indicating spectral broadening of the emission by for example an unstable electric environment of the QD. However, the spectrum in the 2π case can only be fitted by two Gaussian curves where one is governed by the spontaneous decay with the same FWHM as the emission under π-pulse excitation and a broader curve with a linewidth of $\sim 31\,\mu\text{eV}$ which would translate to a lifetime in the order $\sim 20\,\text{ps}$. This strengthens the previous explanation that the first photon is emitted during the pulse interaction ($\tau_{FWHM} = 80\,\text{ps}$)).
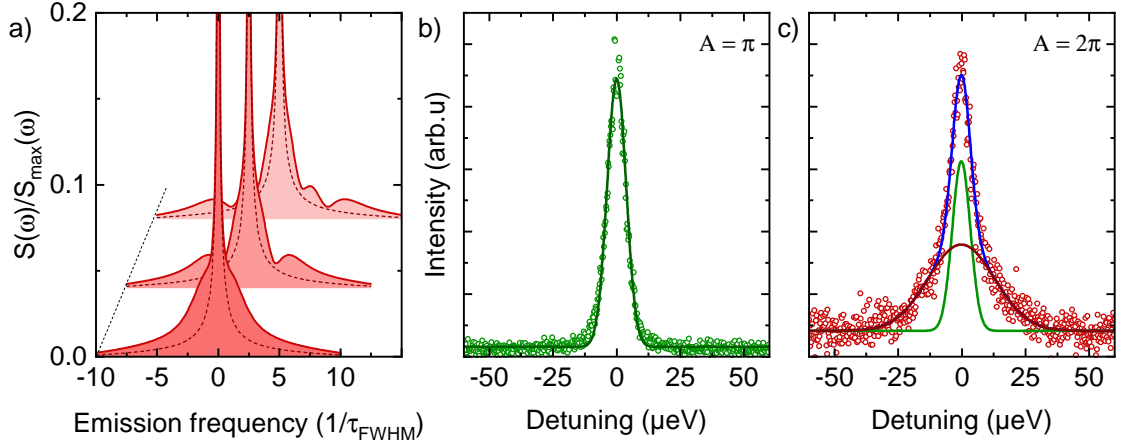
Figure 5.11 | Super-natural linewidth two-photon bundles from a two-level system a, Simulated emission spectra under resonant excitation with a 2π-, 4π- and 6π-pulse (dark to lighter shade). The natural emission linewidth is depicted as dashed line **b**, High resolution spectrum of the QD emission for π-pulse excitation with a Gaussian fit. **c**, QD emission by interaction with a 2π-pulse. The signature of the different linewidth of the two photons is emphasized by a Gaussian cumulative fit.

5.4 High-Purity Single-Photon Emission

Spontaneous emission and re-excitation during the pulse-system interaction sets an intrinsic limit of the achievable single-photon purity for a coherently excited two-level system [Fis18a]. These processes can even lead to the counter-intuitive case of predominant two-photon emission as discussed in the previous section 5.3. However, for prospective quantum applications based on single-photon sources a high purity is crucial to ensure the security of quantum cryptography or to keep the error rate low, boosting the efficiency. In order to tackle that obstacle we propose the use of a three-level quantum ladder system to generate single photons with high purity. This can be realized with a semiconductor QD by including the biexciton level which results in the energy level scheme depicted in Fig. 5.12a [Kod10]. Besides the ground state, given by the empty uncharged QD, and the exciton states split by the fine structure, the biexciton provides a forth level. Disregarding one of the decay branches, for example by polarization filtering, results in a three-level system. The exciton-biexciton transition energy is red-shifted by the binding energy E_B allowing resonant two-photon excitation of the biexciton with a laser field detuned from the exciton transition by $E_b/2$ (purple arrows) [Bru94, Rod03, Mü14]. A typical emission

spectrum is presented in Fig. 5.12b with both emission lines clearly separated and with identical intensity. To deterministically prepare the QD in the biexciton state a short laser pulse tuned to the two-photon resonance is applied. Increasing the laser power, and therefore its pulse area, reveals clean Rabi oscillations in the emission intensity of both decays indicating the coherent nature of the excitation (Fig. 5.13a). Coupling to LA phonons is the main cause for dephasing of the coherent drive resulting in damping of the oscillation [Ram10c]. In addition, the phonon coupling leads to a renormalization of the Rabi frequency and therefore a deviation from the linear behavior of the oscillations with the excitation power [Ram10b]. However, the coherent excitation allow efficient and on demand preparation of the biexciton by applying a π-pulse.
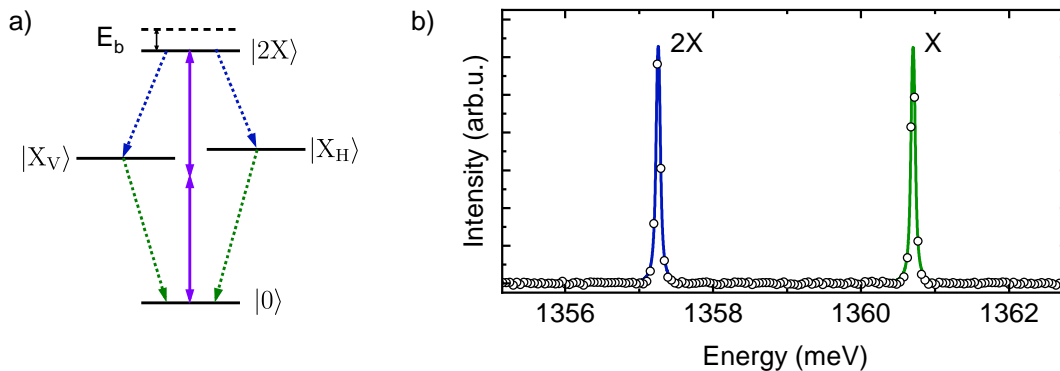
Figure 5.12 | Two-photon excitation of the biexciton a, Level scheme of an uncharged QD including exciton and biexciton levels. The laser couples via two-photon absorbtion to the ground and biexciton state (purple arrows) **b**, Emission spectrum of the cascaded decay of the biexciton. The biexciton line is red shifted with respect to the exciton by the biexciton binding energy E_b

To realize a single-photon source from this system requires spectral filtering due to the sequential decay of the biexciton and exciton. On the other hand, this is also sufficient to suppress backscattered laser light in the detection path facilitating an obtainable brightness of the source exceeding 50% since polarization filtering is not necessary anymore. We continue to investigate the single-photon purity of the biexciton emission under π-pulse excitation using an HBT-setup. The resulting correlation histogram is presented in Fig. 5.13 showing strong anti-bunching. As the center peak nearly vanishes in the detector noise a fitting routine to determine the peak areas is not feasible. Therefore, it is better to integrate the total number of events over

a range that contains the whole peak. In this case the background given by the dark counts of the detectors is the main limiting factor of the achievable accuracy. Following this approach and using a time window of 2.6 ns gives us $g^{(2)}(0) = 9.4 \cdot 10^{-5} \pm 1.9 \cdot 10{-}3$. This extremely high photon purity can be understood as a consequence of the cascaded emission of the biexciton. In the previous section 5.2 it was shown that spontaneous emission and re-excitation during the pulse-system interaction intrinsically limits the obtainable purity of the emission of a resonantly driven two-level system. This also applies for a three-level system, however, the probability to re-excite the system is strongly reduced since two spontaneous decays have to happen during the limited time window when the laser pulse is present. Recently, Schweickert et al. reported a value of $g^{(2)}(0) = (7.5 \pm 1.6) \cdot 10^{-5}$, the highest purity measured so far, with the same excitation scheme but using superconducting nanowire single-photon detectors that feature dark count rates in the mHz range [Sch18b].
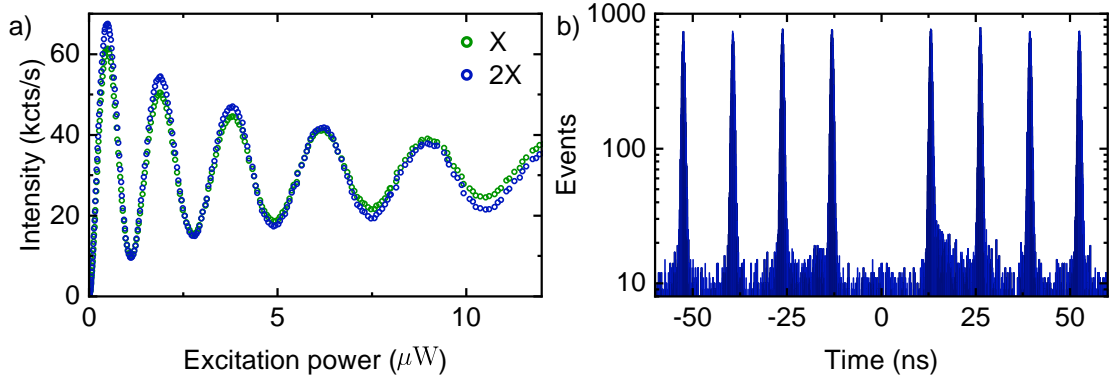
Figure 5.13 | Cascaded emission from the resonantly driven biexciton state a, Rabi oscillations observed via the cascaded emission intensity indicating the coherent nature of the resonant two-photon excitation **b**, Autocorrelation measurement of the filtered biexciton emission showing strong anti-bunching.

Since a single QD can either act as a quantum two- or three-level system we can directly compare their performance in terms of single-photon purity. Hence, we investigate the second-order coherence of the emitted photons as a function of the pulse duration. The result is presented in Fig. 5.14a where the data for the two-level system was reproduced from Fig. 5.4b. The measured $g^{(2)}(0)$-value of the three-level system is up to two orders of magnitude lower compared to the two-level system and indicates higher purity for any pulse duration. We obtain similar results from our theoretical model, presented in Fig. 5.14b, proving the superiority of the

two-photon excitation scheme in terms of single-photon purity. Importantly, for the ladder system the second-order coherence of the emitted photons scales quadratically with the pulse duration compared to a linear behavior for the two-level system which further increases the advantage for shorter pulses.
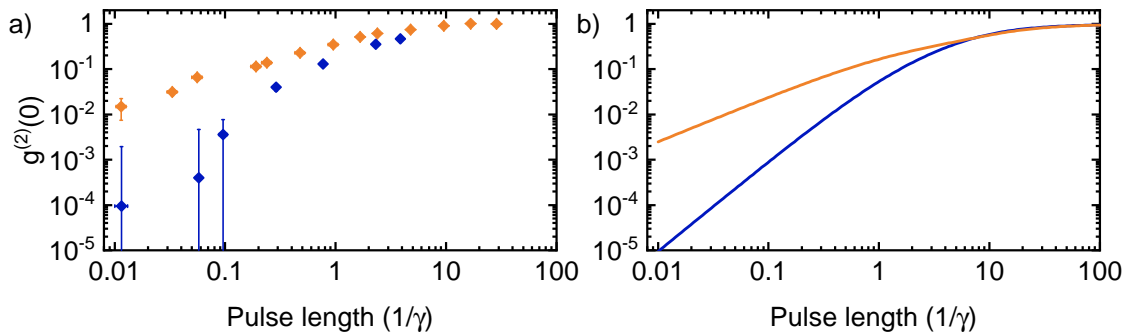
Figure 5.14 | Single-photon purity comparison between a two- and three-level system a, Experimental data of the degree of second-order coherence of the emitted photons from the resonantly driven negative trion transition (orange) and the biexciton recombination (blue) for different pulse length **b**, Simulations reproduce the same behavior, with a $g^{(2)}(0)$ up to two orders of magnitude lower for a three-level system due to suppressed re-excitation.

Chapter *6*

Generation of Highly Indistinguishable Single Photons

Contents

The results of this chapter are published in [Sch19, Sch20, Sbr22]. The analytical model in section 6.2 was provided by Rahul Trivedi using the scattering matrix formalism [Fis18c, Tri18] and Friedrich Sbresny performed the numerical simulations using QuTiP [Joh12, Joh13] for section 6.2 and 6.3.

6.1 Indistinguishability in GaAs QDs

Besides the photon purity, another crucial property of deterministic single-photon sources is the ability to generate indistinguishable photons. This is a requirement for many future applications like boson-sampling [Aar11a, Aar11b] or photon-based quantum simulations [Kni01, Kok07]. While spontaneous parametric down-conversion of laser light in non-linear crystals has been shown to produce highly indistinguishable

photons, this method lacks the high purity achievable with a single quantum emitter [Shi94, Kwi99]. Furthermore, the brightness is limited by the trade-off between overall efficiency and multi-photon events [Som16]. However, InGaAs QDs have also proven to be an excellent source for indistinguishable photons. Improved epitaxial growth and numerous fabrication methods to implement photonic cavities, can strongly reduce the impact of charge fluctuations in the vicinity of the QDs to achieve near-unity indistinguishability of the emitted photons [Din16a, Som16, Kir17, Tom21]. In recent years, the growth of GaAs QDs by droplet etching made great progress and is closing the gap in terms of optical properties and quality to the well established InGaAs QDs [Hub18, Che18, Sch18b]. In the following section, we show that this kind of QDs is also able to generate highly indistinguishable photons. While in chapter 2.3 the advantage of a diode structure enclosing the QD layer was discussed, the investigated samples here with GaAs QDs did not have such a structure. This results in a fluctuating electrical environment introducing spectral wandering to the QD emission. Therefore, additional weak illumination with white light is employed to charge the defects in the vicinity of the investigated QD providing a stabilized environment [Ngu12, Gaz13, Rei17]. A typical emission spectrum under non-resonant excitation ($E_{exc} = 1587.5\,\mathrm{meV}$) is presented in Fig. 6.1a. Besides the bright emission from the neutral exciton at $E = 1571.9\,\mathrm{meV}$ a whole band of sharp features is observed. This is due to the lack of a diode structure causing an uncontrolled charge state of the QD and therefore random capture and tunnel processes of charge carriers and thus, fluorescence from different charged transitions. Switching to resonant excitation of the neutral exciton suppresses excitation of other transition leading to a clean spectrum (Fig. 6.1b). While the exciton line dominates the spectrum a small contribution of the trion transition is visible as well. This indicates a charge carrier capture process after excitation of the exciton or a weak phonon-assisted drive of the trion transition itself [Ard14, Qui15, Bou15]. In addition, the logarithmic scale reveals the asymmetric phonon sideband. Besides those observations we conclude that ∼90% of the QD emission stems purely from the addressed transition. Moreover, tuning the laser in resonance with the trion transition results in a similar behavior as shown in Fig. 6.1c. This allows us to investigate the emission from both transitions separately. Note that the fluctuating charge state of the QD does not affect the fundamental studies presented here but causes blinking of the emission on the µs

to ms time scale which diminish the brightness of the source [Dav14a]. To further neglect effects from other transitions in the emission spectrum as well as the phonon sideband we introduce a self-built transmission spectrometer into the detection path with a resolution of $(19.0 \pm 0.5)\,\text{GHz}$.
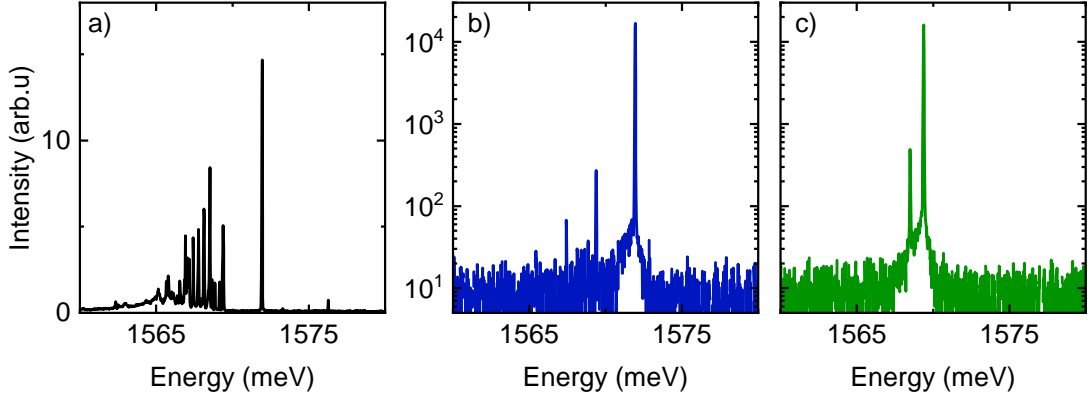
Figure 6.1 | Emission of a single GaAs QD a, Non-resonant excitation results in a rich spectrum featuring several peaks from different charged state transitions. **b**, Resonant excitation of the neutral exciton strongly suppresses emission from other transitions. **c**, RF of the trion transition.

To determine the lifetime of the excited state of the QD we resonantly excite the neutral exciton with a 5.0 ps long laser pulse and record the time-resolved emission. The obtained histogram is presented in Fig. 6.2a on a logarithmic scale. While the excited state population decays following a mono-exponential curve we observe in addition a superimposed modulation. The asymmetric shape of the QD results in two degenerate exciton spin states, with each state having orthogonal linearly polarized optical selection rules. This degeneracy arises from the exchange interaction between the electron and hole spins [Bay02b]. Preparing the QD in a superposition of those two states results in a precession of the spin state and consequently a rotation of the linear polarization of the emitted photons upon recombination [Kod12, Mul13]. The polarization filter in the detection path of the RF setup translates that to an oscillation in time of the detectable photons [Fli01]. Taking the oscillation into account allows excellent agreement of the fitting function with the measured data (solid line) to determine the lifetime to $\tau_X = (196 \pm 2)\,\text{ps}$. Since the oscillation frequency directly depends on the fine structure splitting $\nu = E_{FSS}/h$ we can extract it from the fit and yield $E_{FSS} = (7.44 \pm 0.05)\,\text{µeV}$. The determined lifetime of

∼200 ps is consistent with reported lifetimes of those QDs [Rei17, Rei19] and is considerably shorter than for InGaAs QDs, where the exciton decays on a time scale of 300 ps to 1000 ps [Adl98, Kre05b, Ber07, Liu18]. This facilitates higher repetition rates in the generation of single photons without the need of photonic structures to introduce Purcell enhancement. Moreover, the droplet etch growth method enables QDs with more symmetric shapes leading to a smaller finestructure splitting [Huo13]. This is crucial to generate time-independent polarization entangled photon pairs [War14, Hub18]. The trion lacks the finestructure splitting since either two electrons or holes with opposite spin are present canceling the spin interaction. Hence, the measured time-resolved histogram of the trion emission exhibits a clean mono-exponential decay as depicted in Fig. 6.2b on a logarithmic scale. The extracted lifetime of $\tau_T = (236 \pm 2)$ ps is slightly longer than the exciton lifetime.
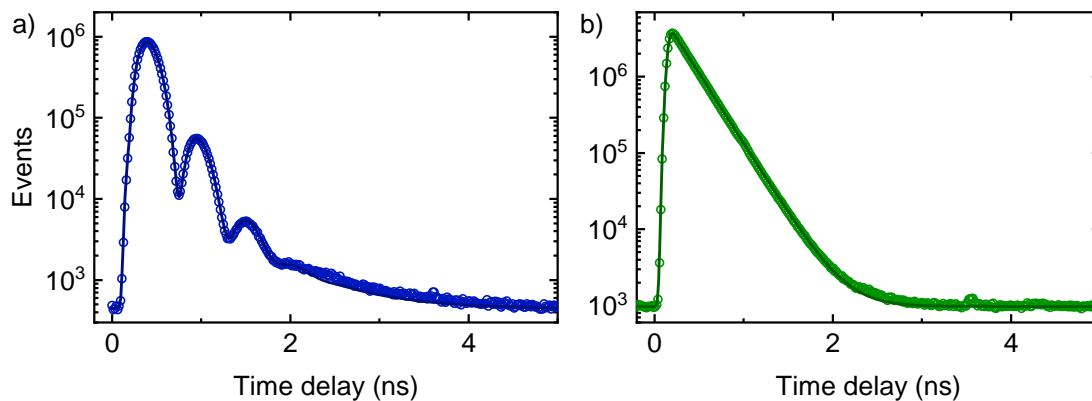
Figure 6.2 | Time-resolved pulsed RF from a GaAs QD a, Temporal evolution of the emission events after pulsed excitation of the neutral exciton. The exponential decay is superimposed by an oscillation caused by the precession of the fine structure. **b**, The trion state lacks a fine structure resulting in a clean mono-exponential decay.

Before we finally investigate the indistinguishability of the emitted photons we examine the photon purity. While a low purity would already spoil the advantage of GaAs QDs compared to SPDC sources, it would also strongly affect the measurement of the indistinguishability. The emission of the exciton decay under resonant π-pulse excitation is analyzed in a HBT-setup with two superconducting single-photon detectors connected to both outputs. The measured correlation histogram is presented in Fig. 6.3a. The low detector dark count rate (< 1 Hz) ensures a near background free histogram which facilitates the analysis of the peak areas by summing up all

correlation events in a 3.2 ns wide time window centered on each peak. This yields $g^{(2)}(0) = (2.5 \pm 0.2) \cdot 10^{-3}$ which we mainly attribute to re-excitation during the pulse-system interaction. It follows, that the laser is fully suppressed in the detection path and no background emission spoils the purity. Repeating the measurement on the trion transition gives us the histogram shown in Fig. 6.3b. Although a high degree of second-order coherence of $g^{(2)}(0) = (6.7 \pm 0.4) \cdot 10^{-3}$ is achieved, the extracted value is higher as for the exciton transition. The longer excited state lifetime would even provide a higher purity when keeping the excitation pulse duration constant which indicates that non-perfect laser or whitelight suppression or leakage from the nearby transition is the reason for the increased value. We
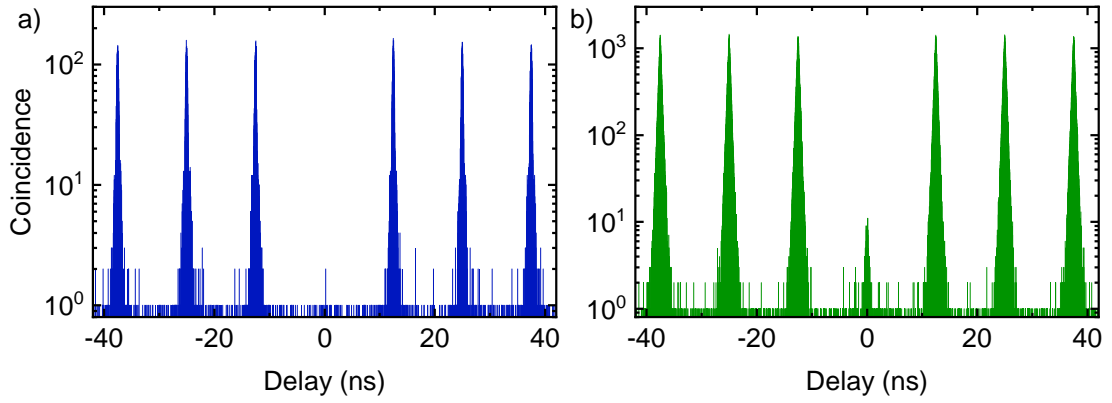
Figure 6.3 | Second-order intensity correlation histogram a, The resonantly driven neutral exciton transition exhibits pure single-photon emission with $g^{(2)}(0) = (2.5 \pm 0.2) \cdot 10^{-3}$. **b**, The correlation histogram obtained from the trion emission yields $g^{(2)}(0) = (6.7 \pm 0.4) \cdot 10^{-3}$

proceed to examine the indistinguishability of the emitted photons using a HOM type experiment as describes in chapter 3.4. To minimize the impact of spectral wandering on the indistinguishability it is beneficial to set the time between the consecutively emitted photons as short as possible. However, this is not an intrinsic limitation of such QDs since a stable electric environment solves this problem and the indistinguishability remains high with increasing temporal separation of their generation. One key requirement is precisely controlled molecular epitaxial growth with negligible impurity implantation which inhibits the creation of defects in the vicinity of the QDs that are randomly charged and uncharged. Another powerful method to reduce spectral wandering is embedding the QDs in a diode structure as

discussed in chapter 2.3.

We experimentally determine the HOM visibility of the photons emitted by the neutral exciton transition resonantly excited with $2\,\text{ns}$ separation. The obtained correlation histogram with a quintuplet of peaks is presented in Fig. 6.4a. Each peak resembles a mirrored copy of the temporal evolution of the exciton state population and as a result exhibits the same modulation as observed for the time resolved RF measurements. To determine the respective peak areas the coincidence events are summed up in a time window including the whole peak. From there the HOM visibility is calculated using Eq. (3.34) to be $V_{\text{HOM}} = 94.9^{+5.1}_{-6.4}\%$ which is proof of the ability of GaAs QDs grown via droplet hole etching to act as excellent sources to generate single indistinguishable photons. Repeating the experiment on the trion transition of the same QD yields $V_{\text{HOM}} = 88.5 \pm 3.3\%$. While this represents still a high degree of indistinguishability it is considerably lower compared to the exciton transition. This can be attributed to stronger spectral wandering due to the charged state being more sensitive to fluctuation of the environment. However, each QD is exposed to an individual environment enabling also higher indistinguishability. Investigating two more QDs provide values up to $V_{\text{HOM}} = 95.0^{+5.0}_{-6.1}\%$.
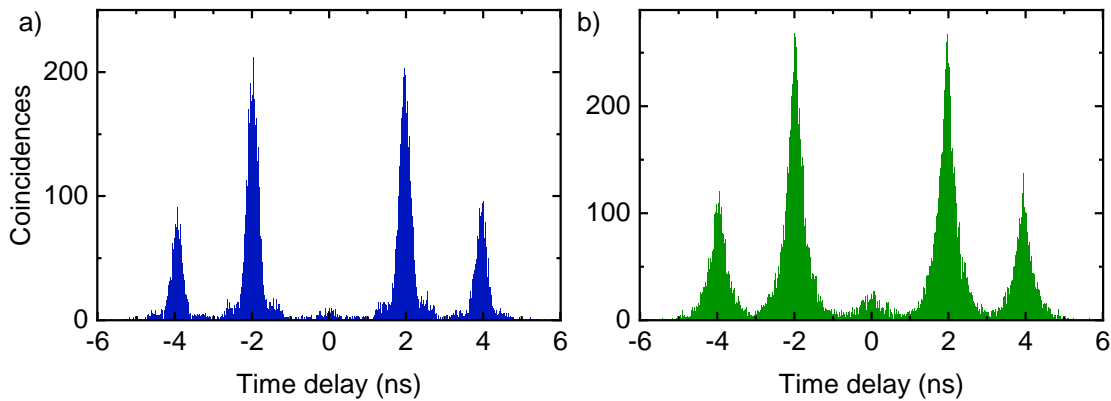
Figure 6.4 | Two-photon interference histogram of RF a, Center quintuplet of the correlation histogram measured at the outputs of an unbalanced Mach-Zehnder interferometer of photons emitted by the neutral exciton transition **b**, and the trion transition under resonant excitation.

6.2 Impact of Cascaded Emission

While GaAs QDs also represent an near ideal two-level quantum system as demonstrated in section 6.1, and are able to serve as an excellent source for single indistinguishable photons, the purity is ultimately limited by re-excitation processes during the pulse-system interaction. We discussed in chapter 5.4 the approach to resonantly excite the biexciton to improve the single-photon purity and investigate now the indistinguishability of the cascaded emission. Assuming that the system was prepared in the biexciton state at $t = 0$ and using a scattering matrix formalism we can describe the emitted two-photon state as [Fis18c, Tri18]:

$$|\psi\rangle = \int_{t=0}^{\infty} \int_{t'=t}^{\infty} dt dt' f(t,t') b_{2X \to X}^{\dagger}(t) b_{X \to 0}^{\dagger}(t') |vac; 0\rangle \tag{6.1}$$

with $b_{2X \to X}^{\dagger}(t)$ and $b_{X \to 0}^{\dagger}(t)$ denoting the time domain creation operators which describe the photonic modes to which the respective transitions couple. While $f(t,t')$ represents the two-photon wave function:

$$f(t,t') = \sqrt{\gamma_X \gamma_{2X}} e^{-i\omega_{2X \to X} t} e^{-i\omega_{X \to 0} t'} e^{-\gamma_X (t'-t)/2} e^{-\gamma_{2X} t/2} \tag{6.2}$$

Here $\omega_{2X \to X}$ and $\omega_{X \to 0}$ denote the respective transition frequencies while γ_{2X} and γ_X are the decay rates of the biexciton and exciton, respectively. Tracing the pure two-photon state over the modes given by the operator $b_{X \to 0}(t)$ allows description of the single-photon state emitted from the $|2X\rangle \to |X\rangle$ transition. We obtain therefore for the density matrix:

$$\rho = \text{Tr}_{b_{X \to 0}} [|\psi\rangle \langle\psi|] \tag{6.3}$$

$$= \int_0^{\infty} \int_0^{\infty} dt dt' \rho(t,t') b_{2X \to X}^{\dagger}(t) |vac\rangle \langle vac| b_{2X \to X}(t'), \tag{6.4}$$

where

$$\rho(t,t') = \gamma_{2X} e^{i\omega_{2X \to X} (t'-t)} e^{-\gamma_{2X} (t+t')/2} e^{-\gamma_X |t-t'|/2}. \tag{6.5}$$

We can see from Eq. (6.4) that the photon state generated by the biexciton decay is non-separable. Since the emitted photons need to be describable as pure states to be

identical, and therefore separable, indicates that the achievable indistinguishability is limited. It follows from the non-separability that the second photon from the cascaded decay is linked to the first one and shares the same indistinguishability. The trace purity $\mathbb{P}$ of the single-photon state allows to quantify the degree of separability [Sim05]:

$$\mathbb{P} = \mathrm{Tr}_{b_{2X} \to X}[\rho^2] = \frac{\gamma_{2X}}{\gamma_{2X} + \gamma_X} \tag{6.6}$$

It follows that for QDs where typically $\gamma_{2X} \approx 2\gamma_X$ the maximum obtainable indistinguishability is ~ 0.66. Note that the trace purity cannot be experimentally accessed. In the previous chapter we determined the HOM visibility from the two-photon interference as a measure of the indistinguishability on the other hand it was recently shown that $\mathrm{V_{HOM}} = \mathbb{P}$ if the single-photon emission exhibits a high purity and therefore negligible multi-photon events [Fis18b, Tri20].
We now continue to experimentally investigate the indistinguishability of the photons emitted by the cascaded decay of the biexciton. Therefore, the QD is deterministically prepared in the biexciton state with a short laser pulse resonant on the two-photon absorption [Stu06, Mü14]. The resulting emission is spectrally filtered to allow separate examination with an unbalanced Mach-Zehnder interferometer of the quantum light generated from the exciton or biexciton decay, respectively. The obtained correlation histograms are presented in Fig. 6.5. For both transitions the center peak of the quintuplet is clearly visible indicating already an reduced indistinguishability. Analysis of the peak areas and applying Eq. 3.34 gives us a HOM visibility of $\mathrm{V}_{HOM,X} = (56.7 \pm 0.6)\%$ and $\mathrm{V}_{HOM,2X} = (60.0 \pm 0.5)\%$. To exclude strong external impact on the achievable indistinguishability the experiment is repeated using RF of the neutral exciton transition of the same QD. The determined HOM visibility $\mathrm{H_{HOM}} = (92.3 \pm 0.1)\%$ proofs that the cascaded emission underlies an intrinsic limitation as suggested by the theory.

Given the high single-photon purity for the two-photon excitation scheme, as shown in chapter 5.4, allows direct comparison of the experimental result with the theoretical trace purity. The low multi-photon event probability was validated for the particular QD under investigation with the same excitation parameter as for the two-photon interference experiment. The extracted degrees of second-order coherence were $g^{(2)}(0)_{TPE,X} = (9.13 \pm 1.61) \cdot 10^{-4}$ and $g^{(2)}(0)_{TPE,2X} = (1.79 \pm 0.30) \cdot 10^{-3}$ and
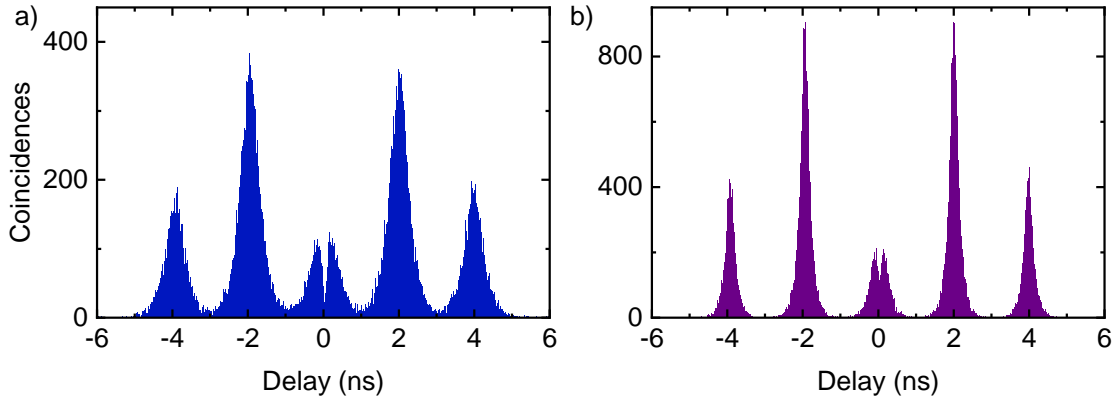
Figure 6.5 | Two-photon interference histogram of the cascaded emission a, The clearly visible peak for zero time delay is a result of the reduced indistinguishability of the exciton emission. **b**, A similar result is observed for the photons emitted by the biexciton decay.

therefore justify direct comparison of the HOM visibility and trace purity $\mathbb{P}$. With the experimentally determined emission rates ($\gamma_X = 5.13\,\mathrm{GHz}$ and $\gamma_{2X} = 7.69\,\mathrm{GHz}$) Eq. (6.6) gives an upper bound of $\mathbb{P} = 0.60$ matching very well the measured HOM visibility.

In a more intuitive picture one can describe the reduced indistinguishability by an additional timing jitter or spectral broadening of the emission. The exciton decay, which can exhibit a near-unity indistinguishability, suffers an uncertainty in time by the decay of the third level when the system is prepared in the biexciton state. While the temporal shape of the photon wave packet stays the same it is randomly shifted in time, governed by the lifetime of the biexciton, reducing the overlap of two photons impinging on the beam splitter. The effect of the temporal shift is influenced by the temporal expansion of the emitted photon, which is determined by the decay dynamics of the exciton. As a result, this reflects the interdependence of the two decay rates. On the other hand, the photon emitted by the biexciton decay suffers an additional spectral broadening due to the limited lifetime of its final state, the exciton. Here, a similar link between the two decays is found, taking into account that the reduction of the spectral overlap caused by the broadening needs to be regarded relative to intrinsic spectral width given by the lifetime of the biexciton. With this in mind, it suggests that modifying the decay rates significantly impact the achievable two-photon interference and could potentially be a method to restore

near-unity indistinguishability of photons emitted by the cascaded decay of a three level system. This is also indicated by the introduced analytical model. For example, Eq. (6.5) shows that the photon state of the biexciton decay becomes separable if the decay rate of the intermediate state vanishes which would allow again emission of identical photons. This becomes even clearer when considering the trace purity given by Eq. (6.6) which approaches 1 for $\gamma_X \to 0$.
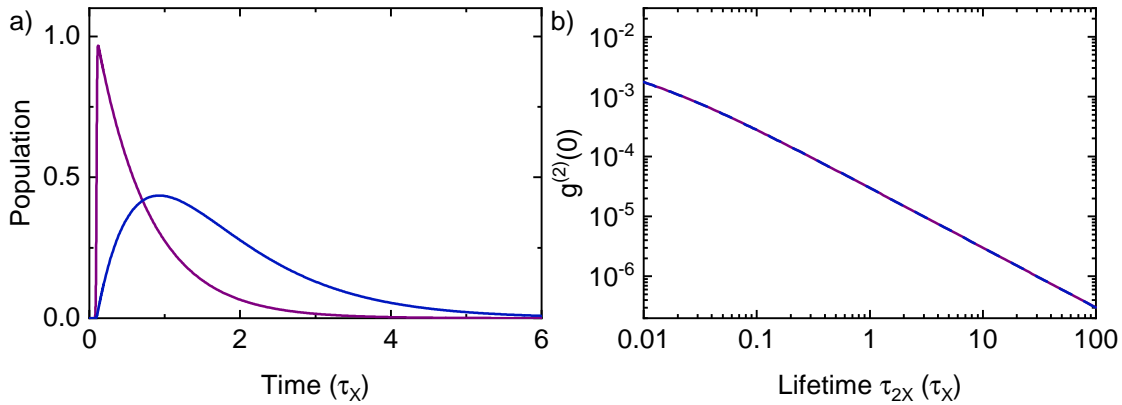
Figure 6.6 | Numeric simulations of the excited quantum three-level ladder system a, Temporal evolution of the state populations upon resonant π-pulse excitation on the two-photon resonance. **b**, Calculated degree of second-order coherence of the cascaded emission as a function of the biexciton lifetime.

We perform numerical simulations to get a quantitative picture of the behavior of the system. This allows us to evaluate the exact temporal evolution of the populations of the QD states after π-pulse excitation (Fig. 6.6a). The laser pulse duration is set to $\tau_X/50$ leading to a steep rise of the biexciton state population close to one when the laser pulse arrives. While the biexciton decay follows directly an exponential function the exciton population builds up in a slow raise with a delayed maximum. The sequential recombination suppresses re-excitation, as discussed in chapter 5.4, implying that modifying the decay rates to improve the indistinguishability also affects the single-photon purity. Therefore, the degree of second-order coherence for the emission of both transitions is presented in Fig. 6.6b as a function of the biexciton lifetime. Increasing the lifetime of the biexciton and keeping it constant for the exciton prolongs the time the system needs to fully relax to the ground state. As a consequence the probability for a second excitation event during the presence

of the laser pulse becomes less likely resulting in a higher single-photon purity of the emission.
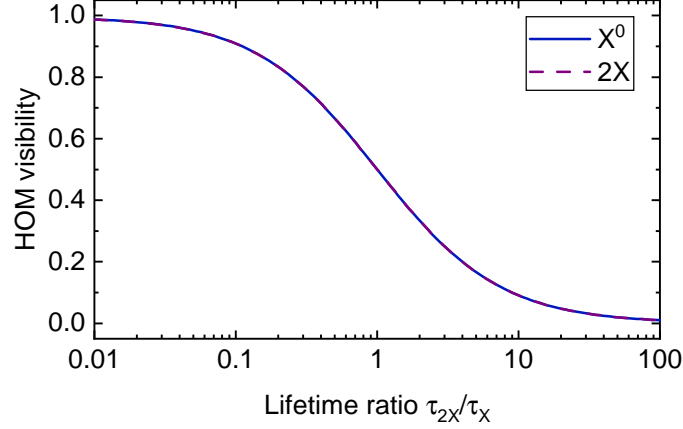
Figure 6.7 | Calculated degree of indistinguishability of the emission of a three-level system as a function of the lifetime ration τ_{2X}/τ_X for constant exciton lifetime.

However, altering the decay rates can restore a high degree of indistinguishability. This is shown in Fig. 6.7 where the HOM visibility is numerically calculated as a function of the lifetime ratio τ_{2X}/τ_X while the exciton decay is kept constant. If the recombination time of the first pair of charge carriers is substantially longer than the exciton lifetime the indistinguishability suffers strongly and approaches zero. While this behavior is directly reproduced by our analytical model it can be also understood in the intuitive picture. Reducing the biexciton decay rate directly transfers to an increase in timing jitter for the preparation of the exciton state. On the other hand, the Fourier limited linewidth of the biexciton emission becomes narrower while the final state broadening stays the same resulting on a larger impact on the achievable HOM visibility. The effect of the timing and spectral jitter can also be reversed for fast decay rates of the biexciton enabling a high degree of indistinguishability for the cascaded emission of the quantum ladder system. This can be realized by embedding the QD in a cavity to selectively enhance the emission rate of the biexciton via the Purcell effect. While this restores a high HOM visibility it degrades the single-photon purity as was shown in Fig. 6.6b.

6.3 Stimulated State Preparation

Another approach to alter the decay rates of the QD transitions is the deterministic stimulation with a resonant coherent light field. Following this method, reduces the generated photons from the cascaded decay from an entangled pair to a single one but allows high indistinguishability while maintaining an excellent purity [Sbr22]. Since the additional laser pulse only enables an overall acceleration of a transition decay this method can only be used to improve the HOM visibility of the exciton transition [Aki06]. The energy levels of the QD representing a four-level system is depicted in Fig. 6.8a. The first laser pulse (green arrows) prepares the QD in the biexciton state while the second light field is resonant with the exciton-biexciton transition (orange arrow). Possible spontaneous decay channels are represented by dashed arrows and divided by polarization selection rules (H/V) [San02a, Bay02b]. Once the biexciton is deterministically excited it decays exponentially as presented in Fig. 6.8b (red line) and at the same time the exciton is slowly populated (blue line). When the stimulation pulse with a pulse area of π interacts ($t = 0.2\tau_X$) with the QD it interchanges the population of exciton and biexciton state (solid lines). This results, for a short delay between the excitation and stimulation pulse, in a faster population of the exciton and therefore a reduction in the timing jitter. The system evolution without the second laser pulse is shown by the dashed lines.
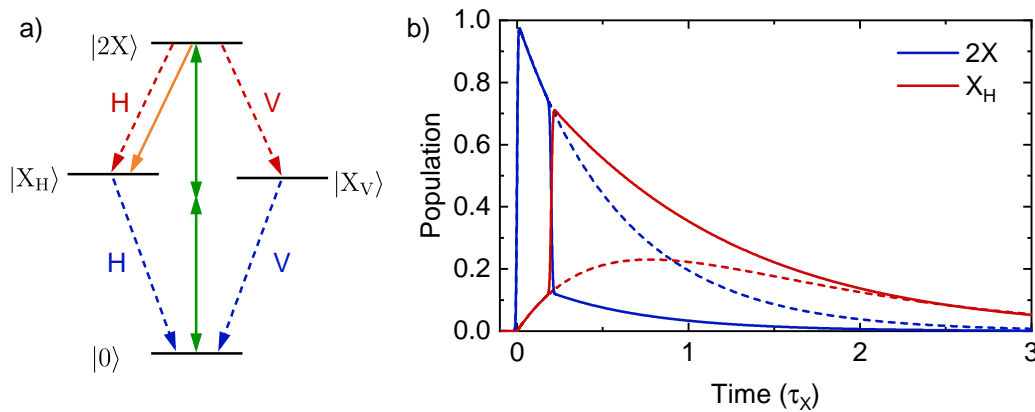
Figure 6.8 | Stimulated preparation of the exciton state a, Energy level scheme of a QD. Solid arrows depicts transitions driven by laser, dashed arrows represent radiative decay channels. **b**, Temporal evolution of the state populations after direct excitation of the biexciton and the stimulation laser applied at $0.2\tau_X$. Dashed lines depict the behavior without the second laser pulse.

We can directly realize this excitation scheme in the experiment by splitting up a single fs-pulse and shaping each pulse separately. Given an initial pulse duration of 150 fs and assuming a Gaussian shape provides a corresponding spectral FWHM of 8.2 nm. This facilitates slicing two pulses with one tuned to the two-photon resonance and the other one in resonance with the exciton-biexciton transition. Introducing a variable delay between the two pulses and having individual control of the respective intensities allows precise modulation of the QD state populations.

The first excitation pulse is able to coherently drive the system to the biexciton state by half a Rabi oscillation as was shown in Fig. 5.13a. The stimulation pulse applied 9 ps later provides additional control over the exciton state population. Actively depopulating the biexciton leads to a reduction of its emission intensity. This is presented in Fig. 6.9a where the biexciton emission intensity follows an oscillation as the stimulation light field power is increased. The clean Rabi oscillations confirm coherent control of the driven transition. While the oscillation scales linearly with the electric field of the laser pulse it exhibits an asymmetric damping. The main contribution to dephasing for a resonantly driven QD is usually caused by coupling to LA phonons, however, this leads to a damping of the oscillation to the incoherent limit of 50% of the excited state population.

To gain further insight we perform numerical simulations without any dephasing. A pulse duration of 5.3 ps is adopted as it was determined by an autocorrelation measurement for the experiment (Fig. 6.9a inset). The calculated populations after the interaction with an excitation pulse with pulse area of π and in dependence of the pulse area of the stimulation pulse which is applied with a delay of 6.7 ps is presented in Fig. 6.9b. The evolution of the biexciton population exhibits a similar asymmetrically damped oscillation as observed in the experiment while the exciton state population shows an overall reduction with increasing pulse area. For the chosen delay and pulse duration the pulses have a finite overlap. As a consequence the first pulse creates a superposition of the ground and biexciton state with a probability to find the system in the excited state in dependence of the interacted pulse area at the time when the second pulse sets in. The stimulation pulse couples the biexciton and exciton state leading then to a superposition of all three QD states with a resulting non zero probability to find the system in its ground state. Increasing the pulse area of the stimulation pulse increases the overlap, and thus, the overall population of

the excited states is reduced. A more illustrative description can be given in the probabilistic picture. At the time the stimulation pulse arrives the system has a high probability to be already driven to the biexciton state by the first pulse. This enables Rabi oscillations by the second pulse of the exciton-biexciton transition. A larger stimulation pulse area creates the possibility to perform a full rotation of the system to the exciton and back to the biexciton state while the excitation laser is still present. In that case the remaining excitation pulse has a finite probability to bring the system back to the ground state.

While the pulse separation in the experiment was significantly larger with a theoretically negligible overlap for Gaussian pulses the observed damping suggest a larger overlap. Comparing the intensity autocorrelation measurements of the shaped laser pulses (Fig. 6.9a inset) with a Gaussian fit reveals additional tails deviating from the Gaussian shape. Their origin stems from the slit which is used in the Fourier plane of the 4f pulse shaper to cut out the desired spectral window. The filtering can then be described by the rectangular function corresponding to its Fourier transform the normalized sinc function in the temporal domain which exhibits additional sidepeaks. Since the opening of the slit is of the order of the resolution limit of the pulse shaper diffraction on the edges of the slit smeares out the actual filter function resulting in a Gaussian-like pulse with the observed tails. This explains the larger overlap of the two pulses despite the large temporal separation and therefore the stronger asymmetric damping in the experiment.

For the remainder of the chapter the pulse area of the excitation and stimulation pulse is set to π respectively.

In order to optimize the excitation scheme and to implement a tuning knob on the biexciton lifetime we study first the temporal evolution of the excited states after excitation. Time-resolved PL measurements of the emission from the cascaded decay are presented in Fig. 6.10a. The red histogram shows the emission of the biexciton. Fitting the data with a monoexponential decay convolved with the Gaussian timing jitter of the SPAD yields a lifetime of $\tau_{2X} \sim 179\,\text{ps}$. In contrast, the exciton emission (blue histogram) has a slow build-up as it is populated by the biexciton decay before it can decay. This leads to a shifted maximum in the emission and an overall delayed decay. To extract the lifetime of the exciton by fitting we take the preceding
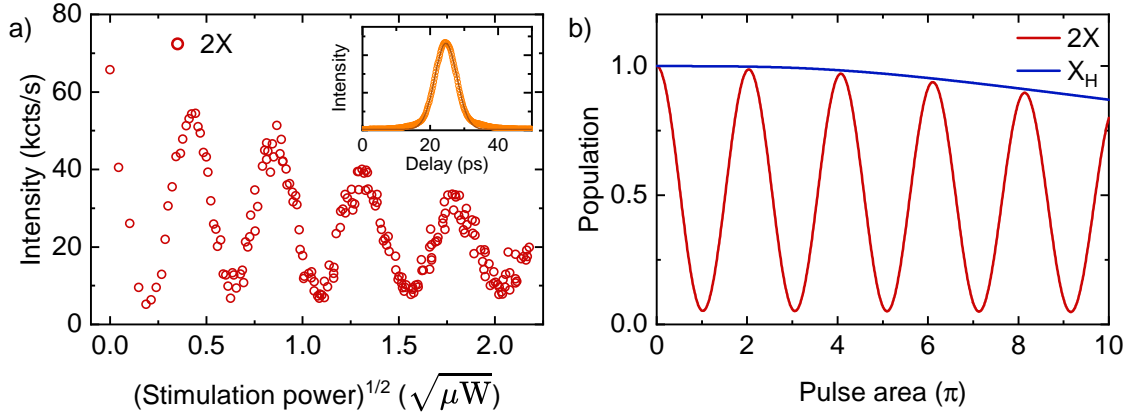
Figure 6.9 | Coherent control of the exciton-biexciton transition a, Emission intensity from the biexciton decay as a function of the stimulation laser power. Inset: Autocorrelation measurement of the laser pulse. The solid line represents a Gaussian fit emphasizing the deviation at the tails. **b**, Numerically simulated Rabi oscillation driven by the stimulation laser pulse.

recombination into account by multiplying a exponential function with the biexciton decay prior to the convolution with the instrument response function. Following this approach we obtain the exciton lifetime of $\tau_X \sim 293$ ps.

Introducing the stimulation pulse only 9 ps after the biexciton excitation directly populates the exciton resulting in an instantaneous simple monoexponential decay (light blue histogram). All histograms are normalized to the same integrated area to facilitate comparison.

Moreover, the second laser pulse is also able to re-excite the biexciton in the case that the first decay already happened and the exciton is still present when the light field interacts with the QD increasing the effective timing jitter of the exciton decay. Therefore, we investigate the emission intensity of the biexciton decay as a function of the pulse delay (Fig. 6.10b). If the stimulation pulse arrives before the biexciton is prepared the QD population is not affected by it since it is energetically red-detuned by $E_b/2$ from the two-photon resonance and the impact of phonon assisted excitation is negligible for a pulse area of π, thus, the measured PL intensity is the same as for sole two-photon excitation. Increasing the pulse delay allows efficient de-population with a minimum of $\sim 6.6\%$ of the initial biexciton emission for a delay of 9 ps $(0.03\tau_X)$. The stimulated excitation is mainly limited by the dephasing of the coherent drive caused by LA-phonons, the temporal overlap of the two laser

light fields and spontaneous decay of the biexciton. While efficiently suppressing the dephasing by phonon coupling was not achieved so far it could be reduced by tailoring the temporal pulse shape or using an adiabatic drive with a strongly chirped laser pulse. In addition, a square temporal pulse shape allows shorter time delays between the pulses without them overlapping and therefore reduces the impact of spontaneous decay.

Further increasing the delay results in a higher observed intensity due to radiative decay before the stimulation pulse arrives. Moreover, a second excitation of the biexciton becomes possible reaching its maximum for a delay of $\sim 1.4\tau_X$ with $\sim 11\%$ higher emission intensity. For longer delays $\geq 3.5\tau_X$ the probability that the full cascaded decay has happened before the second laser pulse arrives becomes higher and the biexciton emission intensity approaches the level of the single excitation.

While the biexciton emission allows us to study the efficiency of the stimulated drive of the biexciton-exciton transition we employ a co-polarized configuration in the measurement setup to investigate the ability of the scheme to deterministically set the polarization of the photon emitted by the exciton decay. The two decay channels of the QD system are either H or V linearly polarized and have equal probability. Introducing a linear polarizer in the detection path of the optical setup, therefore, reduces the signal of the collected photons by 50%. On the other hand, if the polarization of stimulation laser pulse is aligned with one of the polarization axes of the exciton, the decay channel is actively set. The emission intensity of the exciton for this case as a function of the pulse delay is presented in Fig. 6.10c. The stimulation light field does not affect the quantum ladder system for negative time delays since the biexciton state is not yet prepared and the decay path and consequently the polarization is randomly set. For the optimum delay of $0.03\tau_X$, the detected emission intensity is increased by 89% nearly reaching twice the initial value proofing the ability to deterministically define the polarization of the emitted single photon. Further improvement can be achieved by tailoring shorter pulses with a rectangular temporal shape to allow a smaller delay between the two pulses to lower the probability for spontaneous decay of the biexciton. Another reason for the small deviation from the ideal case can be caused by the non-perfect alignment of the polarization axes.

Since the two-photon excitation of the biexciton greatly improves the single-photon
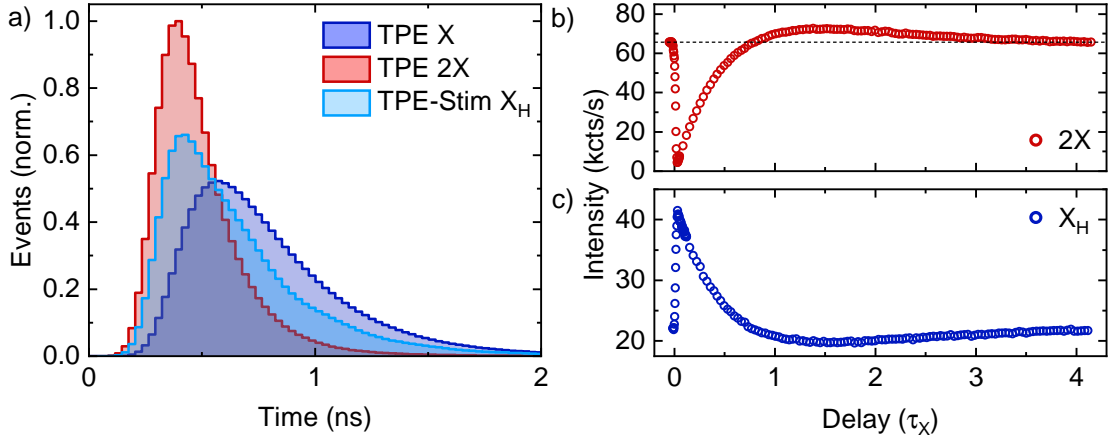
Figure 6.10 | Temporal dependence of the stimulation pulse a, Time-resolved PL measurement of the cascaded emission. **b**, Emission intensity as a function of the stimulation pulse delay of the biexciton decay **c**, and of the exciton decay in a co-polarized setup.

purity of the emission of the cascaded decay, we continue to investigate the impact of the additional stimulation light field on the purity. Our simulations show a decrease of the second-order coherence by nearly three orders of magnitude compared to a resonantly driven two-level system in accordance with previous findings for two-photon excitation (Fig. 6.11a). The second pulse only impacts the purity for very short time delays where the two pulses overlap and interact with the QD simultaneously. Thus, the stimulated drive enables a fast decay of the system to the ground state facilitating re-excitation of the biexciton. This leads to a trade-off between the obtainable single-photon purity of this excitation scheme and the efficiency of the stimulated drive. However, the ideal efficiency is already reached in the falling edge of the peak where the single-photon purity exhibits an improvement by up to two orders of magnitude. Further improvement can be realized by shaping the employed pulses so that the temporal overlap is reduced for even shorter delays by for example using a rectangular pulse shape. To verify our theoretical findings we perform autocorrelation measurements of the emitted photons of the exciton decay. The delay between the two pulses is chosen to fit the point of maximum efficiency of the stimulated drive ($\tau = 0.03\tau_X$). The obtained histogram is presented in Fig. 6.11b with a logarithmic scale on the y-axis to emphasize the vanishing peak at zero time delay. To eliminate the impact of a back reflection in the optical setup

which caused additional events at the time delays of interest the repetition rate of the laser is artificially reduced by a synced fast switching acousto-optic modulator. Non-perfect suppression of the cut-out pulses leads only to minor peaks in the correlation histogram and can be omitted in the analysis of the data. To extract the degree of second-order coherence we determine the peak area by summing up all events in a time window of $5.5\,\text{ns}$ around each peak center. The measured purity with $g^{(2)}(0) = (4.2 \pm 2.3) \cdot 10^{-4}$ is in good agreement with our simulations proofing the maintained property of the excitation scheme to largely suppress re-excitation.
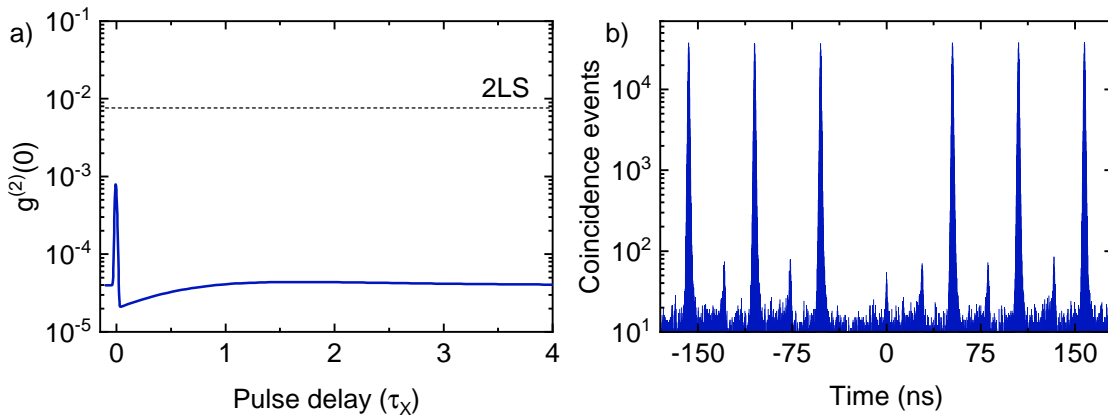
Figure 6.11 | Single-photon purity of the stimulated excitation method a, Simulated degree of second-order coherence. The two pulse excitation scheme enables an up to two orders of magnitude lower $g^{(2)}(0)$ compared to a resonantly driven two-level system (dashed line). **b**, Measured second-order coherence function.

Finally, we investigate the impact of the stimulation pulse on the indistinguishability of the emitted photons. For this, the excitation and stimulation parameters are set as described before while the double pulse is applied again with a delay of $3.3\,\text{ns}$ after the first excitation. The generated photons are sent through an unbalanced Mach-Zehnder interferometer to compensate the time delay and the HOM visibility is determined from the correlation histogram measured at the two outputs of the setup. The center quintuplet of the histogram is presented in Fig. 6.12a. Considering the vanishing center peak indicates a high degree of indistinguishability. Careful analysis of the respective peak areas gives us a raw HOM visibility of $V_{\text{HOM}} = 86.4^{+0.9}_{-1.2}\%$. In conclusion, the stimulated drive of the biexciton-exciton transition after the deterministic preparation of the QD in the biexciton state effectively eliminates the timing jitter suffered by the exciton decay and thus restores the ability of such a

quantum system to generate single photons with excellent indistinguishability. In addition, this excitation method allows further analysis of the consequence of the timing jitter by varying the delay between the two pulses, which provides a turning knob to influence the effective lifetime of the biexciton. The measured HOM visibility as a function of the pulse delay is presented in Fig. 6.12b. In the case where the stimulation pulse arrives before the biexciton is excited, we observe an indistinguishability of $V_{\mathrm{HOM}} = 48.6^{+2.4}_{-2.8}\%$ matching the case of sole two-photon excitation within the error $V_{\mathrm{HOM,TPE}} = 50.1^{+2.3}_{-2.7}\%$ (dashed line). Here, the stimulation light field cannot effectively interact with the quantum ladder system since it is energetically far detuned from the exciton and two-photon resonances and the lifetime of the biexciton is not affected. Increasing the delay between the pulses improves the achieved indistinguishability as soon as the two light fields overlap in time. The maximum is found at the point where the pulses are mostly separated, and at the same time, the delay is still short enough to suppress spontaneous decay of the biexciton ($\tau = 0.03\tau_X$). Further increasing the temporal separation increases the probability of a complete cascaded decay to the ground state and biexciton re-excitation events by the second laser pulse introducing an effective longer lifetime with the consequence of a reduced HOM visibility. Those events gain more importance with larger delay leading to a minimum in observed photon indistinguishability of $V_{\mathrm{HOM,TPE}} = 29.6^{+2.6}_{-2.8}\%$ indicating an effective prolonged lifetime of the biexciton. For larger time delays $\tau \geq 3.5\tau_X$ the population of the system is nearly always decayed to the ground state disabling any effect of the stimulation light field. Theoretical calculations of the photon indistinguishability as a function of the pulse delay (purple line) result in the same behavior in good agreement with the experimental results. However, the overall HOM visibility exceeds the values extracted from the experiment. We attribute this deviation to the neglection of any dephasing in the theoretical model. While coupling to LA phonons during the excitation and stimulation processes is always present and limits the maximum fidelity of the resonant state preparation, charge and spin noise in the QD environment introduce spectral wandering reducing the obtainable indistinguishability. To study the general impact of those dephasing channels, we introduce a phenomenological pure dephasing rate γ_{deph} acting on both excited states with the same strength. This is addressed by adding the two collapse operators $c_{2X} = \sqrt{\gamma_{deph}} \left| 2X \right\rangle \left\langle 2X \right|$ and $c_X = \sqrt{\gamma_{deph}} \left| X \right\rangle \left\langle X \right|$. The calculated HOM

visibility for the dephasing rates from $\gamma_{deph} = 0.05\gamma_X$ to $0.20\gamma_X$ in steps of $0.05\gamma_X$ are presented in Fig. 6.12b as the blue, green, yellow and red lines, respectively. The overall trend is maintained for all cases, while a faster dephasing leads to a lowered indistinguishability of the generated single photons. The remaining slight difference of experiment and theory stems from the simplification of the dephasing, for example, identical rates for both transitions. It is possible that the two charge configurations in the QD couple differently to the charge noise. Moreover, the impact of phonons depends strongly on the drive dynamics, which differ for the two-photon excitation and the stimulated drive. To take into account such fine details, further study of the underlying processes is necessary.
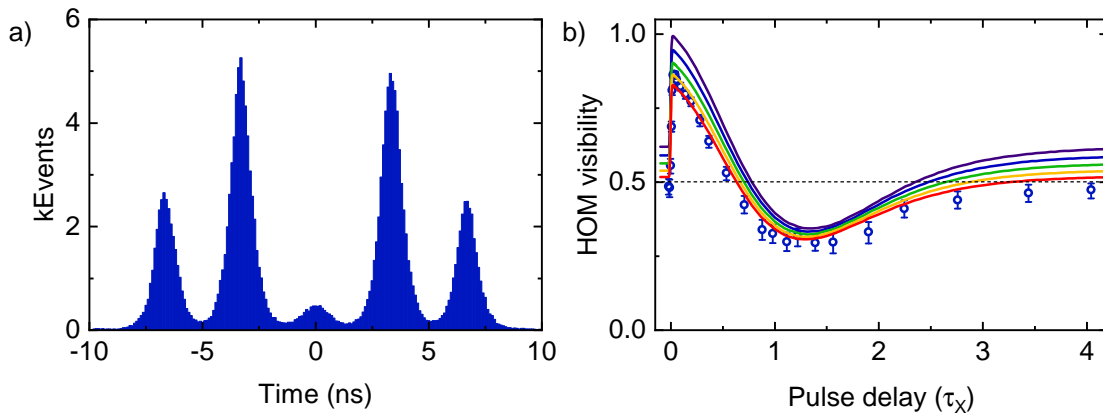
Figure 6.12 | Highly indistinguishable photons generated by the stimulated excitation scheme a, HOM correlation histogram from the exciton emission. **b**, Measured (circles) and simulated (lines) HOM visibility as a function of the stimulation pulse delay. A phenomenological dephasing included in the theoretical model reduces the indistinguishability over the whole range.

To modify the phonon dephasing during the excitation process in the experiment, advanced pulse shaping techniques allowing arbitrary temporal shapes can be employed, however, this is beyond the scope of this thesis. On the other hand, we investigate the indistinguishability of single photons emitted by the resonantly driven exciton transition and vary the time delay between the subsequent executions of the stimulated drive scheme to verify the indication from our simulations that charge noise is one of the main limiting factors of the achieved indistinguishability.
We conduct the following experiments on the same QD that was investigated before allowing direct comparison between the methods of excitation. The emission of the

exciton decay prepared by a single pulse in resonance with the transition allows us to determine the maximum achievable indistinguishability for the QD under investigation. The QD's energy level structure represents in this case a simple quantum two-level system suppressing additional timing jitter of the decay after preparation. It is therefore capable of serving as a source of single photons with near-unity indistinguishability. However, the system is still exposed to the identical sources of dephasing as for the stimulated excitation scheme [Tho16]. To acquire comparable data, we excite the system with two subsequent π-pulses separated by $3.3\,\text{ns}$ and send the generated photons to the unbalanced Mach-Zehnder interferometer to study the HOM visibility by correlating the two outputs. The center quintuplet of the resulting correlation histogram is presented in Fig. 6.13a. We extract the HOM visibility by comparing the center peak area with the two adjacent ones and obtain $V_{\text{HOM}} = 85.8^{+1.8}_{-2.2}\%$. This perfectly coincides with the value within the error reached for the optimum delay for the stimulated excitation method.
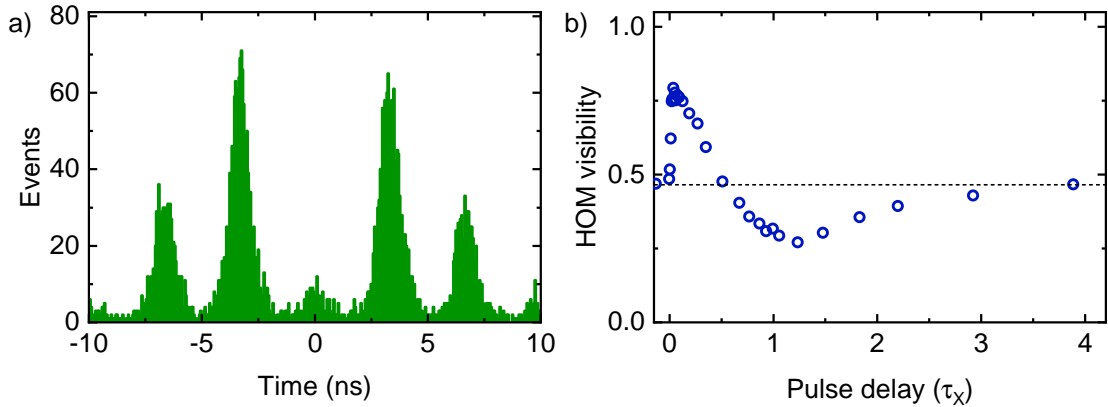
Figure 6.13 | Impact of spectral wandering on the achievable indistinguishability a, Two-photon interference histogram of the neutral exciton RF. **b**, Degree of indistinguishability obtained by the stimulated excitation scheme as a function of the stimulation pulse delay for a $13.1\,\text{ns}$ long delay between consecutive excitations.

Furthermore, we repeat the experiment employing the stimulated drive scheme but increase the time delay between subsequent excitation cycles to $13.1\,\text{ns}$ matching the repetition rate of the laser. Varying the time between the excitation and stimulation pulse and measuring the indistinguishability of the generated photons at each point delivers the same trend as observed before (Fig. 6.13b). Strikingly, the maximum HOM visibility is decreased to $V_{\text{HOM}} = 79.3 \pm 0.3\%$. In agreement with previous

studies, we conclude that spectral wandering caused by charge noise in the QD environment acting on nanosecond time scales is the main limiting factor of the obtainable indistinguishability. On the other hand, the results indicate the ability of the presented excitation scheme to generate highly indistinguishable single photons from a quantum three-level system with vanishing spectral wandering. Furthermore, our simulations yield a HOM visibility of $V_{\mathrm{HOM}} = 97.9\%$ for short time delays between excitation of the biexciton and stimulated drive to the exciton state with Gaussian pulses matching the experimental conditions while omitting any influence of dephasing. The indistinguishability could be further improved for short square pulses facilitating a shorter time delay between the two pulses without temporal overlap.

Chapter 7

Conclusions

In this thesis, we introduced epitaxial QDs as a clean optically active quantum system hosted in a semiconductor chip. Their discrete level structure enables to treat them as a quantum two- or four-level system, providing a platform to explore quantum optical phenomena such as RF and Rabi oscillations. With this at hand, we achieved a deeper understanding of the nature of light emitted by such a system and explored the impact of the excitation process on the properties of the generated photons.

In chapter 2 we outlined the growth process via MBE for two different kind of QDs. The formation of InGaAs QDs is driven by strain relaxation induced by lattice mismatch with the GaAs substrate. While the GaAs QDs are grown by first etching nanoholes in the AlGaAs substrate with an aluminum droplet followed by filling those holes with GaAs. Due to the nanometer sized islands of direct semiconductors embedded in a matrix with larger band gap a discrete energy level structure of the confined charge carriers is created. The growth process facilitates direct implementation of additional functional layers in the sample design. Including a diode structure encapsulating the QDs with small separation to the negatively charged contact enables deterministic adjustment of the ground state. Utilizing this, the QD can either serve as a true two-level system when enabling the negative trion

transition or as a four-level system with cascaded decay from the biexciton state to the ground state given by the uncharged QD.

Interaction of this system with a resonant light field, introduced in chapter 3, induces oscillatory behaviour of the ground and excited state population, known as Rabi oscillations. A short laser pulse with area π thus inverts the state population enabling deterministic and coherent excited state preparation followed by spontaneous decay under emission of a single photon. To harness those photons for further investigation we employed a cross-polarized micro-PL setup to separate them from the laser light. Additionally, precise control over the laser pulse duration and energy is achieved with a 4f-pulse shaper, which spectrally disperses a Fourier-limited femtosecond pulse and converts it into a picosecond pulse by selecting a narrow spectral window. Finally methods to perform time-resolved and correlation measurements of the emitted photons were described to gain insight into the excited state lifetime, the photon purity and indistinguishability.

To verify the quantum two-level character and quality of the QD, we examined the RF under strong continuous driving in chapter 4. The interaction of the two-level system and the light field creates new sets of dressed states, leading to the appearance of the Mollow triplet. Our observations in dependence of the light field's strength and detuning conform perfectly with the theoretical predictions.

On the other hand, performing this experiment in the Rayleight regime, i.e. weak driving, the RF gains a different character. A large component of the emission stems from a coherent scattering process of the laser off the two-level system, inheriting the spectral and coherence properties of the laser field. In chapter 5.1 we investigated the photon statistics of this weak coherent driving and found the interference of the coherently scattered light with the incoherent component of the emission as the basis of photon antibunching. This is an astonishing result considering the negligible fraction of the incoherent component and the Poissonian photon statistics of the coherent emission. However, pulsed excitation is required to deterministically generate single photons, which takes place in the strong driving regime. Here, the antibunching is fully provided by the incoherent emission, where the light field saturates the two-level system driving it to the excited state from where it spontaneously decays in the time frame of the excited state lifetime. Taking the statistic nature of the decay into account, we investigated the single-photon

purity in dependence of the excitation pulse duration in chapter 5.2. We observed a linear dependence between the second-order correlation function and pulse duration. The probability of a decay taking place already during the pulse-system interaction followed by a possible re-excitation increases with longer pulses, making a short pulse favorable to drive a pure single-photon source. In chapter 5.3 we found that those re-excitation processes become also more probable when applying a 2π pulse to the QD. In that case, the system is found in the excited state after absorbing half of the laser pulse. This on one hand increases the probability of a spontaneous decay and on the other hand the remaining half of the pulse, with area π, is perfectly capable to excite the system again leading to a subsequent emission of a second photon. Such two-photon emissions dominate for even π pulse areas over single-photon events. Having found this intrinsic limitation to single-photon purity we turned our attention to the cascaded emission of the biexciton in chapter 5.4. Coherently preparing the QD in the biexciton state via a two-photon excitation process enables the decay of the biexciton under emission of a single photon followed by the exciton decay leading to a second photon emission. Spectrally filtering one of those transitions reveals an up to two orders of magnitude lower second order coherence, since re-excitation becomes only possible after the complete decay to the ground state. This leads to a quadratic relationship between single-photon purity and the excitation pulse duration.

Another important property of quantum light sources is the indistinguishability of the emitted photons, that we investigated in chapter 6. For the first time, we demonstrated close to unity indistinguishability for the emission of GaAs QDs closing the performance gap to the well established InAs QDs. While those measurements were conducted under resonant excitation of the neutral exciton and trion transition, we found an intrinsic limitation to the photon indistinguishability for the cascaded emission from the biexciton state in chapter 6.2. The subsequent decay of the system introduces an inseparability of the two photon states that inherently reduces the maximum observable indistinguishability. In a simple picture this is understood with a final state broadening of the biexciton decay that translates to an inhomogeneous spectral broadening of the emitted photon. While the photon emission of the following exciton decay experiences a temporal jitter due to the statistical nature of the biexciton decay. This links the indistinguishability to the ratio of the state

lifetimes, that is limited to $V_{HOM} = 0.66$ for a typical lifetime ration of $\tau_X/\tau_{2X} = 2$. Finally, in chapter 6.3 we introduced a second laser pulse in the excitation scheme, that stimulates the transition between the biexciton and exciton state. With this additional pulse we gain a turning knob for the biexciton lifetime to experimentally investigate the limited photon indistinguishability of cascaded decays. Driving the population directly after initialization in the biexciton state to the exciton state artificially reduces the timing jitter of the exciton decay and therefore negates the reduction of the indistinguishability. In addition, this excitation scheme still benefits from the improved single-photon purity of the cascaded decay, spectral separation of the excitation lasers from the desired emission and enables funneling the decay path to a single branch, thus allowing selection of the polarization of the emitted photon.

The deeper understanding of the intrinsic limitations of the photon purity and indistinguishability gained within this thesis guides the way to ideal sources for single photons or entangled pairs. For applications that require single photons, like quantum key distribution or linear quantum computing, multi photon emission introduces errors that need to be minimised. On the other hand, a high emission rate is crucial for the efficiency. While this is governed by the excited state lifetime, that can be accelerated by the Purcell enhancement within a cavity it is achieved at the expense of higher probability for re-excitation when maintaining the excitation pulse duration. Proper adjustment of the excitation pulse or scheme can counter this effect while finally an inherent limit cannot be overcome and requires a deliberate trade-off between emission rate and purity. Since the cascaded emission of a QD generates a pair of entangled photons it is considered as a fundamental building block for a quantum repeater based on entanglement swapping. The operation of such a repeater strongly relies on the indistinguishability of the photons that can be enhanced by engineering the decay rate ratio through methods such as using an asymmetric cavity or applying an electric field.

Furthermore, our findings extend to any quantum emitter, such as color centers in diamond and silicon, trapped atoms or ions, since the underlying mechanisms are purely based on quantum two-, three- or four-level systems.

List of Publications

Fis17 K. A. Fischer*, <u>L. Hanschke</u>*, J. Wierzbowski, T. Simmet, C. Dory, J. J. Finley, J. Vučković, and K. Müller, Signatures of two-photon pulses from a quantum two-level system, Nature Phys **13**, 649 (2017).
Contribution: design and preparation of the experiment, data acquisition and analysis, revision of the manuscript

Fis18 K. A. Fischer, <u>L. Hanschke</u>, M. Kremser, J. J. Finley, K. Müller, and J. Vučković, Pulsed Rabi oscillations in quantum two-level systems: beyond the area theorem, Quantum Sci. and Technol. **3**, 014006 (2018).
Contribution: design and preparation of the experiment, data acquisition and analysis, revision of the manuscript

Han18 <u>L. Hanschke</u>*, K. A. Fischer*, S. Appel, D. Lukin, J. Wierzbowski, S. Sun, R. Trivedi, J. Vučković, J. J. Finley, and K. Müller, Quantum dot single-photon sources with ultra-low multi-photon probability, npj Quantum Inf **4**, 43 (2018).
Contribution: design and preparation of the experiment, data acquisition and analysis, writing and revision of the manuscript

Sch19 E. Schöll*, <u>L. Hanschke</u>*, L. Schweickert*, K. D. Zeuner, M. Reindl, S. F. Covre Da Silva, T. Lettner, R. Trotta, J. J. Finley, K. Müller, A. Rastelli, V. Zwiller, and K. D. Jöns, Resonance Fluorescence of GaAs Quantum Dots with Near-Unity Photon Indistinguishability, Nano Lett. **19**, 2404 (2019).
Contribution: preparation of the experiment, data acquisition and analysis, writing and revision of the manuscript

Han20 <u>L. Hanschke</u>*, L. Schweickert*, J. C. L. Carreño*, E. Schöll, K. D. Zeuner, T. Lettner, E. Z. Casalengua, M. Reindl, S. F. C. Da Silva, R. Trotta, J. J. Finley, A. Rastelli, E. Del Valle, F. P. Laussy, V. Zwiller, K. Müller, and K. D. Jöns,

Origin of Antibunching in Resonance Fluorescence, Phys. Rev. Lett. **125**, 170402 (2020).
Contribution: preparation of the experiment, data acquisition and analysis, writing and revision of the manuscript

Sch20 E. Schöll*, L. Schweickert*, <u>L. Hanschke</u>, K. D. Zeuner, F. Sbresny, T. Lettner, R. Trivedi, M. Reindl, S. F. Covre Da Silva, R. Trotta, J. J. Finley, J. Vučković, K. Müller, A. Rastelli, V. Zwiller, and K. D. Jöns, Crux of Using the Cascaded Emission of a Three-Level Quantum Ladder System to Generate Indistinguishable Photons, Phys. Rev. Lett. **125**, 233605 (2020).
Contribution: preparation of the experiment, data acquisition and analysis, revision of the manuscript

Gus21 C. Gustin*, <u>L. Hanschke</u>*, K. Boos*, J. R. A. Müller, M. Kremser, J. J. Finley, S. Hughes, and K. Müller, Highresolution spectroscopy of a quantum dot driven bichromatically by two strong coherent fields, Phys. Rev. Research **3**, 013044 (2021).
Contribution: concept, design and preparation of the experiment, data acquisition and analysis, writing and revision of the manuscript

Sbr22 F. Sbresny*, <u>L. Hanschke</u>*, E. Schöll, W. Rauhaus, B. Scaparra, K. Boos, E. Zubizarreta Casalengua, H. Riedl, E. Del Valle, J. J. Finley, K. D. Jöns, and K.Müller, Stimulated generation of indistinguishable single photons from a quantum ladder system, Phys. Rev. Lett. **128**, 093603 (2022).
Contribution: concept, design and preparation of the experiment, data acquisition and analysis, writing and revision of the manuscript

*contributed equally

Bibliography

[Aar11a] S. Aaronson, *A linear-optical proof that the permanent is #P-hard*, Proceedings of the Royal Society A: Mathematical, Physical and Engineering Sciences **467**, 3393–3405 (2011) (Cited on page 65.)

[Aar11b] S. Aaronson, A. Arkhipov, *The Computational Complexity of Linear Optics*, Proceedings of the forty-third annual ACM symposium on Theory of computing pages 333–342 (2011) (Cited on page 65.)

[Adl98] F. Adler, M. Geiger, A. Bauknecht, D. Haase, P. Ernst, A. Dörnen, F. Scholz, H. Schweizer, *Self-assembled InAs/GaAs quantum dots under resonant excitation*, J. Appl. Phys. **83** (1998) (Cited on page 68.)

[Aki06] I. A. Akimov, J. T. Andrews, F. Henneberger, *Stimulated Emission from the Biexciton in a Single Self-Assembled II-VI Quantum Dot*, Physical Review Letters **96**, 067 401 (2006) (Cited on page 76.)

[Ali04] M. S. Alias, A. A. M. Hassan, *Optical properties of GaAs/AlGaAs DBR mirror for optoelectronics devices*, Solid State Science and Technology **12** (2004) (Cited on page 15.)

[All75] L. Allen, J. Eberly, *Optical resonances and two-level atoms* (Wiley, New York, 1975), ISBN 0-486-65533-4 (Cited on pages 18, 20, and 48.)

[All05] B. Alloing, C. Zinoni, V. Zwiller, L. H. Li, C. Monat, M. Gobet, G. Buchs, A. Fiore, E. Pelucchi, E. Kapon, *Growth and characterization of single quantum dots emitting at 1300 nm*, Applied Physics Letters **86**, 101 908 (2005) (Cited on page 4.)

[Ard14] P. L. Ardelt, L. Hanschke, K. A. Fischer, K. Müller, A. Kleinkauf, M. Koller, A. Bechtold, T. Simmet, J. Wierzbowski, H. Riedl, G. Abstreiter, J. J.

Finley, *Dissipative preparation of the exciton and biexciton in self-assembled quantum dots on picosecond time scales*, Physical Review B - Condensed Matter and Materials Physics **90**, 1–5 (2014) (Cited on page 66.)

[Aru19] F. Arute, K. Arya, R. Babbush, D. Bacon, J. C. Bardin, R. Barends, R. Biswas, S. Boixo, F. G. S. L. Brandao, D. A. Buell, B. Burkett, Y. Chen, Z. Chen, B. Chiaro, R. Collins, W. Courtney, A. Dunsworth, E. Farhi, B. Foxen, A. Fowler, C. Gidney, M. Giustina, R. Graff, K. Guerin, S. Habegger, M. P. Harrigan, M. J. Hartmann, A. Ho, M. Hoffmann, T. Huang, T. S. Humble, S. V. Isakov, E. Jeffrey, Z. Jiang, D. Kafri, K. Kechedzhi, J. Kelly, P. V. Klimov, S. Knysh, A. Korotkov, F. Kostritsa, D. Landhuis, M. Lindmark, E. Lucero, D. Lyakh, S. Mandrà, J. R. McClean, M. McEwen, A. Megrant, X. Mi, K. Michielsen, M. Mohseni, J. Mutus, O. Naaman, M. Neeley, C. Neill, M. Y. Niu, E. Ostby, A. Petukhov, J. C. Platt, C. Quintana, E. G. Rieffel, P. Roushan, N. C. Rubin, D. Sank, K. J. Satzinger, V. Smelyanskiy, K. J. Sung, M. D. Trevithick, A. Vainsencher, B. Villalonga, T. White, Z. J. Yao, P. Yeh, A. Zalcman, H. Neven, J. M. Martinis, *Quantum supremacy using a programmable superconducting processor*, Nature **574**, 505–510 (2019) (Cited on page 2.)

[Asp76] D. E. Aspnes, *GaAs lower conduction-band minima: Ordering and properties*, Physical Review B **14**, 5331–5343 (1976) (Cited on page 10.)

[Asp81] A. Aspect, P. Grangier, G. Roger, *Experimental Tests of Realistic Local Theories via Bell's Theorem*, Physical Review Letters **47**, 460–463 (1981) (Cited on page 1.)

[Asp82] A. Aspect, P. Grangier, G. Roger, *Experimental Realization of Einstein-Podolsky-Rosen-Bohm Gedankenexperiment: A New Violation of Bell's Inequalities*, Physical Review Letters **49**, 91–94 (1982) (Cited on page 1.)

[Bar14] R. Barends, J. Kelly, A. Megrant, A. Veitia, D. Sank, E. Jeffrey, T. C. White, J. Mutus, A. G. Fowler, B. Campbell, Y. Chen, Z. Chen, B. Chiaro, A. Dunsworth, C. Neill, P. O'Malley, P. Roushan, A. Vainsencher, J. Wenner, A. N. Korotkov, A. N. Cleland, J. M. Martinis, *Superconducting quantum*

circuits at the surface code threshold for fault tolerance, Nature **508**, 500–503 (2014) (Cited on page 2.)

[Bas92] T. Basché, W. E. Moerner, M. Orrit, H. Talon, *Photon antibunching in the fluorescence of a single dye molecule trapped in a solid*, Physical Review Letters **69**, 1516–1519 (1992) (Cited on page 2.)

[Bay02a] M. Bayer, A. Forchel, *Temperature dependence of the exciton homogeneous linewidth in $In_{0.60}Ga_{0.40}As/GaAs$ self-assembled quantum dots*, Physical Review B **65**, 041 308 (2002) (Cited on page 22.)

[Bay02b] M. Bayer, G. Ortner, O. Stern, A. Kuther, A. A. Gorbunov, A. Forchel, P. Hawrylak, S. Fafard, K. Hinzer, T. L. Reinecke, S. N. Walck, J. P. Reithmaier, F. Klopf, F. Schäfer, *Fine structure of neutral and charged excitons in self-assembled In(Ga)As/(Al) GaAs quantum dots*, Physical Review B - Condensed Matter and Materials Physics **65**, 195 315 (2002) (Cited on pages 12, 67, and 76.)

[Ben80] P. Benioff, *The computer as a physical system: A microscopic quantum mechanical Hamiltonian model of computers as represented by Turing machines*, Journal of Statistical Physics **22**, 563–591 (1980) (Cited on page 1.)

[Ben84] C. H. Bennett, G. Brassard, *Quantum cryptography: Public key distribution and coin tossing*, Theoretical Computer Science **560**, 7–11 (1984) (Cited on page 1.)

[Ben08] J. Benhelm, G. Kirchmair, C. F. Roos, R. Blatt, *Towards fault-tolerant quantum computing with trapped ions*, Nature Physics **4**, 463–466 (2008) (Cited on page 2.)

[Ber07] T. Berstermann, T. Auer, H. Kurtze, M. Schwab, D. R. Yakovlev, M. Bayer, J. Wiersig, C. Gies, F. Jahnke, D. Reuter, A. D. Wieck, *Systematic study of carrier correlations in the electron-hole recombination dynamics of quantum dots*, Physical Review B - Condensed Matter and Materials Physics **76**, 1–8 (2007) (Cited on page 68.)

[Bim99] D. Bimberg, M. Grundmann, N. N. Ledentsov, *Quantum dot heterostructures* (John Wiley & Sons, 1999) (Cited on pages 7 and 11.)

[Blo12] I. Bloch, J. Dalibard, S. Nascimbène, *Quantum simulations with ultracold quantum gases*, Nature Physics **8**, 267–276 (2012) (Cited on page 2.)

[Bou15] S. Bounouar, M. Müller, A. M. Barth, M. Glässl, V. M. Axt, P. Michler, *Phonon-assisted robust and deterministic two-photon biexciton preparation in a quantum dot*, Physical Review B - Condensed Matter and Materials Physics **91**, 1–5 (2015) (Cited on page 66.)

[Bra59] R. Braunstein, *Intervalence band transitions in gallium arsenide*, Journal of Physics and Chemistry of Solids **8**, 280–282 (1959) (Cited on page 11.)

[Bra00] G. Brassard, N. Lütkenhaus, T. Mor, B. C. Sanders, *Limitations on Practical Quantum Cryptography*, Physical Review Letters **85**, 1330–1333 (2000) (Cited on page 2.)

[Bro56] R. H. Brown, R. Q. Twiss, *Correlation between Photons in two Coherent Beams of Light*, Nature **177**, 27–29 (1956) (Cited on page 26.)

[Bro00] R. Brouri, A. Beveratos, J.-P. Poizat, P. Grangier, *Photon antibunching in the fluorescence of individual color centers in diamond*, Optics Letters **25**, 1294 (2000) (Cited on page 2.)

[Bru90] R. Bruce, D. Clark, S. Eicher, *Low resistance Pd/Zn/Pd Au ohmic contacts to P-type GaAs*, Journal of Electronic Materials **19**, 225–229 (1990) (Cited on page 13.)

[Bru94] K. Brunner, G. Abstreiter, G. Böhm, G. Tränkle, G. Weimann, *Sharp-Line Photoluminescence and Two-Photon Absorption of Zero-Dimensional Biexcitons in a GaAs/AlGaAs Structure*, Physical Review Letters **73**, 1138–1141 (1994) (Cited on pages 12 and 61.)

[Car85] H. J. Carmichael, *Photon Antibunching and Squeezing for a Single Atom in a Resonant Cavity*, Physical Review Letters **55**, 2790–2793 (1985) (Cited on page 44.)

[Car93] H. Carmichael, *An Open Systems Approach to Quantum Optics: Lectures Presented at the Université Libre de Bruxelles, October 28 to November 4 1991*, number v.18 in Lecture Notes in Physics Monographs (Springer

Berlin / Heidelberg, Berlin, Heidelberg, 1993), 1st ed edition, ISBN 978-3-540-56634-2 978-3-540-47620-7 (Cited on page 49.)

[Cas14] S. Castelletto, B. C. Johnson, V. Ivády, N. Stavrias, T. Umeda, A. Gali, T. Ohshima, *A silicon carbide room-temperature single-photon source*, Nature Materials **13**, 151–156 (2014) (Cited on page 3.)

[Che16] D. Chen, G. R. Lander, K. S. Krowpman, G. S. Solomon, E. B. Flagg, *Characterization of the local charge environment of a single quantum dot via resonance fluorescence*, Physical Review B **93**, 115 307 (2016) (Cited on page 42.)

[Che18] Y. Chen, M. Zopf, R. Keil, F. Ding, O. G. Schmidt, *Highly-efficient extraction of entangled photons from quantum dots using a broadband optical antenna*, Nature Communications **9**, 1–7 (2018) (Cited on page 66.)

[Cla74] J. F. Clauser, *Experimental distinction between the quantum and classical field-theoretic predictions for the photoelectric effect*, Physical Review D **9**, 853–860 (1974) (Cited on page 1.)

[CT77] C. Cohen-Tannoudji, S. Reynaud, *Dressed-atom description of resonance fluorescence and absorption spectra of a multi-level atom in an intense laser beam*, Journal of Physics B: Atomic and Molecular Physics **10**, 345–363 (1977) (Cited on page 34.)

[CT98] C. Cohen-Tannoudji, J. Dupont-Roc, G. Grynberg, *Atom-photon interactions: basic processes and applications* (John Wiley & Sons, 1998) (Cited on pages 18, 19, 34, and 35.)

[Dad16] A. C. Dada, T. S. Santana, R. N. E. Malein, A. Koutroumanis, Y. Ma, J. M. Zajac, J. Y. Lim, J. D. Song, B. D. Gerardot, *Indistinguishable single photons with flexible electronic triggering*, Optica **3**, 493 (2016) (Cited on page 49.)

[Dal08] P. A. Dalgarno, J. M. Smith, J. McFarlane, B. D. Gerardot, K. Karrai, A. Badolato, P. M. Petroff, R. J. Warburton, *Coulomb interactions in single charged self-assembled quantum dots: Radiative lifetime and recombination energy*, Physical Review B **77**, 245 311 (2008) (Cited on page 26.)

[Dav14a] M. Davanço, C. S. Hellberg, S. Ates, A. Badolato, K. Srinivasan, *Multiple time scale blinking in InAs quantum dot single-photon sources*, Physical Review B - Condensed Matter and Materials Physics **89**, 1–5 (2014) (Cited on page 67.)

[Dav14b] M. Davanço, C. S. Hellberg, S. Ates, A. Badolato, K. Srinivasan, *Multiple time scale blinking in InAs quantum dot single-photon sources*, Physical Review B **89**, 161 303 (2014) (Cited on page 3.)

[Deb12] A. Debnath, C. Meier, B. Chatel, T. Amand, *Chirped laser excitation of quantum dot excitons coupled to a phonon bath*, Physical Review B **86**, 161 304 (2012) (Cited on page 52.)

[Del12] E. Del Valle, A. Gonzalez-Tudela, F. P. Laussy, C. Tejedor, M. J. Hartmann, *Theory of frequency-filtered and time-resolved N-photon correlations*, Physical Review Letters **109**, 183 601 (2012) (Cited on page 46.)

[Die82] D. Dieks, *Communication by EPR devices*, Physics Letters A **92**, 271–272 (1982) (Cited on page 1.)

[Din16a] X. Ding, Y. He, Z. C. Duan, N. Gregersen, M. C. Chen, S. Unsleber, S. Maier, C. Schneider, M. Kamp, S. Höfling, C. Y. Lu, J. W. Pan, *On-Demand Single Photons with High Extraction Efficiency and Near-Unity Indistinguishability from a Resonantly Driven Quantum Dot in a Micropillar*, Physical Review Letters **116**, 1–6 (2016) (Cited on pages 42 and 66.)

[Din16b] X. Ding, Y. He, Z.-C. Duan, N. Gregersen, M.-C. Chen, S. Unsleber, S. Maier, C. Schneider, M. Kamp, S. Höfling, C.-Y. Lu, J.-W. Pan, *On-Demand Single Photons with High Extraction Efficiency and Near-Unity Indistinguishability from a Resonantly Driven Quantum Dot in a Micropillar*, Physical Review Letters **116**, 020 401 (2016) (Cited on page 3.)

[Din23] X. Ding, Y.-P. Guo, M.-C. Xu, R.-Z. Liu, G.-Y. Zou, J.-Y. Zhao, Z.-X. Ge, Q.-H. Zhang, H.-L. Liu, L.-J. Wang, M.-C. Chen, H. Wang, Y.-M. He, Y.-H. Huo, C.-Y. Lu, J.-W. Pan, *High-efficiency single-photon source above the loss-tolerant threshold for efficient linear optical quantum computing* (2023), arXiv:2311.08347 [quant-ph] (Cited on page 3.)

[DS21]   S. F. C. Da Silva, G. Undeutsch, B. Lehner, S. Manna, T. M. Krieger, M. Reindl, C. Schimpf, R. Trotta, A. Rastelli, *GaAs quantum dots grown by droplet etching epitaxy as quantum light sources*, Applied Physics Letters **119**, 120 502 (2021) (Cited on page 8.)

[Dya08] M. I. Dyakonov, *Spin physics in semiconductors* (Springer Series in Solid-State Sciences, 2008) (Cited on page 11.)

[Ehr60] H. Ehrenreich, *Band Structure and Electron Transport of GaAs*, Physical Review **120**, 1951–1963 (1960) (Cited on page 11.)

[Ein05] A. Einstein, *Über einen die Erzeugung und Verwandlung des Lichtes betreffenden heuristischen Gesichtspunkt*, Annalen der Physik **322**, 132–148 (1905) (Cited on page 1.)

[Eke91] A. K. Ekert, *Quantum cryptography based on Bell's theorem*, Physical Review Letters **67**, 661–663 (1991) (Cited on page 1.)

[Fea89] H. Fearn, R. Loudon, *Theory of two-photon interference*, Journal of the Optical Society of America B **6**, 917 (1989) (Cited on page 28.)

[Fin01a] F. Findeis, M. Baier, E. Beham, A. Zrenner, G. Abstreiter, *Photocurrent and photoluminescence of a single self-assembled quantum dot in electric fields*, Applied Physics Letters **78**, 2958–2960 (2001) (Cited on pages 12 and 15.)

[Fin01b] J. J. Finley, A. D. Ashmore, A. Lemaître, D. J. Mowbray, M. S. Skolnick, I. E. Itskevich, P. A. Maksym, M. Hopkinson, T. F. Krauss, *Charged and neutral exciton complexes in individual self-assembled In(Ga)As quantum dots*, Physical Review B **63**, 073 307 (2001) (Cited on pages 7 and 11.)

[Fis16] K. A. Fischer, K. Müller, K. G. Lagoudakis, J. Vučković, *Dynamical modeling of pulsed two-photon interference*, New Journal of Physics **18**, 113 053 (2016) (Cited on page 50.)

[Fis17] K. A. Fischer, L. Hanschke, J. Wierzbowski, T. Simmet, C. Dory, J. J. Finley, J. Vučković, K. Müller, *Signatures of two-photon pulses from a quantum*

two-level system, Nature Physics **13**, 649—-654 (2017) (Cited on pages 5, 41, and 49.)

[Fis18a] K. A. Fischer, L. Hanschke, M. Kremser, J. J. Finley, K. Müller, J. Vučković, *Pulsed Rabi oscillations in quantum two-level systems: Beyond the area theorem*, Quantum Science and Technology **43** (2018) (Cited on pages 5, 41, 48, 49, and 61.)

[Fis18b] K. A. Fischer, R. Trivedi, D. Lukin, *Particle emission from open quantum systems*, Physical Review A **98**, 023 853 (2018) (Cited on page 72.)

[Fis18c] K. A. Fischer, R. Trivedi, V. Ramasesh, I. Siddiqi, J. Vučković, *Scattering into one-dimensional waveguides from a coherently-driven quantum-optical system*, Quantum **2**, 69 (2018), arXiv:1710.02875 [quant-ph] (Cited on pages 65 and 71.)

[Fli01] T. Flissikowski, A. Hundt, M. Lowisch, M. Rabe, F. Henneberger, *Photon beats from a single semiconductor quantum dot*, Physical Review Letters **86**, 3172–3175 (2001) (Cited on page 67.)

[Fox06] M. Fox, *Quantum optics: an introduction* (Oxford University Press, Oxford, 2006), ISBN 978-0-19-856672-4 (Cited on pages 19, 27, and 48.)

[Fox24] A. M. Fox, *Solid-State Quantum Emitters*, Advanced Quantum Technologies page 2300390 (2024) (Cited on page 48.)

[Fre72] S. J. Freedman, J. F. Clauser, *Experimental Test of Local Hidden-Variable Theories*, Physical Review Letters **28**, 938–941 (1972) (Cited on page 1.)

[Fry00a] P. W. Fry, J. J. Finley, L. R. Wilson, A. Lemaître, D. J. Mowbray, M. S. Skolnick, M. Hopkinson, G. Hill, J. C. Clark, *Electric-field-dependent carrier capture and escape in self-assembled InAs/GaAs quantum dots*, Applied Physics Letters **77**, 4344–4346 (2000) (Cited on pages 8, 12, and 15.)

[Fry00b] P. W. Fry, I. E. Itskevich, D. J. Mowbray, M. S. Skolnick, J. J. Finley, J. A. Barker, E. P. O'Reilly, L. R. Wilson, I. A. Larkin, P. A. Maksym, M. Hopkinson, M. Al-Khafaji, J. P. R. David, A. G. Cullis, G. Hill, J. C. Clark,

Inverted Electron-Hole Alignment in InAs-GaAs Self-Assembled Quantum Dots, Physical Review Letters **84**, 733–736 (2000) (Cited on pages 8 and 14.)

[Gae16] J. Gaebler, T. Tan, Y. Lin, Y. Wan, R. Bowler, A. Keith, S. Glancy, K. Coakley, E. Knill, D. Leibfried, D. Wineland, *High-Fidelity Universal Gate Set for $^9Be^+$ Ion Qubits*, Physical Review Letters **117**, 060 505 (2016) (Cited on page 2.)

[Gaz13] O. Gazzano, S. Michaelis De Vasconcellos, C. Arnold, A. Nowak, E. Galopin, I. Sagnes, L. Lanco, A. Lemaître, P. Senellart, *Bright solid-state sources of indistinguishable single photons*, Nature Communications **4** (2013) (Cited on page 66.)

[Gib73] H. M. Gibbs, *Incoherent Resonance Fluorescence from a Rb Atomic Beam Excited by a Short Coherent Optical Pulse*, Physical Review A **8**, 446–455 (1973) (Cited on page 21.)

[Gis02] N. Gisin, G. Ribordy, W. Tittel, H. Zbinden, *Quantum cryptography*, Reviews of Modern Physics **74**, 145–195 (2002) (Cited on page 1.)

[Gol85] L. Goldstein, F. Glas, J. Y. Marzin, M. N. Charasse, G. Le Roux, *Growth by molecular beam epitaxy and characterization of InAs/GaAs strained-layer superlattices*, Applied Physics Letters **47**, 1099–1101 (1985) (Cited on pages 3 and 8.)

[Gri19] D. J. Griffiths, D. F. Schroeter, *Introduction to quantum mechanics* (Cambridge university press, 2019) (Cited on pages 19 and 34.)

[Grü19] P. Grünwald, *Effective second-order correlation function and single-photon detection*, New Journal of Physics **21**, 093 003 (2019) (Cited on page 28.)

[Gus18] C. Gustin, R. Manson, S. Hughes, *Spectral asymmetries in the resonance fluorescence of two-level systems under pulsed excitation*, Optics Letters **43**, 779 (2018) (Cited on pages 33 and 39.)

[Gé98] J. Gérard, B. Sermage, B. Gayral, B. Legrand, E. Costard, V. Thierry-Mieg, *Enhanced Spontaneous Emission by Quantum Boxes in a Monolithic*

Optical Microcavity, Physical Review Letters **81**, 1110–1113 (1998) (Cited on page 3.)

[Han18] L. Hanschke, K. A. Fischer, S. Appel, D. Lukin, J. Wierzbowski, S. Sun, R. Trivedi, J. Vučković, J. J. Finley, K. Müller, *Quantum dot single photon sources with ultra-low multi-photon probability*, npj Quantum Information **4** (2018) (Cited on pages 5 and 41.)

[Han20] L. Hanschke, L. Schweickert, J. C. L. Carreño, E. Schöll, K. D. Zeuner, T. Lettner, E. Z. Casalengua, M. Reindl, S. F. C. Da Silva, R. Trotta, J. J. Finley, A. Rastelli, E. Del Valle, F. P. Laussy, V. Zwiller, K. Müller, K. D. Jöns, *Origin of Antibunching in Resonance Fluorescence*, Physical Review Letters **125**, 170 402 (2020) (Cited on pages 4 and 41.)

[Haw99] P. Hawrylak, *Excitonic artificial atoms: Engineering optical properties of quantum dots*, Physical Review B **60**, 5597–5608 (1999) (Cited on pages 7, 11, and 12.)

[Haw03] P. Hawrylak, M. Korkusiński, *Electronic Properties of Self-Assembled Quantum Dots*, pages 25–92 (Springer Berlin Heidelberg, Berlin, Heidelberg, 2003), ISBN 978-3-540-39180-7 (Cited on page 11.)

[Hei54] W. Heitler, *The quantum theory of radiation* (Oxford University Press, London, 1954) (Cited on page 42.)

[Hen21] N. W. Hendrickx, W. I. L. Lawrie, M. Russ, F. Van Riggelen, S. L. De Snoo, R. N. Schouten, A. Sammak, G. Scappucci, M. Veldhorst, *A four-qubit germanium quantum processor*, Nature **591**, 580–585 (2021) (Cited on page 2.)

[Hey09a] C. Heyn, A. Stemmann, W. Hansen, *Dynamics of self-assembled droplet etching*, Applied Physics Letters **95** (2009) (Cited on page 10.)

[Hey09b] C. Heyn, A. Stemmann, T. Köppen, C. Strelow, T. Kipp, M. Grave, S. Mendach, W. Hansen, *Highly uniform and strain-free GaAs quantum dots fabricated by filling of self-assembled nanoholes*, Applied Physics Letters **94**, 2007–2010 (2009) (Cited on page 10.)

[Hey11] C. Heyn, *Kinetic model of local droplet etching*, Physical Review B - Condensed Matter and Materials Physics **83**, 1–5 (2011) (Cited on page 10.)

[Höf97] J. T. Höffges, H. W. Baldauf, T. Eichler, S. R. Helmfrid, H. Walther, *Heterodyne measurement of the fluorescent radiation of a single trapped ion*, Optics Communications **133**, 170–174 (1997) (Cited on page 45.)

[Hon87] C. K. Hong, Z. Y. Ou, L. Mandel, *Measurement of subpicosecond time intervals between two photons by interference*, Physical Review Letters **59**, 2044–2046 (1987) (Cited on page 28.)

[Hor89] M. A. Horne, A. Shimony, A. Zeilinger, *Two-particle interferometry*, Physical Review Letters **62**, 2209–2212 (1989) (Cited on page 1.)

[Hto02] H. Htoon, T. Takagahara, D. Kulik, O. Baklenov, A. L. Holmes, C. K. Shih, *Interplay of Rabi Oscillations and Quantum Interference in Semiconductor Quantum Dots*, Physical Review Letters **88**, 087 401 (2002) (Cited on page 3.)

[Hub18] D. Huber, M. Reindl, S. F. Covre Da Silva, C. Schimpf, J. Martín-Sánchez, H. Huang, G. Piredda, J. Edlinger, A. Rastelli, R. Trotta, *Strain-Tunable GaAs Quantum Dot: A Nearly Dephasing-Free Source of Entangled Photon Pairs on Demand*, Physical Review Letters **121**, 33 902 (2018) (Cited on pages 3, 66, and 68.)

[Huo13] Y. H. Huo, A. Rastelli, O. G. Schmidt, *Ultra-small excitonic fine structure splitting in highly symmetric quantum dots on GaAs (001) substrate*, Applied Physics Letters **102** (2013) (Cited on pages 10 and 68.)

[Hut95] B. Huttner, N. Imoto, N. Gisin, T. Mor, *Quantum cryptography with coherent states*, Physical Review A **51**, 1863–1869 (1995) (Cited on page 2.)

[Hwa03] W.-Y. Hwang, *Quantum Key Distribution with High Loss: Toward Global Secure Communication*, Physical Review Letters **91**, 057 901 (2003) (Cited on page 2.)

[Int09] P. M. Intallura, M. B. Ward, O. Z. Karimov, Z. L. Yuan, P. See, P. Atkinson, D. A. Ritchie, A. J. Shields, *Quantum communication using single*

photons from a semiconductor quantum dot emitting at a telecommunication wavelength, Journal of Optics A: Pure and Applied Optics **11**, 054 005 (2009) (Cited on page 4.)

[Iwa15] T. Iwasaki, F. Ishibashi, Y. Miyamoto, Y. Doi, S. Kobayashi, T. Miyazaki, K. Tahara, K. D. Jahnke, L. J. Rogers, B. Naydenov, F. Jelezko, S. Yamasaki, S. Nagamachi, T. Inubushi, N. Mizuochi, M. Hatano, *Germanium-Vacancy Single Color Centers in Diamond*, Scientific Reports **5**, 12 882 (2015) (Cited on page 2.)

[Iwa17] T. Iwasaki, Y. Miyamoto, T. Taniguchi, P. Siyushev, M. H. Metsch, F. Jelezko, M. Hatano, *Tin-Vacancy Quantum Emitters in Diamond*, Physical Review Letters **119**, 253 601 (2017) (Cited on page 2.)

[Jak05] D. Jaksch, P. Zoller, *The cold atom Hubbard toolbox*, Annals of Physics **315**, 52–79 (2005) (Cited on page 2.)

[Joh12] J. Johansson, P. Nation, F. Nori, *QuTiP: An open-source Python framework for the dynamics of open quantum systems*, Computer Physics Communications **183**, 1760–1772 (2012) (Cited on page 65.)

[Joh13] J. Johansson, P. Nation, F. Nori, *QuTiP 2: A Python framework for the dynamics of open quantum systems*, Computer Physics Communications **184**, 1234–1240 (2013) (Cited on pages 41, 53, and 65.)

[Kam01] H. Kamada, H. Gotoh, J. Temmyo, T. Takagahara, H. Ando, *Exciton Rabi Oscillation in a Single Quantum Dot*, Physical Review Letters **87**, 246 401 (2001) (Cited on page 3.)

[Kan17] A. Kandala, A. Mezzacapo, K. Temme, M. Takita, M. Brink, J. M. Chow, J. M. Gambetta, *Hardware-efficient variational quantum eigensolver for small molecules and quantum magnets*, Nature **549**, 242–246 (2017) (Cited on page 2.)

[Kap24] F. Kappe, R. Schwarz, Y. Karli, T. Bracht, V. M. Axt, A. Rastelli, V. Remesh, D. E. Reiter, G. Weihs, *Keeping the photon in the dark: Enabling full quantum dot control by chirped pulses and magnetic fields* (2024), arXiv:2404.10708 [cond-mat, physics:quant-ph] (Cited on page 12.)

[Kim76]   H. J. Kimble, L. Mandel, *Theory of resonance fluorescence*, Physical Review A **13**, 2123–2144 (1976) (Cited on page 28.)

[Kim77a] H. J. Kimble, M. Dagenais, L. Mandel, *Photon antibunching in resonance fluorescence*, Physical Review Letters **39**, 691–695 (1977) (Cited on pages 1 and 42.)

[Kim77b] H. J. Kimble, L. Mandel, *Resonance fluorescence with excitation of finite bandwidth*, Physical Review A **15**, 689–699 (1977) (Cited on page 28.)

[Kir17]   G. Kiršanske, H. Thyrrestrup, R. S. Daveau, C. L. Dreeßen, T. Pregnolato, L. Midolo, P. Tighineanu, A. Javadi, S. Stobbe, R. Schott, A. Ludwig, A. D. Wieck, S. I. Park, J. D. Song, A. V. Kuhlmann, I. Söllner, M. C. Löbl, R. J. Warburton, P. Lodahl, *Indistinguishable and efficient single photons from a quantum dot in a planar nanobeam waveguide*, Physical Review B **96**, 1–11 (2017) (Cited on page 66.)

[Kni01]   E. Knill, R. Laflamme, G. J. Milburn, *A scheme for efficient quantum computation with linear optics*, Nature **409**, 46–52 (2001) (Cited on pages 1 and 65.)

[Kod10]   Y. Kodriano, E. Poem, N. H. Lindner, C. Tradonsky, B. D. Gerardot, P. M. Petroff, J. E. Avron, D. Gershoni, *Radiative cascade from quantum dot metastable spin-blockaded biexciton*, Physical Review B **82**, 155 329 (2010) (Cited on page 61.)

[Kod12]   Y. Kodriano, I. Schwartz, E. Poem, Y. Benny, R. Presman, T. A. Truong, P. M. Petroff, D. Gershoni, *Complete control of a matter qubit using a single picosecond laser pulse*, Physical Review B - Condensed Matter and Materials Physics **85**, 1–5 (2012) (Cited on page 67.)

[Kok07]   P. Kok, W. J. Munro, K. Nemoto, T. C. Ralph, J. P. Dowling, G. J. Milburn, *Linear optical quantum computing with photonic qubits*, Reviews of Modern Physics **79**, 135–174 (2007) (Cited on page 65.)

[Kon12]   K. Konthasinghe, J. Walker, M. Peiris, C. K. Shih, Y. Yu, M. F. Li, J. F. He, L. J. Wang, H. Q. Ni, Z. C. Niu, A. Muller, *Coherent versus incoherent*

light scattering from a quantum dot, Physical Review B - Condensed Matter and Materials Physics **85**, 235 315 (2012) (Cited on page 42.)

[Kre05a] H. J. Krenner, S. Stufler, M. Sabathil, E. C. Clark, P. Ester, M. Bichler, G. Abstreiter, J. J. Finley, A. Zrenner, *Recent advances in exciton-based quantum information processing in quantum dot nanostructures*, New Journal of Physics **7** (2005) (Cited on page 8.)

[Kre05b] A. Kress, F. Hofbauer, N. Reinelt, M. Kaniber, H. J. Krenner, R. Meyer, G. Böhm, J. J. Finley, *Manipulation of the spontaneous emission dynamics of quantum dots in two-dimensional photonic crystals*, Physical Review B - Condensed Matter and Materials Physics **71**, 1–4 (2005) (Cited on page 68.)

[Kuh13a] A. V. Kuhlmann, J. Houel, D. Brunner, A. Ludwig, D. Reuter, A. D. Wieck, R. J. Warburton, *A dark-field microscope for background-free detection of resonance fluorescence from single semiconductor quantum dots operating in a set-and-forget mode*, Review of Scientific Instruments **84** (2013) (Cited on pages 3, 22, and 42.)

[Kuh13b] A. V. Kuhlmann, J. Houel, A. Ludwig, L. Greuter, D. Reuter, A. D. Wieck, M. Poggio, R. J. Warburton, *Charge noise and spin noise in a semiconductor quantum device*, Nature Physics **9**, 570–575 (2013) (Cited on pages 3, 14, and 26.)

[Kuh15] A. V. Kuhlmann, J. H. Prechtel, J. Houel, A. Ludwig, D. Reuter, A. D. Wieck, R. J. Warburton, *Transform-limited single photons from a single quantum dot*, Nature Communications **6**, 8204 (2015) (Cited on pages 3, 14, and 52.)

[Kur00] C. Kurtsiefer, S. Mayer, P. Zarda, H. Weinfurter, *Stable Solid-State Source of Single Photons*, Physical Review Letters **85**, 290 (2000) (Cited on page 2.)

[Kwi95] P. G. Kwiat, K. Mattle, H. Weinfurter, A. Zeilinger, A. V. Sergienko, Y. Shih, *New High-Intensity Source of Polarization-Entangled Photon Pairs*, Physical Review Letters **75**, 4337–4341 (1995) (Cited on page 1.)

[Kwi99] P. G. Kwiat, E. Waks, A. White, I. Appelbaum, P. H. Eberhard, *Ultrabright source of polarization-entangled photons*, Physical Review A - Atomic, Molecular, and Optical Physics **60**, R771–R776 (1999) (Cited on page 66.)

[Lan04] W. Langbein, P. Borri, U. Woggon, V. Stavarache, D. Reuter, A. Wieck, *Radiatively limited dephasing in InAs quantum dots*, Physical Review B **70**, 033 301 (2004) (Cited on page 26.)

[LC18] J. C. López Carreño, E. Z. Casalengua, F. P. Laussy, E. Del Valle, *Joint subnatural-linewidth and single-photon emission from resonance fluorescence*, Quantum Science and Technology **3**, 045 001 (2018) (Cited on pages 5 and 46.)

[Lee23] C.-M. Lee, F. Islam, S. Harper, M. A. Buyukkaya, D. Higginbottom, S. Simmons, E. Waks, *High-Efficiency Single Photon Emission from a Silicon T-Center in a Nanobeam*, ACS Photonics **10**, 3844–3849 (2023) (Cited on page 3.)

[Leo93] D. Leonard, M. Krishnamurthy, C. M. Reaves, S. P. Denbaars, P. M. Petroff, *Direct formation of quantum-sized dots from uniform coherent islands of InGaAs on GaAs surfaces*, Applied Physics Letters **63**, 3203–3205 (1993) (Cited on page 3.)

[Lew86] M. Lewenstein, J. Zakrzewski, K. Rzazewski, *Theory of fluorescence spectra induced by short laser pulses*, Journal of the Optical Society of America B **3**, 22 (1986) (Cited on page 49.)

[Liu18] F. Liu, A. J. Brash, J. O'Hara, L. M. Martins, C. L. Phillips, R. J. Coles, B. Royall, E. Clarke, C. Bentham, N. Prtljaga, I. E. Itskevich, L. R. Wilson, M. S. Skolnick, A. M. Fox, *High Purcell factor generation of indistinguishable on-chip single photons*, Nature Nanotechnology **13**, 835–840 (2018) (Cited on page 68.)

[Lo05] H.-K. Lo, X. Ma, K. Chen, *Decoy State Quantum Key Distribution*, Physical Review Letters **94**, 230 504 (2005) (Cited on page 2.)

[Loh16] A. Lohrmann, S. Castelletto, J. R. Klein, T. Ohshima, M. Bosi, M. Negri, D. W. M. Lau, B. C. Gibson, S. Prawer, J. C. McCallum, B. C. Johnson,

Activation and control of visible single defects in 4H-, 6H-, and 3C-SiC by oxidation, Applied Physics Letters **108**, 021 107 (2016) (Cited on page 3.)

[Lou84] R. Loudon, *Squeezing in resonance fluorescence*, Optics Communications **49**, 24–28 (1984) (Cited on page 44.)

[Lou00] R. Loudon, *The quantum theory of light* (OUP Oxford, 2000) (Cited on page 56.)

[Ma15] X. Ma, N. F. Hartmann, J. K. S. Baldwin, S. K. Doorn, H. Htoon, *Room-temperature single-photon generation from solitary dopants of carbon nanotubes*, Nature Nanotechnology **10**, 671–675 (2015) (Cited on page 3.)

[Mad22] L. S. Madsen, F. Laudenbach, M. F. Askarani, F. Rortais, T. Vincent, J. F. F. Bulmer, F. M. Miatto, L. Neuhaus, L. G. Helt, M. J. Collins, A. E. Lita, T. Gerrits, S. W. Nam, V. D. Vaidya, M. Menotti, I. Dhand, Z. Vernon, N. Quesada, J. Lavoie, *Quantum computational advantage with a programmable photonic processor*, Nature **606**, 75–81 (2022) (Cited on page 2.)

[Man82] L. Mandel, *Squeezed states and sub-poissonian photon statistics*, Physical Review Letters **49**, 136–138 (1982) (Cited on page 44.)

[Mar24] N. Maring, A. Fyrillas, M. Pont, E. Ivanov, P. Stepanov, N. Margaria, W. Hease, A. Pishchagin, A. Lemaître, I. Sagnes, T. H. Au, S. Boissier, E. Bertasi, A. Baert, M. Valdivia, M. Billard, O. Acar, A. Brieussel, R. Mezher, S. C. Wein, A. Salavrakos, P. Sinnott, D. A. Fioretto, P.-E. Emeriau, N. Belabas, S. Mansfield, P. Senellart, J. Senellart, N. Somaschi, *A versatile single-photon-based quantum computing platform*, Nature Photonics **18**, 603–609 (2024) (Cited on page 2.)

[Mat12] C. Matthiesen, A. N. Vamivakas, M. Atatüre, *Subnatural linewidth single photons from a quantum dot*, Physical Review Letters **108**, 093 602 (2012) (Cited on pages 4, 42, and 45.)

[Mat13] C. Matthiesen, M. Geller, C. H. Schulte, C. Le Gall, J. Hansom, Z. Li, M. Hugues, E. Clarke, M. Atatüre, *Phase-locked indistinguishable photons*

with synthesized waveforms from a solid-state source, Nature Communications **4**, 1600 (2013) (Cited on page 42.)

[Mey07] P. Meystre, M. Sargent, *Elements of quantum optics* (Springer, 2007), ISBN 9783540742098 (Cited on pages 4, 19, 26, 34, and 43.)

[Mic00a] P. Michler, A. Kiraz, C. Becher, W. V. Schoenfeld, P. M. Petroff, L. Zhang, E. Hu, A. Imamoglu, *A Quantum Dot Single-Photon Turnstile Device*, Science **290**, 2282–2285 (2000) (Cited on page 3.)

[Mic00b] P. Michler, A. Kiraz, C. Becher, W. V. Schoenfeld, P. M. Petroff, L. Zhang, E. Hu, A. Imamoğlu, *A quantum dot single-photon turnstile device*, Science **290**, 2282–2285 (2000) (Cited on page 42.)

[Mig85] A. L. Migdall, J. V. Prodan, W. D. Phillips, T. H. Bergeman, H. J. Metcalf, *First Observation of Magnetically Trapped Neutral Atoms*, Physical Review Letters **54**, 2596–2599 (1985) (Cited on page 1.)

[Miy05] T. Miyazawa, K. Takemoto, Y. Sakuma, S. Hirose, T. Usuki, N. Yokoyama, M. Takatsu, Y. Arakawa, *Single-Photon Generation in the 1.55-µm Optical-Fiber Band from an InAs/InP Quantum Dot*, Japanese Journal of Applied Physics **44**, L620 (2005) (Cited on page 4.)

[Mn14] C. S. Muñoz, E. Del Valle, A. G. Tudela, K. Müller, S. Lichtmannecker, M. Kaniber, C. Tejedor, J. J. Finley, F. P. Laussy, *Emitters of N-photon bundles*, Nature Photonics **8**, 550–555 (2014) (Cited on pages 55 and 56.)

[Moi94] J. M. Moison, F. Houzay, F. Barthe, L. Leprince, E. André, O. Vatel, *Self-organized growth of regular nanometer-scale InAs dots on GaAs*, Applied Physics Letters **64**, 196–198 (1994) (Cited on page 8.)

[Mol69] B. R. Mollow, *Power Spectrum of Light Scattered by Two-Level Systems*, Physical Review **188**, 1969–1975 (1969) (Cited on pages 18 and 31.)

[Mon10] A. Monmayrant, S. Weber, B. Chatel, *A newcomer's guide to ultrashort pulse shaping and characterization*, Journal of Physics B: Atomic, Molecular and Optical Physics **43**, 103 001 (2010) (Cited on page 24.)

[Mul13] K. Muller, T. Kaldewey, R. Ripszam, J. S. Wildmann, A. Bechtold, M. Bichler, G. Koblmuller, G. Abstreiter, J. J. Finley, *All optical quantum control of a spin-quantum state and ultrafast transduction into an electric current*, Scientific Reports **3**, 1–7 (2013) (Cited on page 67.)

[Mü14] M. Müller, S. Bounouar, K. D. Jöns, M. Glässl, P. Michler, *On-demand generation of indistinguishable polarization-entangled photon pairs*, Nature Photonics **8**, 224–228 (2014) (Cited on pages 61 and 72.)

[Mą22] M. T. Mądzik, S. Asaad, A. Youssry, B. Joecker, K. M. Rudinger, E. Nielsen, K. C. Young, T. J. Proctor, A. D. Baczewski, A. Laucht, V. Schmitt, F. E. Hudson, K. M. Itoh, A. M. Jakob, B. C. Johnson, D. N. Jamieson, A. S. Dzurak, C. Ferrie, R. Blume-Kohout, A. Morello, *Precision tomography of a three-qubit donor quantum processor in silicon*, Nature **601**, 348–353 (2022) (Cited on page 2.)

[Neu80] W. Neuhauser, M. Hohenstatt, P. E. Toschek, H. Dehmelt, *Localized visible Ba^+ mono-ion oscillator*, Physical Review A **22**, 1137–1140 (1980) (Cited on page 1.)

[Neu11] E. Neu, D. Steinmetz, J. Riedrich-Möller, S. Gsell, M. Fischer, M. Schreck, C. Becher, *Single photon emission from silicon-vacancy colour centres in chemical vapour deposition nano-diamonds on iridium*, New Journal of Physics **13**, 025 012 (2011) (Cited on page 2.)

[Ngu11] H. S. Nguyen, G. Sallen, C. Voisin, P. Roussignol, C. Diederichs, G. Cassabois, *Ultra-coherent single photon source*, Applied Physics Letters **99** (2011) (Cited on pages 4, 42, and 45.)

[Ngu12] H. S. Nguyen, G. Sallen, C. Voisin, P. Roussignol, C. Diederichs, G. Cassabois, *Optically gated resonant emission of single quantum dots*, Physical Review Letters **108**, 057 401 (2012) (Cited on pages 3 and 66.)

[Nov01] L. Novotny, R. D. Grober, K. Karrai, *Reflected image of a strongly focused spot*, Optics Letters **26**, 789 (2001) (Cited on page 23.)

[Ou88]   Z. Y. Ou, L. Mandel, *Violation of Bell's Inequality and Classical Probability in a Two-Photon Correlation Experiment*, Physical Review Letters **61**, 50–53 (1988) (Cited on page 1.)

[Pai00] M. Paillard, X. Marie, E. Vanelle, T. Amand, V. K. Kalevich, A. R. Kovsh, A. E. Zhukov, V. M. Ustinov, *Time-resolved photoluminescence in self-assembled InAs/GaAs quantum dots under strictly resonant excitation*, Applied Physics Letters **76**, 76–78 (2000) (Cited on page 26.)

[Par70] J. L. Park, *The concept of transition in quantum mechanics*, Foundations of Physics **1**, 23–33 (1970) (Cited on page 1.)

[Par22] A. J. Park, J. Trautmann, N. Šantić, V. Klüsener, A. Heinz, I. Bloch, S. Blatt, *Cavity-Enhanced Optical Lattices for Scaling Neutral Atom Quantum Technologies to Higher Qubit Numbers*, PRX Quantum **3**, 030 314 (2022) (Cited on page 2.)

[Pau91] S. Paul, J. B. Roy, P. K. Basu, *Empirical expressions for the alloy composition and temperature dependence of the band gap and intrinsic carrier density in $Ga_xIn_{1-x}As$*, Journal of Applied Physics **69**, 827–829 (1991) (Cited on page 10.)

[Phi20] C. L. Phillips, A. J. Brash, D. P. McCutcheon, J. Iles-Smith, E. Clarke, B. Royall, M. S. Skolnick, A. M. Fox, A. Nazir, *Photon Statistics of Filtered Resonance Fluorescence*, Physical Review Letters **125**, 043 603 (2020) (Cited on page 4.)

[Pla01] M. Planck, *Ueber das Gesetz der Energieverteilung im Normalspectrum*, Annalen der Physik **309**, 553–563 (1901) (Cited on page 1.)

[Poe10] E. Poem, Y. Kodriano, C. Tradonsky, N. H. Lindner, B. D. Gerardot, P. M. Petroff, D. Gershoni, *Accessing the dark exciton with light*, Nature Physics **6**, 993–997 (2010) (Cited on page 12.)

[Pog21] I. Pogorelov, T. Feldker, C. D. Marciniak, L. Postler, G. Jacob, O. Krieglsteiner, V. Podlesnic, M. Meth, V. Negnevitsky, M. Stadler, B. Höfer, C. Wächter, K. Lakhmanskiy, R. Blatt, P. Schindler, T. Monz,

Compact Ion-Trap Quantum Computing Demonstrator, PRX Quantum **2**, 020 343 (2021) (Cited on page 2.)

[Poh08] U. W. Pohl, A. Strittmatter, *Control of Self-Organized In(Ga)As/GaAs Quantum Dot Growth*, in D. Bimberg (Editor) *Semiconductor Nanostructures*, pages 41–65 (Springer Berlin Heidelberg, 2008), ISBN 978-3-540-77898-1 (Cited on page 8.)

[Qui15] J. H. Quilter, A. J. Brash, F. Liu, M. Glässl, A. M. Barth, V. M. Axt, A. J. Ramsay, M. S. Skolnick, A. M. Fox, *Phonon-Assisted Population Inversion of a Single InGaAs/GaAs Quantum Dot by Pulsed Laser Excitation*, Physical Review Letters **114**, 1–5 (2015) (Cited on page 66.)

[Ram10a] A. J. Ramsay, T. M. Godden, S. J. Boyle, E. M. Gauger, A. Nazir, B. W. Lovett, A. M. Fox, M. S. Skolnick, *Phonon-Induced Rabi-Frequency Renormalization of Optically Driven Single InGaAs/GaAs Quantum Dots*, Physical Review Letters **105**, 177 402 (2010) (Cited on page 52.)

[Ram10b] A. J. Ramsay, T. M. Godden, S. J. Boyle, E. M. Gauger, A. Nazir, B. W. Lovett, A. M. Fox, M. S. Skolnick, *Phonon-induced Rabi-frequency renormalization of optically driven single InGaAs/GaAs quantum dots*, Physical Review Letters **105**, 1–4 (2010) (Cited on page 62.)

[Ram10c] A. J. Ramsay, A. V. Gopal, E. M. Gauger, A. Nazir, B. W. Lovett, A. M. Fox, M. S. Skolnick, *Damping of exciton rabi rotations by acoustic phonons in optically excited InGaAs/GaAs quantum dots*, Physical Review Letters **104**, 20–23 (2010) (Cited on page 62.)

[Rar90] J. G. Rarity, P. R. Tapster, *Experimental violation of Bell's inequality based on phase and momentum*, Physical Review Letters **64**, 2495–2498 (1990) (Cited on page 1.)

[Rau03] R. Raussendorf, D. E. Browne, H. J. Briegel, *Measurement-based quantum computation on cluster states*, Physical Review A **68**, 022 312 (2003) (Cited on page 1.)

[Rei17] M. Reindl, K. D. Jöns, D. Huber, C. Schimpf, Y. Huo, V. Zwiller, A. Rastelli, R. Trotta, *Phonon-Assisted Two-Photon Interference from Remote Quantum Emitters*, Nano Letters **17**, 4090–4095 (2017) (Cited on pages 66 and 68.)

[Rei19] M. Reindl, J. H. Weber, D. Huber, C. Schimpf, S. F. Covre Da Silva, S. L. Portalupi, R. Trotta, P. Michler, A. Rastelli, *Highly indistinguishable single photons from incoherently excited quantum dots*, Physical Review B **100**, 155 420 (2019) (Cited on page 68.)

[Rob75] G. Robinson, *Metallurgical and electrical properties of alloyed Ni/Au-Ge films on n-type GaAs*, Solid-State Electronics **18**, 331–338 (1975) (Cited on page 12.)

[Rod87] P. A. Rodgers, S. Swain, *Time-dependent pulses in quantum optics: the use of Light's perturbation theory*, Journal of Physics B: Atomic and Molecular Physics **20**, 617–628 (1987) (Cited on pages 21 and 48.)

[Rod03] S. Rodt, R. Heitz, A. Schliwa, R. L. Sellin, F. Guffarth, D. Bimberg, *Repulsive exciton-exciton interaction in quantum dots*, Physical Review B **68**, 035 331 (2003) (Cited on page 61.)

[Rud98] T. G. Rudolph, H. S. Freedhoff, Z. Ficek, *Multiphoton ac Stark effect in a bichromatically driven two-level atom*, Physical Review A **58**, 1296–1309 (1998) (Cited on page 33.)

[San01] C. Santori, M. Pelton, G. Solomon, Y. Dale, Y. Yamamoto, *Triggered Single Photons from a Quantum Dot*, Physical Review Letters **86**, 1502–1505 (2001) (Cited on page 3.)

[San02a] C. Santori, D. Fattal, M. Pelton, G. S. Solomon, Y. Yamamoto, *Polarization-correlated photon pairs from a single quantum dot*, Physical Review B **66**, 045 308 (2002) (Cited on page 76.)

[San02b] C. Santori, D. Fattal, J. Vučković, G. S. Solomon, Y. Yamamoto, *Indistinguishable photons from a single-photon device*, Nature **419**, 594–597 (2002) (Cited on pages 3, 29, and 30.)

[Sax80] A. K. Saxena, *The conduction band structure and deep levels in Ga$_{1-x}$Al$_x$As alloys from a high-pressure experiment*, Journal of Physics C: Solid State Physics **13**, 4323–4334 (1980) (Cited on page 10.)

[Sbr22] F. Sbresny, L. Hanschke, E. Schöll, W. Rauhaus, B. Scaparra, K. Boos, E. Zubizarreta Casalengua, H. Riedl, E. del Valle, J. J. Finley, K. D. Jöns, K. Müller, *Stimulated Generation of Indistinguishable Single Photons from a Quantum Ladder System*, Physical Review Letters **128**, 93 603 (2022) (Cited on pages 65 and 76.)

[Sch15] C. H. H. Schulte, J. Hansom, A. E. Jones, C. Matthiesen, C. Le Gall, M. Atatüre, *Quadrature squeezed photons from a two-level system*, Nature **525**, 222–225 (2015) (Cited on page 4.)

[Sch16] I. Schwartz, D. Cogan, E. R. Schmidgall, Y. Don, L. Gantz, O. Kenneth, N. H. Lindner, D. Gershoni, *Deterministic generation of a cluster state of entangled photons*, Science **354**, 434–437 (2016) (Cited on page 12.)

[Sch18a] L. Schweickert, K. D. Jöns, K. D. Zeuner, S. F. Covre Da Silva, H. Huang, T. Lettner, M. Reindl, J. Zichi, R. Trotta, A. Rastelli, V. Zwiller, *On-demand generation of background-free single photons from a solid-state source*, Applied Physics Letters **112** (2018) (Cited on page 3.)

[Sch18b] L. Schweickert, K. D. Jöns, K. D. Zeuner, S. F. Covre Da Silva, H. Huang, T. Lettner, M. Reindl, J. Zichi, R. Trotta, A. Rastelli, V. Zwiller, *On-demand generation of background-free single photons from a solid-state source*, Applied Physics Letters **112**, 093 106 (2018) (Cited on pages 63 and 66.)

[Sch19] E. Schöll, L. Hanschke, L. Schweickert, K. D. Zeuner, M. Reindl, S. F. Covre Da Silva, T. Lettner, R. Trotta, J. J. Finley, K. Müller, A. Rastelli, V. Zwiller, K. D. Jöns, *Resonance Fluorescence of GaAs Quantum Dots with Near-Unity Photon Indistinguishability*, Nano Letters **19**, 2404–2410 (2019) (Cited on page 65.)

[Sch20] E. Schöll, L. Schweickert, L. Hanschke, K. D. Zeuner, F. Sbresny, T. Lettner, R. Trivedi, M. Reindl, S. F. Covre Da Silva, R. Trotta, J. J. Finley,

J. Vučković, K. Müller, A. Rastelli, V. Zwiller, K. D. Jöns, *Crux of Using the Cascaded Emission of a Three-Level Quantum Ladder System to Generate Indistinguishable Photons*, Physical Review Letters **125**, 1–7 (2020) (Cited on page 65.)

[Scu97] M. O. Scully, M. S. Zubairy, *Quantum optics* (Cambridge university press, 1997) (Cited on pages 18, 19, 34, and 35.)

[Sem08] E. S. Semenova, R. Hostein, G. Patriarche, O. Mauguin, L. Largeau, I. Robert-Philip, A. Beveratos, A. Lemaître, *Metamorphic approach to single quantum dot emission at 1.55µm on GaAs substrate*, Journal of Applied Physics **103**, 103 533 (2008) (Cited on page 4.)

[Shi94] Y. H. Shih, A. V. Sergienko, M. H. Rubin, T. E. Kiess, C. O. Alley, *Two-photon entanglement in type-II parametric down-conversion*, Physical Review A **50** (1994) (Cited on page 66.)

[Sho94] P. Shor, *Algorithms for quantum computation: discrete logarithms and factoring*, in *Proceedings 35th Annual Symposium on Foundations of Computer Science*, pages 124–134 (IEEE Comput. Soc. Press, Santa Fe, NM, USA, 1994), ISBN 978-0-8186-6580-6 (Cited on page 2.)

[Sim05] C. Simon, J.-P. Poizat, *Creating Single Time-Bin-Entangled Photon Pairs*, Physical Review Letters **94**, 030 502 (2005) (Cited on page 72.)

[Sni18] H. Snijders, J. A. Frey, J. Norman, V. P. Post, A. C. Gossard, J. E. Bowers, M. P. Van Exter, W. Löffler, D. Bouwmeester, *Fiber-Coupled Cavity-QED Source of Identical Single Photons*, Physical Review Applied **9**, 31 002 (2018) (Cited on page 42.)

[Som16] N. Somaschi, V. Giesz, L. De Santis, J. C. Loredo, M. P. Almeida, G. Hornecker, S. L. Portalupi, T. Grange, C. Antón, J. Demory, C. Gómez, I. Sagnes, N. D. Lanzillotti-Kimura, A. Lemaítre, A. Auffeves, A. G. White, L. Lanco, P. Senellart, *Near-optimal single-photon sources in the solid state*, Nature Photonics **10**, 340–345 (2016) (Cited on pages 3, 42, and 66.)

[Son12] D. Sonnenberg, A. Graf, V. Paulava, W. Hansen, C. Heyn, *Highly versatile ultra-low density GaAs quantum dots fabricated by filling of self-assembled nanoholes*, Applied Physics Letters **101** (2012) (Cited on page 10.)

[Sta04] J. Stangl, V. Holý, G. Bauer, *Structural properties of self-organized semiconductor nanostructures*, Reviews of Modern Physics **76**, 725–783 (2004) (Cited on page 8.)

[Ste15] D. A. Steck, *Quantum and Atom Optics* (2015) (Cited on pages 4, 20, 32, and 34.)

[Sti01] T. H. Stievater, X. Li, D. G. Steel, D. Gammon, D. S. Katzer, D. Park, C. Piermarocchi, L. J. Sham, *Rabi Oscillations of Excitons in Single Quantum Dots*, Physical Review Letters **87**, 133 603 (2001) (Cited on pages 3, 48, and 52.)

[Str71] C. R. Stroud, *Quantum-Electrodynamic Treatment of Spontaneous Emission in the Presence of an Applied Field*, Physical Review A **3**, 1044–1052 (1971) (Cited on page 34.)

[Stu06] S. Stufler, P. Machnikowski, P. Ester, M. Bichler, V. M. Axt, T. Kuhn, A. Zrenner, *Two-photon Rabi oscillations in a single $In_xGa_{1-x}As/GaAs$ quantum dot*, Physical Review B **73**, 125 304 (2006) (Cited on page 72.)

[Tak10] K. Takemoto, Y. Nambu, T. Miyazawa, K. Wakui, S. Hirose, T. Usuki, M. Takatsu, N. Yokoyama, K. Yoshino, A. Tomita, S. Yorozu, Y. Sakuma, Y. Arakawa, *Transmission Experiment of Quantum Keys over 50 km Using High-Performance Quantum-Dot Single-Photon Source at 1.5 µm Wavelength*, Applied Physics Express **3**, 092 802 (2010) (Cited on page 4.)

[Tak15] K. Takemoto, Y. Nambu, T. Miyazawa, Y. Sakuma, T. Yamamoto, S. Yorozu, Y. Arakawa, *Quantum key distribution over 120 km using ultrahigh purity single-photon source and superconducting single-photon detectors*, Scientific Reports **5**, 14 383 (2015) (Cited on page 4.)

[Tan95] K. Tanaka, T. Nakamura, W. Takamatsu, M. Yamanishi, Y. Lee, T. Ishihara, *Cavity-Induced Changes of Spontaneous Emission Lifetime in One-*

Dimensional Semiconductor Microcavities, Physical Review Letters **74**, 3380–3383 (1995) (Cited on page 15.)

[Tho16] A. Thoma, P. Schnauber, M. Gschrey, M. Seifried, J. Wolters, J.-H. Schulze, A. Strittmatter, S. Rodt, A. Carmele, A. Knorr, T. Heindel, S. Reitzenstein, *Exploring Dephasing of a Solid-State Quantum Emitter via Time- and Temperature-Dependent Hong-Ou-Mandel Experiments*, Physical Review Letters **116**, 033 601 (2016) (Cited on page 85.)

[Tom21] N. Tomm, A. Javadi, N. O. Antoniadis, D. Najer, M. C. Löbl, A. R. Korsch, R. Schott, S. R. Valentin, A. D. Wieck, A. Ludwig, R. J. Warburton, *A bright and fast source of coherent single photons*, Nature Nanotechnology **16**, 399–403 (2021) (Cited on pages 3 and 66.)

[Tra16] T. T. Tran, K. Bray, M. J. Ford, M. Toth, I. Aharonovich, *Quantum emission from hexagonal boron nitride monolayers*, Nature Nanotechnology **11**, 37–41 (2016) (Cited on page 3.)

[Tri18] R. Trivedi, K. Fischer, S. Xu, S. Fan, J. Vuckovic, *Few-photon scattering and emission from low-dimensional quantum systems*, Physical Review B **98**, 144 112 (2018) (Cited on pages 65 and 71.)

[Tri20] R. Trivedi, K. A. Fischer, J. Vučković, K. Müller, *Generation of Non-Classical Light Using Semiconductor Quantum Dots*, Advanced Quantum Technologies **3**, 1900 007 (2020) (Cited on page 72.)

[Ulh12] A. Ulhaq, S. Weiler, S. M. Ulrich, R. Roßbach, M. Jetter, P. Michler, *Cascaded single-photon emission from the Mollow triplet sidebands of a quantum dot*, Nature Photonics **6**, 238–242 (2012) (Cited on page 39.)

[Ulh13] A. Ulhaq, S. Weiler, C. Roy, S. M. Ulrich, M. Jetter, S. Hughes, P. Michler, *Detuning-dependent Mollow triplet of a coherently-driven single quantum dot*, Optics Express **21**, 4382 (2013) (Cited on pages 33 and 39.)

[Upp20] R. Uppu, F. T. Pedersen, Y. Wang, C. T. Olesen, C. Papon, X. Zhou, L. Midolo, S. Scholz, A. D. Wieck, A. Ludwig, P. Lodahl, *Scalable integrated single-photon source*, Science Advances **6** (2020) (Cited on page 42.)

[Urb13] B. Urbaszek, X. Marie, T. Amand, O. Krebs, P. Voisin, P. Maletinsky, A. Högele, A. Imamoglu, *Nuclear spin physics in quantum dots: An optical investigation*, Reviews of Modern Physics **85**, 79–133 (2013) (Cited on pages 11 and 26.)

[Vaj22] D. A. Vajner, L. Rickert, T. Gao, K. Kaymazlar, T. Heindel, *Quantum Communication Using Semiconductor Quantum Dots*, Advanced Quantum Technologies **5**, 2100 116 (2022) (Cited on page 1.)

[Vog91] W. Vogel, *Squeezing and anomalous moments in resonance fluorescence*, Physical Review Letters **67**, 2450–2452 (1991) (Cited on page 44.)

[Wal81] D. F. Walls, P. Zoller, *Reduced Quantum Fluctuations in Resonance Fluorescence*, Physical Review Letters **47**, 709–711 (1981) (Cited on page 44.)

[Wal08] D. Walls, G. Milburn, *Quantum Optics* (Springer Berlin, Heidelberg, 2008), ISBN 978-3-540-28573-1 (Cited on page 28.)

[Wan06] C. Wang, C. Kurtsiefer, H. Weinfurter, B. Burchard, *Single photon emission from SiV centres in diamond produced by ion implantation*, Journal of Physics B: Atomic, Molecular and Optical Physics **39**, 37–41 (2006) (Cited on page 2.)

[Wan07] Z. M. Wang, B. L. Liang, K. A. Sablon, G. J. Salamo, *Nanoholes fabricated by self-assembled gallium nanodrill on GaAs(100)*, Applied Physics Letters **90** (2007) (Cited on page 10.)

[War98] R. J. Warburton, B. T. Miller, C. S. Dürr, C. Bödefeld, K. Karrai, J. P. Kotthaus, G. Medeiros-Ribeiro, P. M. Petroff, S. Huant, *Coulomb interactions in small charge-tunable quantum dots: A simple model*, Physical Review B **58**, 16 221–16 231 (1998) (Cited on pages 7 and 11.)

[War00] R. J. Warburton, C. Schäflein, D. Haft, F. Bickel, A. Lorke, K. Karrai, J. M. Garcia, W. Schoenfeld, P. M. Petroff, *Optical emission from a charge-tunable quantum ring*, Nature **405**, 926–929 (2000) (Cited on pages 3, 12, and 15.)

[War05] M. B. Ward, O. Z. Karimov, D. C. Unitt, Z. L. Yuan, P. See, D. G. Gevaux, A. J. Shields, P. Atkinson, D. A. Ritchie, *On-demand single-photon source*

for 1.3µm telecom fiber, Applied Physics Letters **86**, 201 111 (2005) (Cited on page 4.)

[War14] M. B. Ward, M. C. Dean, R. M. Stevenson, A. J. Bennett, D. J. Ellis, K. Cooper, I. Farrer, C. A. Nicoll, D. A. Ritchie, A. J. Shields, *Coherent dynamics of a telecom-wavelength entangled photon source*, Nature Communications **5**, 3–8 (2014) (Cited on page 68.)

[Wei88] A. M. Weiner, J. P. Heritage, E. M. Kirschner, *High-resolution femtosecond pulse shaping*, Journal of the Optical Society of America B **5**, 1563 (1988) (Cited on page 24.)

[Wei95] A. Weiner, *Femtosecond optical pulse shaping and processing*, Progress in Quantum Electronics **19**, 161–237 (1995) (Cited on page 24.)

[Wei00] A. M. Weiner, *Femtosecond pulse shaping using spatial light modulators*, Review of Scientific Instruments **71**, 1929–1960 (2000) (Cited on page 24.)

[Woo82] W. K. Wootters, W. H. Zurek, *A single quantum cannot be cloned*, Nature **299**, 802–803 (1982) (Cited on page 1.)

[Yan20] C. H. Yang, R. C. C. Leon, J. C. C. Hwang, A. Saraiva, T. Tanttu, W. Huang, J. Camirand Lemyre, K. W. Chan, K. Y. Tan, F. E. Hudson, K. M. Itoh, A. Morello, M. Pioro-Ladrière, A. Laucht, A. S. Dzurak, *Operation of a silicon quantum processor unit cell above one kelvin*, Nature **580**, 350–354 (2020) (Cited on page 2.)

[ZC20] E. Zubizarreta Casalengua, J. C. López Carreño, F. P. Laussy, E. D. Valle, *Conventional and Unconventional Photon Statistics*, Laser & Photonics Reviews **14**, 1900 279 (2020) (Cited on page 44.)

[Zha22] L. Zhai, G. N. Nguyen, C. Spinnler, J. Ritzmann, M. C. Löbl, A. D. Wieck, A. Ludwig, A. Javadi, R. J. Warburton, *Quantum interference of identical photons from remote GaAs quantum dots*, Nature Nanotechnology **17**, 829–833 (2022) (Cited on page 15.)

[Zho20] H.-S. Zhong, H. Wang, Y.-H. Deng, M.-C. Chen, L.-C. Peng, Y.-H. Luo, J. Qin, D. Wu, X. Ding, Y. Hu, P. Hu, X.-Y. Yang, W.-J. Zhang, H. Li,

Y. Li, X. Jiang, L. Gan, G. Yang, L. You, Z. Wang, L. Li, N.-L. Liu, C.-Y. Lu, J.-W. Pan, *Quantum computational advantage using photons*, Science **370**, 1460–1463 (2020) (Cited on page 2.)

[Zre02] A. Zrenner, E. Beham, S. Stufler, F. Findeis, M. Bichler, G. Abstreiter, *Coherent properties of a two-level system based on a quantum-dot photodiode*, Nature **418**, 612–614 (2002) (Cited on pages 3 and 52.)

[Zub20] E. Zubizarreta Casalengua, J. C. López Carreño, F. P. Laussy, F. P. Laussy, E. Del Valle, E. Del Valle, *Tuning photon statistics with coherent fields*, Physical Review A **101**, 1–21 (2020) (Cited on page 45.)

[Zwe22] A. M. J. Zwerver, T. Krähenmann, T. F. Watson, L. Lampert, H. C. George, R. Pillarisetty, S. A. Bojarski, P. Amin, S. V. Amitonov, J. M. Boter, R. Caudillo, D. Correas-Serrano, J. P. Dehollain, G. Droulers, E. M. Henry, R. Kotlyar, M. Lodari, F. Lüthi, D. J. Michalak, B. K. Mueller, S. Neyens, J. Roberts, N. Samkharadze, G. Zheng, O. K. Zietz, G. Scappucci, M. Veldhorst, L. M. K. Vandersypen, J. S. Clarke, *Qubits made by advanced semiconductor manufacturing*, Nature Electronics **5**, 184–190 (2022) (Cited on page 2.)

Acknowledgments